ISSN:2538-516X

Journal of Civil Engineering Researchers

Volume: 6; Number: 2; June 2024

J-Researchers

J-Researchers

JOURNAL OF CIVIL ENGINEERING RESEARCHERS

Volume 6, Number 2, June 2024

Contents

J-Researchers

Journal of Civil Engineering Researchers

Journal homepage: www.journals-researchers.com

Comprehensive Sinkhole Mitigation: A Case Study and Application of Compaction Grouting in Karstic Environments in the State of Tennessee, USA

Hossein Alimohammadi,[a,*] Ashfaq A. Memon [a]

[a] *Terracon Consultants, Inc., Nashville, TN, USA 37217*

ABSTRACT

Sinkholes pose significant risks to infrastructure, requiring detailed investigation and effective repair strategies. This paper details a case study of a persistent sinkhole along a driveway in Nashville, Tennessee, which has caused repeated pavement subsidence despite multiple repairs. The investigation included site visits, drilling operations, soil and rock analysis, and groundwater assessment. Three mitigation approaches were evaluated including conventional inverted rock filter repair, constructing a land bridge, and compaction grouting. After considering technical, situational, and cost factors, compaction grouting was chosen as the optimal solution. The paper outlines the compaction grouting repair strategy, including methodology, materials, and construction specifications. The findings aim to enhance design standards and construction practices for sinkhole repairs in Tennessee and similar geotechnical regions.

ARTICLE INFO

Received: May 01, 2024
Accepted: June 10,2024

Keywords:
Sinkholes
Remediation and Repair Methods
Case Study
Future Design and Construction
Compaction Grouting

DOI: 10.61186/JCER.6.2.1
DOR: 20.1001.1.2538516.2024.6.2.1.2

1. Introduction and literature review on sinkhole remediation methods and case studies

Sinkholes pose significant challenges to infrastructure, safety, and environmental stability in regions susceptible to subsidence. These natural phenomena, often triggered by geological factors or human activities, necessitate effective remediation and repair strategies to mitigate their impact [1] to [5]. Repairing sinkholes requires careful planning, engineering expertise, and innovative solutions tailored to each unique case. Sinkholes occur when underground voids collapse, leading to sudden depressions on the surface. They can vary in size from small cavities to large craters, causing substantial damage to buildings, roads, and other structures. The occurrence of sinkholes is often unpredictable and can be triggered by factors such as heavy rainfall, changes in groundwater levels, or human activities like mining and construction [6]. Over the years, extensive research has been conducted to develop methodologies for addressing sinkhole occurrences, ranging from preventive measures to post-collapse interventions [7] to [49]. This literature review examines several case studies on sinkhole

* Corresponding author. Tel.: +12254853307; e-mail: Hossein.Alimohammadi@terracon.com.

repairs, highlighting different approaches, challenges faced, and lessons learned, and aims to provide an overview of the current state of knowledge regarding sinkhole remediation and repair techniques. Development in karst-prone geologies poses significant risks, necessitating careful attention during site preparation to mitigate potential hazards. Key considerations include ensuring positive drainage to prevent water ponding, capturing surface runoff in stormwater systems, and vigilant observation for incipient sinkholes during construction [45] to [49]. Given the inherent risks associated with karst formations, it is imperative to involve geotechnical engineers in site assessments and grading operations to detect and remediate karst features promptly [20]. Several approaches exist for mitigating the risks of sinkholes in karst areas. These approaches encompass both preventive measures and reactive strategies. Preventive measures aim to minimize the occurrence of sinkholes by assessing and managing the geological hazards associated with karst terrain [28]. This may involve comprehensive geological surveys, monitoring of groundwater levels, land-use planning regulations, and the implementation of engineering practices that consider the unique characteristics of karst landscapes [34]. Reactive strategies, on the other hand, focus on addressing sinkhole formation after it has occurred. These strategies encompass a range of techniques aimed at stabilizing sinkholes, repairing damaged infrastructure, and restoring affected areas. Reactive measures often involve a combination of geotechnical engineering, structural reinforcement, and ecological restoration to mitigate the impacts of sinkholes on the surrounding environment [1] to [3].

The choice of mitigation techniques and sinkhole repair strategies depends on various factors, including the size and severity of the sinkhole, the geological conditions of the site, and the socio-economic considerations of the affected community [1] to [3], [45] to [49]. Furthermore, the effectiveness of these strategies may vary depending on local environmental factors and the availability of resources. Recent advancements in technology and scientific understanding have led to the development of innovative approaches for karst mitigation and sinkhole repair. These include the use of geophysical surveys, remote sensing techniques, and advanced modeling tools to assess and monitor karst hazards accurately [8]. Additionally, the integration of nature-based solutions, such as bioengineering and ecological restoration, offers sustainable approaches to mitigating the impacts of sinkholes while enhancing ecosystem resilience. Despite these advancements, challenges remain in effectively managing karst hazards and mitigating the risks associated with sinkholes. Limited resources, inadequate infrastructure, and competing land-use priorities often constrain the implementation of comprehensive mitigation measures in karst regions [45]. Furthermore, the dynamic nature of karst landscapes presents ongoing challenges in assessing and managing geological hazards effectively. Karst mitigation techniques could be performed by some methods such as avoidance strategies, inverted rock filter, and cap and permeation grouting.

Preventing sinkhole formation is crucial in minimizing their potential hazards. Comprehensive geological surveys, monitoring of ground conditions, and land use planning are essential components of preventive strategies. Early detection techniques such as ground-penetrating radar (GPR), electrical resistivity imaging (ERI), and LiDAR have proven effective in identifying potential sinkhole locations. Moreover, proper management of groundwater resources through controlled extraction and recharge programs can help stabilize subsurface conditions and reduce the likelihood of sinkhole formation. Avoidance remains one of the most cost-effective strategies for mitigating karst-related risks. This involves situating developments away from areas prone to karst activity, minimizing exposure to potential hazards. Critical structures should be located in areas with minimal karst features, and detention/retention ponds should be positioned outside karst-prone zones. Furthermore, measures such as lining ponds with geomembranes can help prevent water infiltration into subsurface voids, reducing the risk of sinkhole formation triggered by fluctuating water levels.

Sinkhole repair entails restoring affected infrastructure and preventing further subsidence. Excavation and backfilling are commonly employed to fill collapsed sinkholes and rebuild damaged foundations. However, conventional repair methods may be insufficient for large or deep sinkholes, necessitating innovative solutions such as the use of geosynthetic reinforcements or soil stabilization techniques. In karst geologies, surface collapses during construction are a significant concern due to vibrations and water intrusion. The inverted rock filter method offers an economical and practical solution for remediation. This technique involves excavating the collapse area to the sinkhole throat, lining it with geotextile fabric, and filling it with rip-rap stone. The fabric prevents soil erosion while allowing water drainage, and the stone provides structural support. This method is suitable for pavement and slab areas but may require alternative approaches, such as concrete backfill, for collapses beneath foundations. Figure 1a to 1e illustrate sinkhole remediation via inverted rock filter method.

When sinkholes do occur, prompt and effective mitigation measures are necessary to prevent further damage. One common approach is the injection of grout materials into subsurface cavities to fill voids and provide structural support. Various types of grouts, including

a) b) c)

d) e)

Figure 1. a to e) Sinkhole Remediation via Inverted Rock Filter

cement-based, chemical, and foam formulations, have been employed depending on the specific geological conditions and desired outcomes. Ground improvement techniques such as compaction grouting and vibro-compaction have also been utilized to stabilize loose or compressible soils prone to sinkhole development. In some cases, advanced grouting technologies combined with ground improvement methods may offer more durable and cost-effective repair alternatives. Cap and permeation grouting are effective methods for stabilizing subsurface voids and enhancing soil strength. Cap grouting involves injecting low-mobility cement grout into voids to fill them and increase soil density, while permeation grouting uses more viscous grout under low pressure to fill smaller voids. Cap grouting, performed by specialty contractors, creates a grout blanket at the bedrock surface and extends columns of grout to stabilize the soil. Permeation grouting, on the other hand, targets smaller voids to prevent further subsidence. It is advisable to perform cap grouting before permeation grouting to seal off bedrock surfaces from water infiltration. Grouting can also be considered for pavement areas at sinkhole features, with consultation from specialty contractors recommended to determine the extent of the grouting program. Figure 2 shows sinkhole remediation via cap and permeation grouting method.

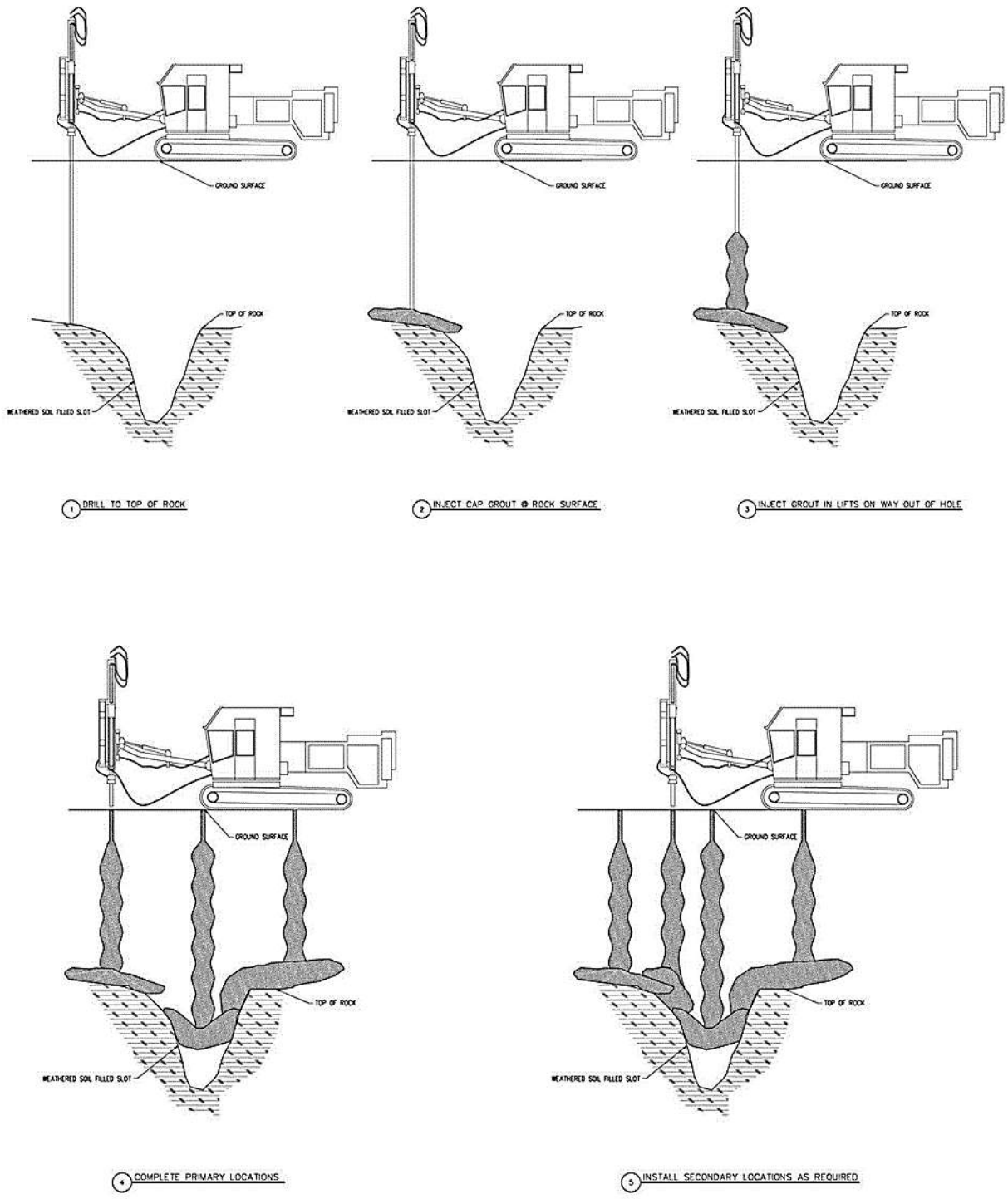

Figure 2. Sinkhole Remediation via Cap and Permeation Grouting

The remediation of sinkholes must also address environmental concerns, particularly regarding groundwater contamination and habitat restoration. Sustainable remediation practices aim to minimize

ecosystem disruption and promote long-term environmental resilience. Techniques such as phytoremediation, which utilize plants to uptake contaminants from soil and water, have shown promise in mitigating the environmental impact of sinkhole collapse.

Sinkhole repairs present complex challenges requiring interdisciplinary approaches, innovative techniques, and proactive risk management strategies. Case studies from around the world highlight the diverse methods employed to stabilize sinkholes and mitigate associated risks. These include grouting techniques, soil stabilization, structural reinforcement, and ground improvement measures. Lessons learned from these case studies underscore the importance of early detection, rapid response, community engagement, and long-term monitoring in effective sinkhole remediation. Smith et al. (2015) reviewed a massive sinkhole formed in Winter Park, Florida, threatening nearby homes and infrastructure in 2013. This case study utilized a combination of compaction grouting and permeation grouting to fill voids and stabilize the surrounding soil. Monitoring systems were installed to track ground movement and ensure the effectiveness of the repairs. The project highlighted the importance of early detection, rapid response, and collaboration between stakeholders to mitigate sinkhole risks effectively. Garcia et al. reviewed the sinkhole incident in Guatemala City in 2010, which drew international attention due to its sheer size and impact on urban infrastructure. This case study employed a combination of geophysical surveys, soil stabilization techniques, and structural reinforcement to stabilize the sinkhole and prevent further collapse. The project showcased the complexities of urban sinkhole remediation, including logistical constraints, public safety concerns, and socio-economic implications. Lessons learned from this case emphasized the need for interdisciplinary collaboration, community engagement, and long-term monitoring to ensure the effectiveness of sinkhole repairs. Barton et al. reviewed a sinkhole formed beneath the National Corvette Museum in Bowling Green, Kentucky, in 2014, swallowing several rare cars on display. This case study employed a combination of geotechnical investigations, ground improvement techniques, and structural reinforcement to stabilize the sinkhole and restore the museum building. The project required careful coordination between preservation experts, engineers, and museum stakeholders to balance structural integrity with historical preservation goals. The Corvette Museum sinkhole restoration highlighted the importance of adaptive strategies, risk communication, and public outreach in managing sinkhole incidents in sensitive environments.

Wang et al. reviewed a sinkhole formed near a metro construction site in Xi'an, China, in 2018, prompting emergency response efforts to stabilize the area. This case study examined the application of innovative repair techniques, including jet grouting and ground improvement, to mitigate sinkhole risks in urban settings. They employed advanced monitoring systems and numerical modeling to assess ground stability and optimize grouting operations. The project demonstrated the effectiveness of proactive risk management and rapid intervention in preventing sinkhole-related disasters in urbanizing areas. Lessons learned from the Xi'an sinkhole remediation underscored the importance of early warning systems, geotechnical analysis, and contingency planning in mitigating sinkhole hazards. Another case study, performed by O'Connor et al., reviewed one of the most visually striking sinkhole incidents to occur in Guatemala City in 2010, when a massive crater measuring approximately 60 feet in diameter and 300 feet deep suddenly appeared, swallowing buildings and roads. The sinkhole was attributed to a combination of factors, including heavy rainfall, volcanic activity, and inadequate infrastructure maintenance. They faced significant challenges in repairing the sinkhole due to its size and the surrounding unstable soil conditions. Traditional repair methods such as grouting and soil stabilization were deemed impractical due to the scale of the sinkhole. Instead, they opted for a combination of backfilling with compacted soil and reinforced concrete structures to stabilize the sinkhole's edges and restore the affected area. The Guatemala City sinkhole serves as a sobering reminder of the catastrophic consequences of neglecting infrastructure maintenance and geological risk assessment.

In 2015, a sinkhole emerged on Oakwood Drive in Toledo, Ohio, prompting emergency repairs to prevent further subsidence. Investigation revealed that the sinkhole was caused by a leaking stormwater pipe, which eroded the surrounding soil and created a void beneath the road surface. Repair efforts involved excavating the damaged pipe, backfilling the void with compacted soil, and reinforcing the roadbed with concrete. Geotechnical monitoring was implemented to detect any signs of instability and ensure the effectiveness of the repair measures. In Beit She'an, Israel, a massive sinkhole formed due to extensive groundwater extraction for agricultural purposes. A unique solution was employed, involving the injection of expansive polyurethane foam to fill the void and stabilize the surrounding soil. This innovative approach provided rapid and cost-effective repairs, minimizing disruption to the local community and infrastructure. Long-term monitoring indicated the stability of the repaired sinkhole, demonstrating the effectiveness of this unconventional technique. In Ripon, North Yorkshire, UK, a large sinkhole formed in 2016, posing a threat to residential areas and infrastructure. Engineers implemented a multifaceted approach, combining traditional grouting methods with innovative

geophysical techniques such as ground-penetrating radar (GPR) and electrical resistivity tomography (ERT) to accurately assess subsurface conditions. This comprehensive approach enabled targeted grouting to fill voids and stabilize the sinkhole effectively. Continuous monitoring following the repair ensured the long-term stability of the site, demonstrating the efficacy of integrating advanced technologies with conventional repair methods.

This paper provides an overview of karst mitigation techniques and sinkhole repair strategies, highlighting recent advancements, challenges, and future directions in the field. By synthesizing existing knowledge and emerging trends, this paper aims to contribute to the development of effective strategies for mitigating the risks associated with sinkholes in karst landscapes. Future research should continue to explore novel repair strategies, enhance predictive modeling capabilities, and promote collaboration between stakeholders to address the ongoing threat of sinkhole hazards.

2. Practical case study

2.1. Project Description

The sinkhole is situated on Whispering Hills Drive just north of Bonerwood Drive in Nashville, Tennessee. Whispering Hills Drive is a two-lane asphalt roadway, approximately 30 feet wide, sloping gently downward to the north-northeast. Subsidence, spanning the width of the travel lanes, is visibly apparent along a segment of approximately 50 feet in length. Additionally, an isolated dropout of approximately 6 feet in diameter is observed in the east (northbound) lane of the roadway. Within the affected area, there reportedly exists a 36-inch diameter water main and a 12-inch diameter water line. A storm drain traverses through the pavement subsidence area, located along the eastern end of the pavement. A stone-lined ditch is situated on the western side of the roadway.

This problematic area has been a persistent issue for several years. Personnel from Metro Public Works recall visiting the site in the late 1990s, observing isolated dropouts and subsidence related to soil piping. It appears that conventional sinkhole repair methods involving excavation of overburden and placement of rock fill have been implemented on multiple occasions since then. The most recent repair of the pavement settlement area, reportedly conducted about four months ago, involved the removal of asphalt pavement and undercutting of the soft subgrade soils to an unspecified depth. The undercut area was subsequently backfilled with crushed rock fill, topped with a thick layer of asphalt pavement. However, noticeable and measurable subsidence, along with a significant dropout, occurred shortly after the repair efforts, prompting the initiation of the current exploration and study to investigate and mitigate the issue. The affected section of the road has been closed to traffic since the latter part of May 2009. The site location map and the approximate location of dropout within the roadway are depicted in figures 3a and 3b respectively. Figures 4a to 4k also illustrate the existing site situations and dropouts and subsidence along the driveway on the site.

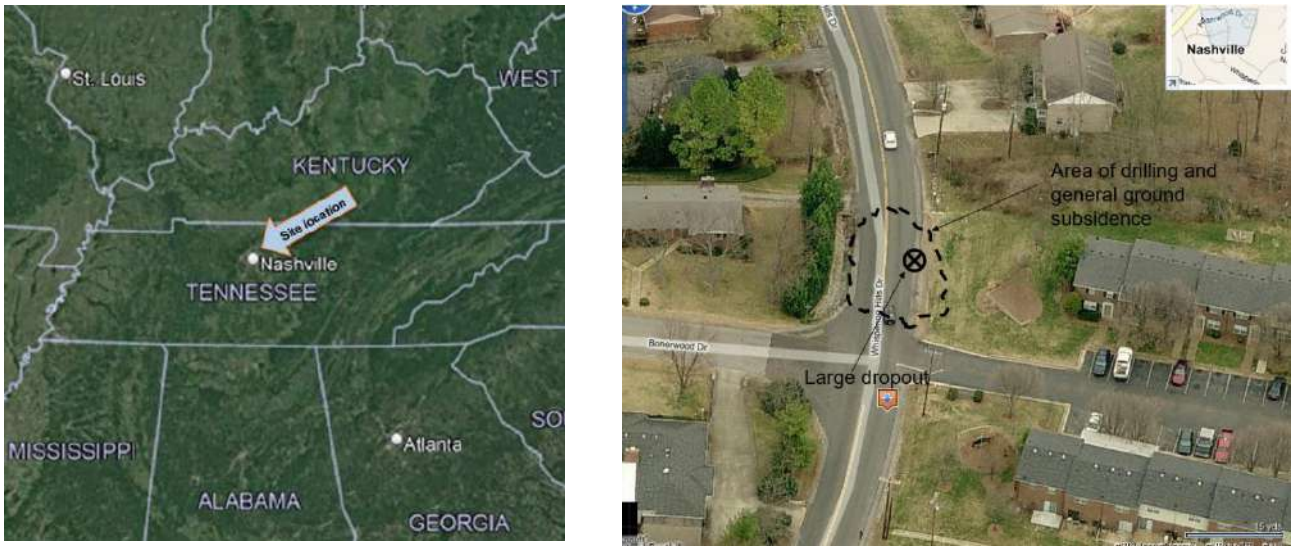

a) b)

Figure 3. a) Site location, and b) the approximate location of dropout within the roadway

a)

b)

c)

d)

e)

f)

Figure 4. Continued on the next page

g) h)

i) j) k)

Figure 4. a to k) the existing site situations and dropouts within the roadway

2.2. Field Exploration and Laboratory Testing

The subsurface exploration comprised two distinct phases. The initial phase, conducted from April 24 to 28, 2009, involved the drilling of seven borings in the vicinity of the sinkhole area. These borings delved to depths ranging between approximately 17 and 48½ feet below existing grade. Subsequently, the second phase occurred from June 8 to 9, 2009, during which an additional five borings were drilled to augment the subsurface data. The locations of these borings were determined by Terracon personnel and were positioned relative to the features delineated in Figure 3. Both truck-mounted rotary drill rigs and ATV rigs equipped with hollow stem augers were utilized to advance the boreholes. Soil sampling was conducted using the split barrel sampling procedure, whereby the standard penetration resistance value (N) was determined based on the number of blows required to advance a standard 2-inch O.D. split barrel sampler the final 12 inches of an 18-inch penetration, using a 140-pound hammer with a free fall of 30 inches. This value facilitated estimates of in situ relative density for cohesionless soils and the consistency of cohesive soils. The depths of sampling, penetration distances, and standard penetration resistance values were meticulously documented on the boring logs, with the samples subsequently sealed and transported to the laboratory for comprehensive testing and classification. Field logs detailing the visual classifications of encountered materials and the driller's interpretation of subsurface conditions between samples were meticulously prepared. Final boring logs represented an amalgamation of field observations and laboratory analyses, with modifications made based on the

latter. Figure 5 illustrates locations of the performed borings within the roadway and Figure 6 shows cross section of pavement and location of some borings within the existing dropout.

All boreholes were extended until auger refusal was encountered, typically occurring at depths ranging from approximately 7½ to 48½ feet below existing grade. For seven of the twelve borings, refusal materials were penetrated using a diamond bit affixed to the outer barrel of a double core barrel. The inner barrel collected cored material while the outer barrel, rotating at high speeds, facilitated rock cutting. Upon completion of each drilling operation, the barrel was retrieved, and the core samples were boxed and logged. Subsequent rock classification by an engineer involved determining the "percent recovery" and the rock quality designation (RQD), with the former representing the ratio of retrieved sample length to drilled length, and the latter providing an indication of in-situ rock quality based on the length of intact core segments.

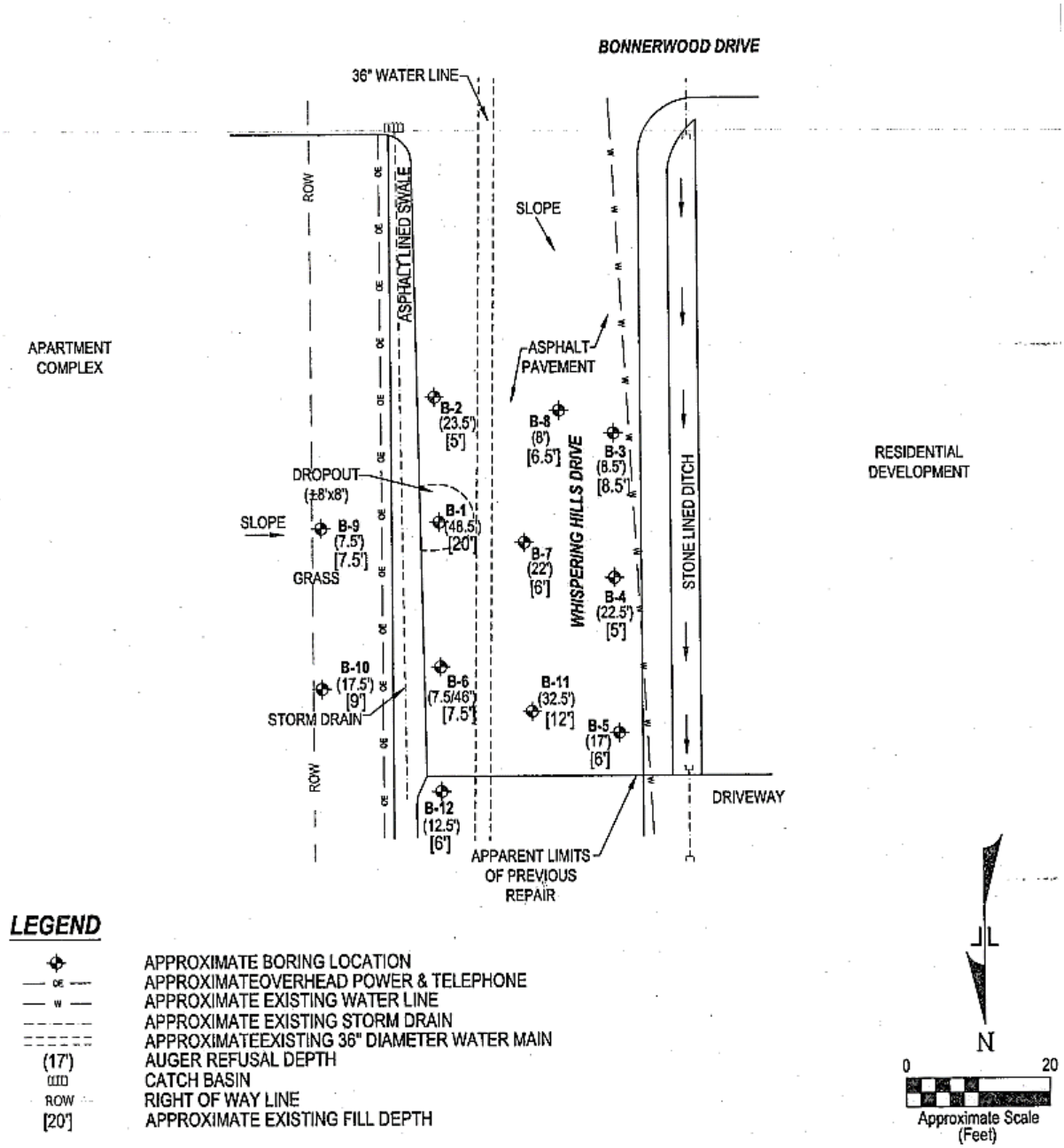

Figure 5. Locations of the borings within the roadway

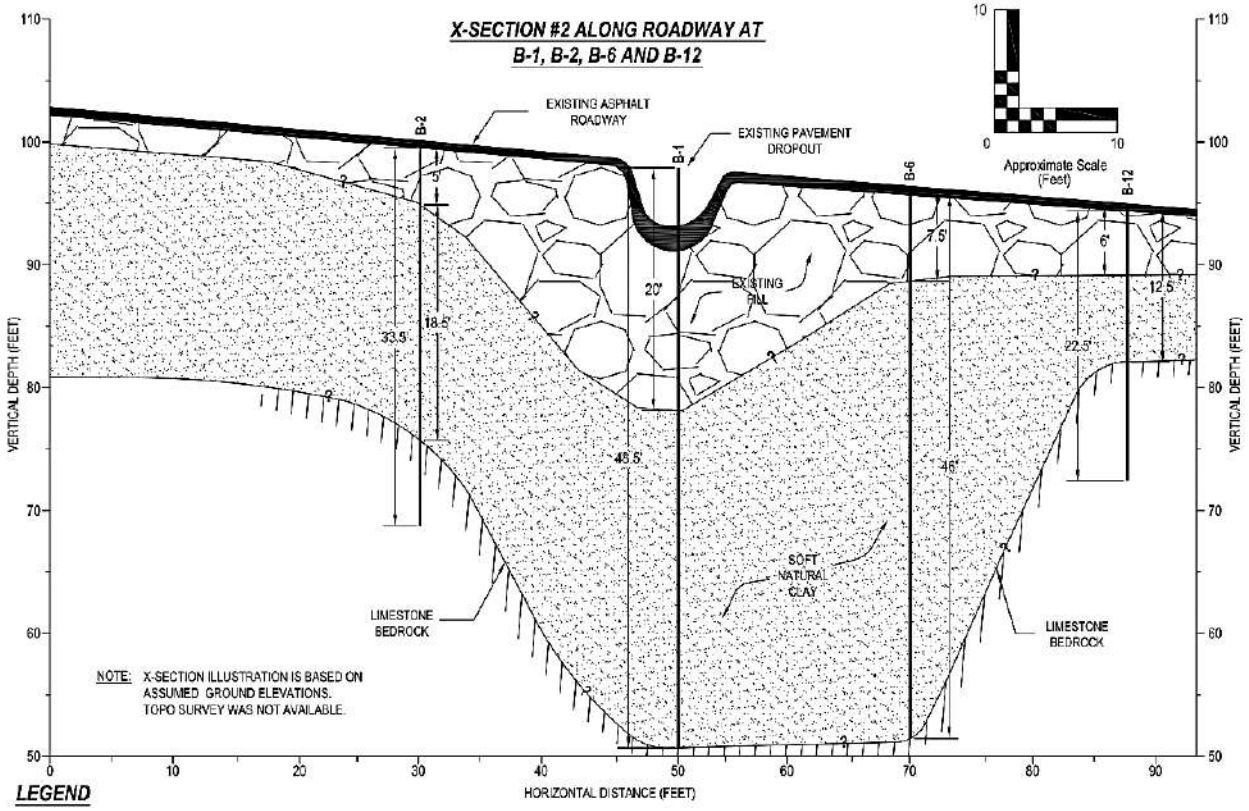

Figure 6. Cross section of pavement and location of some borings within the existing dropout

Laboratory testing encompassed water content tests and Atterberg Limits tests on representative soil samples. These tests, coupled with field penetration data, facilitated assessments of soil strength in-situ, volume change potential, and soil classification, with results documented on the boring logs. Classification and descriptions of rock core samples adhered to established guidelines and were primarily based on visual and tactile assessments, although petrographic analysis of thin sections could potentially reveal additional rock types. Percent recovery and RQD calculations for these samples were documented at their respective depths on the boring logs.

3. Subsurface Conditions

3.1. Geology

A comprehensive review of available geological data reveals that the site is underlain by the Hermitage Formation from the Ordovician Period. This formation comprises four distinct facies (sections), including the granular phosphatic limestone facies at the uppermost level, followed by the Coquina and laminated argillaceous limestone facies in the middle, and the Curdsville Limestone at the base. The granular phosphatic limestone facies is identified by its medium light gray to brownish-gray coloration, medium bedding, and crossbedding, along with brown phosphatic pallets. The Coquina facies exhibits a medium gray to brownish-gray hue, medium bedding, and contains disseminated silt and shale partings. The laminated argillaceous facies consists of medium to dark gray, very fine-grained limestone with numerous thin shale partings. The Curdsville Limestone, on the other hand, is characterized by a medium to dark gray coloration, fine to medium grain size, thin bedding, and thin shale partings. These facies undergo weathering processes resulting in a transition to pale to dark yellowish-brown silty, sandy clay material, akin to the conditions observed beneath the fill in our boreholes.

The subject property is located within a region characterized by karst-prone geology. Any development in such topography carries inherent risks of future internal soil erosion and ground subsidence, potentially impacting the stability of pavements and buried utilities. Presently, the state of the art in geotechnical engineering does not facilitate accurate prediction of the location and probability of karst-related subsidence. The subsidence of the existing pavement, along with associated dropout within the

Table 1. depths of fill and auger refusal encountered at each boring locations

Boring	Approximate fill depth (ft)	Approx. depth to refusal (ft)	Boring	Approximate fill depth (ft)	Approx. depth to refusal (ft)
B-1	20	48 ½	B-7	6	22
B-2	5	23 ½ *	B-8	6 ½	8 *
B-3	8 ½	8 ½ *	B-9	7 ½	7 ½ *
B-4	5	22 ½ *	B-10	9	17 ½
B-5	6	17	B-11	12	32 ½
B-6 **	7 ½	46 *	B-12	6	12 ½ *

* Boring where rock coring was performed

** Initial auger refusal occurred at a depth of about 7½ feet on weathered limestone rock

roadway, is seemingly linked to karst-related soil piping, and is typified as a sinkhole occurrence.

3.2. Soil and Rock Conditions

The subsurface conditions inferred from the borehole investigations can be summarized as follows: Borings B-1 through B-8, B-11, and B-12 were conducted within the asphalt pavement area, revealing a layer of asphalt ranging from 0.3 to 2 feet in thickness. Borings B-9 and B-10, located off the pavement at the right-of-way limits east of the roadway, encountered approximately 0.4 to 0.6 feet of topsoil. Beneath the surface cover, the boreholes generally penetrated 5 to 20 feet of fill material overlying natural lean to fat clay and/or limestone bedrock. Boring B-1, situated within the pavement dropout area, revealed a deeper fill of about 20 feet, primarily comprised of crushed rock with or without clay. The fill material appeared to be uniformly graded with minimal fines, with variations noted such as the presence of soil and rock at B-3 and large limestone fragments, possibly shot rock, at B-9 and B-10. The depths of fill and auger refusal encountered at each boring location are summarized in Table 1.

Natural clay was encountered beneath the fill layer, extending to auger refusal on limestone bedrock at depths ranging from 8 to 48½ feet below the existing grade. A void of approximately 1 foot was observed between the bottom of the asphalt and the surface of the crushed rock at Boring B-4. The fill material exhibited a variable relative density, ranging from very loose to medium dense, with standard penetration resistance (N) values typically ranging from 0 to 23 blows per foot (bpf). It is noted that higher N-values may be inflated due to the presence of large limestone fragments and do not accurately represent the true relative density of the fill. The natural clay beneath the existing fill generally displayed a very soft to medium stiff consistency, with most N-values ranging from 0 to 6 bpf, except for borings B-4 and B-12 where stiff clays were encountered down to the bedrock. This softening of soil is indicative of karst activity and suggests soil piping at these locations.

All boreholes were extended to auger refusal on apparent limestone bedrock, with depths ranging from about 7½ to 48½ feet below the existing grade. Deeper refusal depths, ranging from 46 to 48½ feet below grade, were observed at B-1 and B-6. Rock core sampling was performed at selected boring locations (B-2 through B-4, B-6, B-8, B-9, and B-12) to further investigate the materials encountered at auger refusal. The sampled bedrock materials primarily consisted of light to medium gray, thin to very thin bedded limestone with weathered shaly seams. Core recovery ranged from 30 to 100 percent, with poorer recovery noted at B-9 and B-12. The quality of the cores obtained was generally assessed as very poor to fair based on the Rock Quality Designation (RQD) values, typically ranging from 0 to 75 percent. At Boring B-6, initial auger refusal was encountered at approximately 7½ feet below grade on weathered limestone, which extended to a depth of about 14 feet below grade. Below this depth, the core barrel encountered minimal resistance down to approximately 46 feet below grade, with no recovery of subsurface material due to an apparent clay-filled slot resulting from solution weathering, a common feature in the Hermitage Limestone formation present at the site. At Boring B-9, the sampled bedrock material comprised moderately to highly weathered limestone with voids and crevices filled with concrete grout. Additionally, a 3-inch thick asphalt piece was encountered during coring at approximately 12 feet below grade, indicating the possibility of prior compaction grouting to fill voids within the rock mass.

3.3. Groundwater Conditions

The borings were meticulously monitored during and immediately after drilling to assess the presence and depth of groundwater. Upon completion of the boring process,

groundwater was observed in borings B-1, B-3, B-4, and B-8, with depths ranging from approximately 5 to 28 feet below the existing grade. These observations offer a preliminary insight into the groundwater conditions prevailing on the site at the time of drilling. However, owing to the low permeability of the cohesive soils encountered in the borings, more extensive monitoring over the long term, possibly through cased holes or piezometers, would be necessary for a comprehensive and precise evaluation of groundwater conditions. It is essential to recognize that fluctuations in groundwater levels may arise due to seasonal variations in rainfall, runoff, and other factors that may not have been evident during the initial boring operations.

4. Evaluations and Recommendations

Based on subsurface data and our professional experience, the pavement distress and dropout are attributed to active soil piping and ground subsidence, likely associated with an apparent sinkhole. Previous repair efforts have been largely superficial and insufficient to halt the ongoing soil piping at significant depths.

Initially, a conventional inverted rock filter sinkhole repair method was contemplated for this project. However, optimal execution of such a repair would necessitate the rock fill to extend down to the bedrock. The excavation required to reach the bedrock is anticipated to be considerable, possibly extending beyond the road right-of-way into adjacent private properties. Consequently, temporary shoring of excavation sidewalls may be necessary due to space constraints. Furthermore, this approach would mandate the relocation of all buried utilities within the excavation area. Considering the substantial depth of excavation, reaching up to 48½ feet below grade, along with the potential need for temporary shoring, this sinkhole repair option is deemed impractical and cost-ineffective.

Alternatively, the project team explored a structural solution involving the construction of a land bridge spanning the affected area. Extensive research and review were conducted regarding the costs and logistical challenges associated with this approach. However, it was concluded that the construction of a land bridge would be prohibitively expensive and time-consuming, with the design and construction phases spanning several months. The adverse impacts on both cost and schedule were deemed unacceptable, leading to the abandonment of this approach.

Based on our extensive experience, research, and consultations with specialty contractors, a compaction grouting program, sometimes referred to as cap grouting, emerges as a viable and practical solution for enhancing subgrade conditions and mitigating ground subsidence. Compaction grouting entails the precise injection of low-slump grout in a grid pattern to displace soft soils, fill voids above the bedrock surface, and establish a grouted matrix aimed at solidifying and stabilizing the affected area. The primary objective of the initial grouting phase is to create a grout blanket or cap across the bedrock surface, sealing voids without filling those within the bedrock itself. This targeted grouting strategy involves placing grout bulbs at the bedrock surface to prevent further loss of overburden into bedrock voids and crevices, while also reducing voids within the overburden above. As the lower reaches of the target area are grouted, casings are gradually withdrawn, and grout is injected at predetermined intervals. This incremental approach effectively reduces voids within the overburden, contributing to the solidification of the zone. Subsequent rounds of grouting, if necessary, will be determined based on the outcomes of the primary injection cycle. The grouting operations are expected to extend up to near the invert of the existing 36-inch diameter water line, reaching a depth of approximately 8 feet below the road surface. Typically, such specialized work is undertaken by a dedicated grouting contractor.

Following the completion of grouting operations, the near-surface subgrades in the affected area will undergo undercutting and replacement with engineered fill, followed by repaving. The engineered fill will primarily comprise granular materials such as well-graded crushed mineral aggregate, conforming to TDOT Section 903.05 (Type A, Grading D), and/or approved clean shot rock. The granular fill will be placed in maximum 10-inch thick loose lifts, with each layer compacted to at least 95% of the material's standard Proctor maximum dry density. The upper 12 inches of fill subgrade will be compacted to at least 100% of the same standard. Graded solid rock fill shall comprise well-graded, durable shot rock with a maximum fragment size of 18 inches, with 20 to 30 percent passing the No. 4 sieve and no more than 5 percent passing the No. 200 sieve. The fragments should exhibit roughly equidimensional shapes, with thin, slabby, or shaly material deemed unacceptable. The material's performance under five iterations of the sodium sulfate soundness test (AASHTO T-104) should yield a weighted percentage of loss not exceeding 12%. It is not recommended to mix shot rock with natural clayey soils. Placement and compaction of uniform fill materials will aid in densification and testing during construction. Graded solid rock material must be approved by the engineer before use on the project. Shot rock fill should be compacted in lifts not exceeding 2 feet using a D-8 class Dozer (10-ton class vibratory roller) or equivalent equipment. Undercut material is expected to comprise open-graded crushed rock with minimal or no fines, large limestone fragments, and soil-rock mixture.

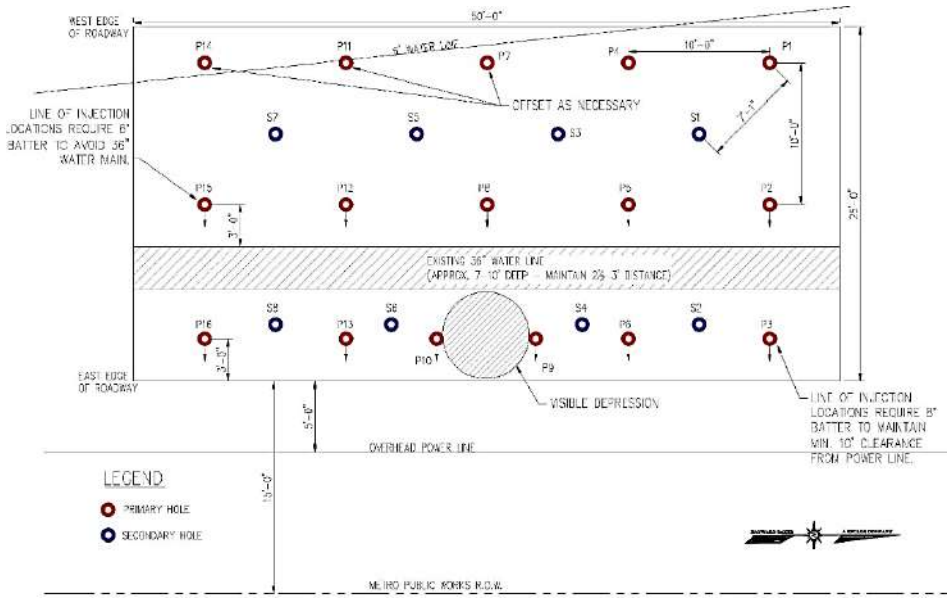

Figure 7. Primary hole and secondary hole locations of the studied site

Reuse of this material is not recommended; it should be hauled off-site.

We recommended that the new engineered fill be properly benching with the existing subgrade to establish a positive bond between the new fill and the existing soils. Finish pavement grades should be properly sloped to ensure positive drainage, thereby reducing water ponding on the pavement and infiltration into the underlying subgrade. Based on our discussions, we understand that the Owner agrees with the compaction grouting repair option and has authorized the project team to prepare bid documents accordingly. In compliance with their request, we have previously prepared and forwarded a permit for the work as required by the regulatory division of the state of Tennessee.

The compaction grouting program has been determined to be a viable treatment plan for the problem area, based on our discussions. Our experience indicates that compaction or cap grouting has effectively addressed sinkhole/karst-related ground subsidence in the past. The objective of the current work is to provide a permanent repair to the current problems in the affected road segment. This was discussed with the Owner and nearby residents in a project-related public meeting, and communicated to the regulatory agency. The intent of the grouting is to inject sufficient low slump material into the subsurface to create a solidified but porous mass, forming a plug over the bedrock voids to support the road subgrade for many years. It's important to note that the work is not intended to fill every bedrock void within the upper weathered bedrock profile at the problem area. Instead, an associated goal is to permit the continued passage of groundwater through the zone. The aim of this objective is to reduce potential negative impacts of groundwater movement in peripheral areas where such movement had not previously occurred. However, it's crucial for the Owner and nearby residents to understand that this targeted remedy is not a widespread treatment expected to address or reduce the risk of sinkholes on adjacent public right of way or nearby properties. Figure 7 shows proposed primary hole and secondary hole locations of the studied site. Sinkhole formation risk is inherent in this geologic setting, as adamantly stated in the public meeting, and local risk cannot be entirely eliminated. Future sinkhole occurrences in this neighborhood cannot be predicted but should not be totally unexpected. Any future sinkhole incidents should be addressed on a case-by-case basis, and any such occurrence would be considered coincidental to the currently proposed repair work.

5. Conclusions

In conclusion, the comprehensive investigation detailed in this paper sheds light on the complexities surrounding sinkhole occurrences and their remediation, as exemplified by the persistent sinkhole along Whispering Hills Drive in Nashville, Tennessee. The interdisciplinary approach employed, combining geotechnical expertise, geological analysis, and engineering solutions, underscores the multifaceted nature of sinkhole mitigation. Through meticulous field exploration and laboratory testing, the geological and subsurface conditions were thoroughly characterized, revealing the presence of karst-prone geology and variable soil and rock compositions. Evaluation of potential repair strategies highlighted the limitations of conventional methods and led to the selection

of a compaction grouting program as the most viable solution. This approach, involving precise injection of low-slump grout to stabilize the affected area, offers a practical and cost-effective means of addressing soil piping and ground subsidence. The proposed repair strategy, detailed with specifications for material selection and construction methodologies, aims to provide a long-lasting solution to the persistent sinkhole issue. The recommendations put forth emphasize the importance of proactive risk management and continued monitoring to address potential future sinkhole occurrences. While the selected repair strategy targets the specific problem area, it is essential to recognize the inherent risks associated with sinkhole formation in karstic landscapes. Stakeholders must remain vigilant and prepared to address any future incidents on a case-by-case basis. Continued research and collaboration among stakeholders are essential to further enhance the effectiveness and sustainability of sinkhole remediation efforts. The findings presented in this paper underscore the significance of proactive risk management and adaptive strategies in addressing sinkhole hazards. While the selected compaction grouting program offers a promising solution for the current problem area, it is essential to acknowledge the inherent risks associated with sinkhole formation in karstic landscapes. Continued research, monitoring, and community engagement are imperative in enhancing our understanding of sinkhole dynamics and developing resilient infrastructure systems capable of withstanding such geological challenges. Ultimately, the lessons learned from this study contribute to the advancement of design standards and construction practices for sinkhole repairs, fostering safer and more sustainable development in karstic areas and beyond.

6. Acknowledgments

The authors would like to acknowledge the engineers in the soil mechanic laboratory facility, the field group members, and the drilling crews who performed SPT in the Terracon company in Nashville, TN, and thank them for their help in providing the data for this research. The opinions, findings, and conclusions presented herein are those of the authors and do not necessarily reflect any sponsors.

7. Conflict of interest

The authors declare that they have no conflict of interest.

References

[1] Jitendra Khatti, Kamaldeep Singh Grover, "Prediction of compaction parameters for fine-grained soil: Critical comparison of the deep learning and standalone models," T Journal of Rock Mechanics and Geotechnical Engineering, Volume 15, Issue 11, November 2023, Pages 3010-3038, https://doi.org/10.1016/j.jrmge.2022.12.034

[2] Gutiérrez, F., Cooper, A.H. & Johnson, K.S. Identification, prediction, and mitigation of sinkhole hazards in evaporite karst areas. Environ Geol 53, 1007–1022 (2008). https://doi.org/10.1007/s00254-007-0728-4

[3] Qing-Long Cui, et al, "Mitigation of geohazards during deep excavations in karst regions with caverns: A case study" Engineering Geology, Volume 195, 10 September 2015, Pages 16-27, https://doi.org/10.1016/j.enggeo.2015.05.024

[4] M. Abu-Farsakh, H. Alimohammadi, and L. N. Mohammad, "Finite Element Analysis to Evaluate the Benefits of Geosynthetic Reinforcement in Flexible Pavements Over Weak Subgrade for Low-Volume Traffic Roads," Transp. Res. Board Conf. 99th Annu. Meet., 2020. https://annualmeeting.mytrb.org/OnlineProgramArchive/Details/12333

[5] H. Alimohammadi and B. Izadi Babokani, "Finite element electrodynamics modeling of a layered piezoelectric composite shell with different materials by using numerical software," ISSS J. Micro Smart Syst., 2020.

[6] H. Alimohammadi, "A framework for evaluation of existing pavement conditions and selection of feasible maintenance/rehabilitation alternatives; a case study in some routes of Livingston Parish in the state of Louisiana," SN Appl. Sci., vol. 2, no. 2, p. 289, Feb. 2020. https://doi.org/10.1007/s42452-020-1999-6

[7] G. Zheng, H. Alimohammadi, J. Zheng, and V. R. Schaefer, "Effectiveness of Geosynthetics in the Construction of Roadways: A Full-Scale Field Studies Review," International Foundations Congress and Equipment Expo 2021, 2021, pp. 223–232. https://doi.org/10.1061/9780784483411.022

[8] H. Alimohammadi, V. R. Schaefer, J. Zheng, and H. Li, "Performance evaluation of geosynthetic reinforced flexible pavement: a review of full-scale field studies," Int. J. Pavement Res. Technol., 2020. https://doi.org/10.1007/s42947-020-0019-y

[9] H. Alimohammadi, V. Schaefer, J. Ashlock, A. Buss, C. Rutherford, and B. Li, "Effectiveness of geogrids in roadway construction; determine a granular equivalent (G.E.) factor."

[10] H. Alimohammadi, J. Zheng, A. Buss, V. R. Schaefer, C. Williams, and G. Zheng, "Field and simulated rutting behavior of hot mix and warm mix asphalt overlays," Constr. Build. Mater., vol. 265, p. 120366, Dec. 2020. https://doi.org/10.1016/j.conbuildmat.2020.120366

[11] Koosha Kalhor 1, Reza Ghasemizadeh, Ljiljana Rajic, Akram Alshawabkeh, "Assessment of groundwater quality and remediation in karst aquifers: A review," Groundwater for Sustainable Development, Volume 8, April 2019, Pages 104-121. https://doi.org/10.1016/j.gsd.2018.10.004

[12] H. Alimohammadi and · Jamal Tahat, "A case study experimental pile load testing (PLT) for evaluation of driven pile behaviors," Arab. J. Geosci. 2022 159, vol. 15, no. 9, pp. 1–11, Apr. 2022. https://doi.org/10.1007/s12517-022-10176-5

[13] H. Alimohammadi and · Jamal Tahat, "A Case Study Pile Load Testing (PLT) to Evaluate Driven Pile Behaviors," Indian Geotechnical Journal. Volume 52, pages 959–968, 2022. https://doi.org/10.1007/s40098-022-00613-3

[14] H. Alimohammadi, M. Amirmojahedi, and J. N. Tahat, "A Case History of Application of Deep Compaction Method with Comparison to Different Ground Improvement Techniques," Transp.

Infrastruct. Geotechnol., pp. 1–26, Mar. 2022. https://doi.org/10.1007/s40515-022-00229-3

[15] S. Satvati, H. Alimohammadi, M. A. Rowshanzamir, and S. M. Hejazi, "Evaluation the Effects of Geosynthetic Reinforcement on Bearing Capacity of Shallow Foundations in Soil Slopes," 101st Transp. Res. Board Annu. Meet., 2022. https://annualmeeting.mytrb.org/OnlineProgram/Details/17240

[16] H. Alimohammdi, V. R. Schaefer, J. Zheng, C. T. Jahren, G. Zheng, and D. White, "Effectiveness of Geotextiles/Geogrids in Roadway Construction; Determine a Granular Equivalent (GE) Factor," Minnesota Dep. Transp., 2021. https://www.dot.state.mn.us/research/reports/2021/202126.pdf

[17] H. Alimohammadi, V. Schaefer, J. Zheng, D. J. White, and G. Zheng, "A State-of-the-art Large-scale Laboratory Approach to Evaluating the Effectiveness of Geogrid Reinforcement in Flexible Pavements," Geosynthetics Conference 2021, 2021. https://osf.io/2d4gk/

[18] H. Alimohammadi, A. Buss, V. R. Schaefer, J. Zheng, and G. Z. Christopher Williams, "Finite element viscoelastic simulations of rutting behavior of hot mix and warm mix asphalt overlay on flexible pavements," Int. J. Pavement Res. Technol., 2020. https://doi.org/10.1007/s42947-020-0057-5

[19] H. Alimohammadi, J. Zheng, A. Buss, V. R. Schaefer, and G. Zheng, "Rutting Performance Evaluation of Hot Mix Asphalt and Warm Mix Asphalt Mixtures by Using Dynamic Modulus, Hamburg Wheel Tracking Tests, and Viscoelastic Finite Element Simulations," International Conference on Transportation and Development 2020, pp. 83– 94. https://doi.org/10.1061/9780784483183.009

[20] J. Zheng, H. He, and H. Alimohammadi, "Three-dimensional Wadell roundness for particle angularity characterization of granular soils," Acta Geotech., vol. 9, p. 2020. https://doi.org/10.1007/s11440-020-01004-9

[21] H. Alimohammadi, K. Yashmi Dastjerdi, and M. Lotfollahi Yaghin, "The study of progressive collapse in dual systems," Civ. Environ. Eng., vol. 16, 2020. https://doi.org/10.2478/cee-2020-0009

[22] H. Alimohammadi, J. Zheng, A. Buss, V. Schaefer, C. Williams, and Guangfan Zheng, "Performance Evaluation of Hot Mix and Warm Mix Asphalt Overlay Layers Based on Field Measurements and Finite Element Viscoelastic Simulations," Transp. Res. Board Conf. 99th Annu. Meet., 2020. https://annualmeeting.mytrb.org/OnlineProgramArchive/Details/13743

[23] H. Alimohammadi, A. Hesaminejad, and M. Lotfollahi Yaghin, "Effects of different parameters on inelastic buckling behavior of composite concrete-filled steel tubes," Int. Res. J. Eng. Technol., vol. 6, no. 12, 2019. https://www.researchgate.net/publication/337856971_Effects_of_different_parameters_on_inelastic_buckling_behavior_of_composite_concrete-filled_steel_tubes

[24] H. Alimohammadi, M. D. Esfahani, and M. L. Yaghin, "Effects of openings on the seismic behavior and performance level of concrete shear walls," Int. J. Eng. Appl. Sci., 2019. https://www.researchgate.net/publication/337596926_Effects_of_openings_on_the_seismic_behavior_and_performance_level_of_concrete_shear_walls

[25] H. Alimohammadi, "Finite element analysis of a Piezoelectric layered plate with different materials," International Journal of Engineering and Applied Sciences, vol. 6, no. 7, 2019. DOI: 10.31873/IJEAS.6.8.2019.09

[26] H. Alimohammadi and M. Lotfollahi Yaghin, "Study on the Effect of the Concentric Brace and Lightweight Shear Steel Wall on Seismic Behavior of Lightweight Steel Structures," Int. Res. J. Eng. Technol., vol. 6, no. 8, pp. 1358–1362, 2019. https://www.researchgate.net/publication/336846191_Study_on_the_Effect_of_the_Concentric_Brace_and_Lightweight_Shear_Steel_Wall_on_Seismic_Behavior_of_Lightweight_Steel_Structures

[27] H. Alimohammadi and M. Abu-Farsakh, "Finite Element Parametric Study on Rutting Performance of Geosynthetic Reinforced Flexible Pavements," Transp. Res. Board, vol. 98th, 2019. https://trid.trb.org/view/1572248

[28] H. Alimohammadi and A. Memon "A Case Study of Mechanically Stabilized Earth (MSE) Retaining Wall Failure in the State of Tennessee; Recommendations for Future Design and Constructions" OSF Preprints, https://doi.org/10.31219/osf.io/uy76r

[29] H. Alimohammadi, V. R. Schaefer, J. Zheng, and D. White, " A full-scale field approach for evaluating the geogrid reinforcement effectiveness in flexible pavement", 22nd International Conference on Soil Mechanics and Geotechnical Engineering, 2022

[30] H. Alimohammadi, J. Tahat, " A State-of-The-Art Evaluation of Driven Pile Behaviors Using Pile Load Testing (PLT)", 101st Transportation Research Board Annual Meeting, TRBAM-22-01453, 2022, https://annualmeeting.mytrb.org/OnlineProgram/Details/17332

[31] H. Alimohammadi, " Effectiveness of Geogrids in Roadway Construction: Determine a Granular Equivalent (G.E.) Factor", Iowa State University, 2021, https://www.proquest.com/docview/2576937127

[32] H. Alimohammadi, " Rutting Behavior of Laboratory, Field, and Finite Element Simulated Hot Mix and Warm Mix Asphalt Overlays", Iowa State University, 2021.

[33] H. Alimohammadi, M. Abu-Farsakh, " Evaluating Geosynthetic Reinforcement Benefits of Flexible Pavement", 8th Annual Graduate Student Research Conference, 2019

[34] H. Alimohammadi and A. Memon "Failure Analysis and Recommendations For Improving Mechanically Stabilized Earth (MSE) Retaining Wall Design and Construction: A Case Study from Tennessee, USA" Transportation Research Board 103rd Annual Meeting, TRBAM-24-00338, 2024

[35] H. Alimohammadi and A. Memon "A Case Study of Failure Analysis of an MSE Retaining Wall in Tennessee: Lessons Learned and Recommendations for Reconstruction" OSF Preprints, 2023, https://doi.org/10.31219/osf.io/nf95e

[36] H. Alimohammadi and A. Memon "Forensic Investigation of Slope Stability Issues and Design Practices: A Case Study in Nashville, Tennessee" OSF Preprints, 2023, https://doi.org/10.31219/osf.io/9yx82

[37] H. Alimohammadi and J. Tahat "Evaluation of Driven Pile Using Pile Load Testing: A Case Study in the State of Ohio" Geo-Congress 2024 conference, ID: 0732_1077_000720, 2024.

[38] H. Alimohammadi and J. Tahat "Evaluating Driven Pile Behaviors Through Case Study Experimental Pile Load Testing (PLT)" 48th Annual Conference on Deep Foundations, 2023.

[39] S. Satvati, H. Alimohammadi, M. Rowshanzamir, and S. M. Hejazi, "Bearing Capacity of Shallow Footings Reinforced with Braid and Geogrid Adjacent to Soil Slope," Int. J. Geosynth. Gr. Eng., vol. 6, no. 41, p. 2020. https://doi.org/10.1007/s40891-020-00226-x

[40] H. Alimohammadi, J. Zheng, A. Buss, V. R. Schaefer, and G. Zheng, "Evaluating the Rutting Performance of Hot Mix Asphalt and Warm Mix Asphalt Mixtures by Using Viscoelastic Finite Element Simulations," Int. Conf. Transp. Dev. 2020, https://doi.org/10.1061/9780784483183.009

[41] H. Alimohammadi, J. Zheng, V. Schaefer, J. Siekmeier, and R. Velasqueze, "Evaluation of Geogrid Reinforcement of Flexible Pavement Performance: A Review of Large-Scale Laboratory Studies," Transp. Geotech., p. 2020. https://doi.org/10.1016/j.trgeo.2020.100471

[42] H. Alimohammadi and B. Izadi Babokani, "Finite element electrodynamics modeling of a layered piezoelectric composite shell

with different materials by using numerical software," ISSS J. Micro Smart Syst., 2020. https://doi.org/10.1007/s41683-020-00052-3

[43] H. Alimohammadi, M. D. Esfahani, "Investigating the Opening Effect of Constant Cross-Section and Various Forms of Seismic Behavior and Performance levels in Concrete Shear Walls" First international conference on civil engineering architecture and stable urban development, 2015.

[44] H. Alimohammadi, and M. Lotfollahi Yaghin "Evaluation of seismic properties of light weight concentric brace on seismic behavior of light weight steel structures" National Conference in applied civil engineering and new advances, 2014.

[45] H. Alimohammadi, and M. Lotfollahi Yaghin "Evaluation of seismic properties of lightweight steel frames coated with lightweight steel shear wall" First international conference on urban development based on new technologies and 4th national conference on urban development, 2014.

[46] Wang, X., Lai, J., He, S. et al. Karst geology and mitigation measures for hazards during metro system construction in Wuhan, China. Nat Hazards 103, 2905–2927 (2020). https://doi.org/10.1007/s11069-020-04108-3

[47] Ki-Il Song, Gye-Chun Cho, Seok-Bue Chang, Identification, remediation, and analysis of karst sinkholes in the longest railroad tunnel in South Korea. NEngineering Geology, Volumes 135–136, 15 May 2012, Pages 92-105, https://doi.org/10.1016/j.enggeo.2012.02.018

[48] Gracia, A.; Torrijo, F.J.; Garzón-Roca, J.; Pérez-Picallo, M.; Alonso-Pandavenes, O. Identification and Mitigation of Subsidence and Collapse Hazards in Karstic Areas: A Case Study in Alcalá de Ebro (Spain). Appl. Sci. 2023, 13, 5687. https://doi.org/10.3390/app13095687

[49] Goldscheider, N. A holistic approach to groundwater protection and ecosystem services in karst terrains. Carbonates Evaporites 34, 1241–1249 (2019). https://doi.org/10.1007/s13146-019-00492-5

J-Researchers

Journal of Civil Engineering Researchers

Journal homepage: www.journals-researchers.com

A review on progressive collapse and its types

Niloufar Allahverdi,[a] Seyed Mohammd Mirhoseini,[a,*] Emadaldin Hezavehi,[b] Vahid Rahimi[a]

[a] *Department of Civil Engineering, Arak Branch, Islamic Azad University, Arak, Iran*

[b] *Department of Textile Engineering, Arak Branch, Islamic Azad University, Arak, Iran*

ABSTRACT

The occurrence of progressive structural damage during seismic events and nearby explosions presents a significant challenge. Progressive failure refers to the situation in which a localized failure in a structural element triggers the failure of neighboring elements, leading to further collapses within the building. There are limited instances of structures experiencing either partial or complete progressive failure. Notably, such occurrences were observed following the partial collapse of the renowned Ronan Point1 residential building in London in 1968 and the destruction of the World Trade Center buildings on September 11, 2001. The engineering community and various standardization committees have focused their attention on this significant issue and have initiated the implementation of enhanced design methods to mitigate progressive failure.

ARTICLE INFO

Received: April 22, 2024
Accepted: May 25, 2024

Keywords:
Progressive collapse
Progressive failure
Structural damage
Column failure
Load redistribution

DOI: 10.61186/JCER.6.2.17
DOR: 20.1001.1.2538516.2024.6.2.2.3

1. Introduction

Progressive failure is the process by which the initial local failure in one structural member spreads to other members, ultimately resulting in the rupture of the entire structure or a significant portion of it. Potential factors contributing to progressive failure may encompass design or manufacturing errors, fire, explosive gases, accidental overloading, impact events, bomb explosions, and other similar hazards. Due to the typically low probability of these risks, they are not typically accounted for in the structural design or are mitigated through indirect measures. During a relatively brief timeframe, the majority of these incidents involve dynamic responses and exhibit characteristics of rapid action. Researchers first focused on progressive deterioration in the 1970s following the partial collapse of a tower in Ronan Point2, England. Additionally, the renewed examination of progressive rupture occurred after the terrorist attacks on the World Trade Center on September 11, 2001[1].

In the majority of studies carried out in the field of progressive failure, the main cause of failure is often disregarded. Consequently, regardless of the specific cause of failure, certain columns are eliminated under various

* Corresponding author. Tel.: +989216275438; e-mail: mo.mirhosseini@iau.ac.ir.

scenarios, and the structure's response is examined in the absence of these columns. This approach overlooks the fact that each primary factor leading to failure can elicit distinct responses from structures. As a result, the present study endeavors to scrutinize the causes of progressive collapse in structures more meticulously, evaluating the progression and designing structures with this issue in mind.

The current building regulations involve designing structures to withstand anticipated loads over their lifespan, rather than accounting for extreme events that could result in widespread damage. Common codes provide general recommendations for mitigating the impact of progressive failure in structures loaded beyond their design limits. Consequently, further study and investigation of this phenomenon's effects on structures appears necessary.

2. Examples of progressive failure

The number of reported examples of progressive failure of all or part of a structure is very small and spread over a period. Progressive damage is a phenomenon that is gradually being incorporated into design standards, and the desire to incorporate it into design increased dramatically after the destruction of the World Trade Center on September 11, 2001[1].

2.1. Alfred P Murrah building

It was designed and built in Oklahoma City between 1970 and 1976 as an administrative building for the United States government. On April 19, 1995, an explosion on the north side hit a truck. The structural system consists of a nine-story reinforced concrete frame. Its particularity is the presence of a Transfer girder5 on the third floor on the north side. Thus the columns on the ground floor are twice as far apart as on the other upper floors. The explosion destroyed all three columns and the entire cantilever was eventually moved, as shown in Fig. 1. The accident was considered an example of progressive failure due to the inability of the transport frame and beam system to handle the increased anchorage and shear forces near the three columns that were removed at the level of the ground [1].

2.2. Ronan point

Ronan Point is a 22-storey residential tower built between 1966 and 1968. The structural system of the walls and roof was prefabricated reinforced concrete. The walls and ceiling are joined with screws and the joints are filled with mortar. In other words, if the lower retaining wall is removed, the roof will not have much capacity to resist bending. Therefore, when the wall panels on the 18th floor were blown away by the explosion, the upper floors were destroyed and falling debris began to damage the lower floors down to the ground floor.

Fig.1. Progressive collapse in Alfred P Murrah

Fig. 2. Progressive collapse in Ronan point

Fig. 3. Kobar towers

As shown in Fig. 2, the failure of the building occurred gradually because the building did not take advantage of the necessary uncertainty and resistance of the roof connections to bending caused by distributed loads. This is an example of progressive failure, where the loss of supporting elements leads to total failure of the structure [3].

2.3. Kobar towers

Kobar Towers was one of several apartment buildings in Al-Kobar near Dhahran, Saudi Arabia. On June 25, 1996, one of the apartment buildings was severely damaged when a heavy bomb exploded on the street in front of the building (Fig. 3). The eight-story Kobar Towers building was built with a T-shaped plan and a system of prefabricated reinforced concrete walls and roof. All vertical and lateral loads were supported by the prefabricated wall system. Although the shear wall was destroyed by the blast, damage was limited to the opposite and exterior openings leading to the building, and only continued within the initial damage zone. Research shows that precast reinforced concrete systems are plastic enough to handle abnormal events. In addition, the connections within the ceiling and walls remain mostly intact and unbroken [2].

2.4. Bunkers Trust bulding

This building is an example of undisturbed architecture remaining from progressive collapse. This 40-story building was built in the early 1970s in New York. Right on the site of the original South World Trade Center. The structural system consists of a steel frame with beams connected to the columns by two-way bent connections. The structure withstood the impact of the debris from the destruction of the South World Trade Center. A portion of the exterior wall of the south tower impacted the 23rd floor of the building, including the roof system damage and perimeter beams between floors 9 and 23, as well as damage to exterior columns between floors 9 and 18, as shown. in Fig. 4. Despite the loss of vertical load-bearing members, no additional damage occurred beyond that caused directly by debris from the destroyed South Tower of the World Trade Center. It is clear that the bending frame is ductile enough and sufficient to withstand the distributed load stresses after the column removal and to absorb the kinetic energy generated by the sudden column removal and debris falling [1].

2.5. Sky line plaza

In 1973, during the concreting of floor 24, there was progressive damage to the entire height of the tower, and progressive horizontal damage to the entire parking lot adjacent to the tower due to debris impact [3] (Fig. 5).

2.6. The world trade center twin towers

The vulnerability of these structures to unusual and unexpected constraints was demonstrated when two aircraft struck the United States' Twin Towers on September 11, 2001, causing damage and total and partial damage to ten adjacent buildings [4] (Fig. 6).

Fig. 4. Bukners Trust

Fig. 5. Sky line plaza

3. Types of progressive collapse

3.1. Pancake destruction

An example of this type of destruction is the prograssive destruction of the World Trade Towers. Airstrikes and fires caused local damage in the impact areas. Therefore, with the loss of load-bearing capacity of a limited number of layers, the upper part of the structure begins to fall and accumulates kinetic energy. The collision with the bottom of the sound results in a large impact force, which is much greater than the bearing capacity of the actual design of the structure. This structural impact causes a loss of bearing capacity of the entire section of the tower within the impact area. The suggested word for this type of destruction was used after the destruction of a smaller building than the Twin Towers. The buildings have shingles stacked on top of each other to form cookie-like objects. This type of destruction mechanism has the following functions:

- Initial failure of vertical bearing elements
- Detachment of structural components and their falling in the movement of a vertical rigid body
- Converting gravitational potential energy into kinetic energy
- Impact of separated and fallen components on the rest of the structure
- Failure of other vertical bearing elements due to compressive forces resulting from impact loading.

Fig. 6. The world trade center twin towers

- And finally, the spread of failure in the vertical direction [5,6]

3.2. Domino destruction

The mechanism of this type of destruction is as follows:

- Initial reversal of an element
- Falling of the mentioned element in the form of angular rigid body movement around the lower edge
- Converting gravitational potential energy into kinetic energy
- Side impact of the upper edge of the overturned element to the side view of the similar element on the side
- The overturning of adjacent elements due to the horizontal pushing force caused by the impacting element
- Expansion of failure in the direction of overturning [1,13].

3.3. Zipper destruction

An example of this type of failure is a cable-stayed bridge failure, which occurs because one cable breaks and the break spreads to other cables, eventually causing the entire bridge to fail. The zipper destruction mechanism has the following characteristics:

- Initial failure of one or more elements
- Redistributing the forces borne by these elements to the rest of the structure
- Dynamic impact loading due to a sudden initial failure and redistribution of forces
- The dynamic response of the remaining structure, to that dynamic impact loading
- Concentration of forces in load-bearing elements that are similar in type and function and are in the vicinity or close to the primary damaged elements.
- Overloading and failure of those elements
- Progression of damage in the transverse direction compared to the main forces of the damaged elements [13,14].

3.4. Instability destruction

Structural failure due to instability during small deflections (defect and lateral loads) can cause significant deformation or damage. These structures are generally designed so that instable failure does not occur. This is achieved by providing additional structural components to brace and stiffen the structure. Under static conditions, this type of failure is called buckling. The unstable damage mechanism has the following characteristics:

- Initial failure of bracing or stiffening elements that have stabilized the load-bearing elements in pressure.
- Instability of compression elements
- Sudden loss of stability of these pressure elements due to a small deviation
- The spread of destruction or damage [13,14].

3.5. Compound destruction

Some progressive collapse does not fit completely into the above categories. The partial destruction of the Alfred P Murrah building shows not only a pancake scenario, but also some characteristics of a domino scenario.

4. Research foundations

After the destruction of the World Trade Center towers on September 11, 2001, special attention was paid to the problem of progressive failure of the more important buildings, special progressive failure loads were incorporated into the design, and it was necessary that buildings were designed to withstand localized failures. Reduce and resist abnormal loads by integrating structural elements to improve energy redistribution and load redistribution (creating alternative load transfer pathways) [1].

For this reason, in this section we present some tests carried out by engineers and their results.

In 2010, Zhang et al. Experiments were conducted on steel sheets to study the effect of the membrane and the bending strength of steel sheets against the progressive collapse phenomenon. [5] The suitability of the sudden column removal method used in the study was verified as an ideal local damage resulting from a real explosion event. To this end, a combination of computational and rigorous experimental modeling has been used to perform large-scale, real-world simulations of steel structures with bending frame systems. Finally, the results obtained from the numerical and experimental models were compared. The previous study paid special attention to the interaction of composite systems used in structural slabs during the removal of columns [6].

By testing the concrete structure in 2012, K. Qian and B. Li were able to control progressive failure by modifying the longitudinal and transverse reinforcement of the column sections. The results showed that the load displacement scheme and crushing mechanism were modified to reduce the effects of progressive failure.

In E. 2013, Song, B., Sezen,H et al discuss numerical and experimental simulations to evaluate the probability of progressive failure of the Ohio Union Building by removing four first-floor columns. Sap2000 software is used to perform numerical simulations in the form of 2D and 3D models. The analyzes used are non-linear static and dynamic analyses. Also in the experimental study, after removing four columns of a floor in three conditions, the straining generated in the elements adjacent to the removed columns were measured using strain gauges installed in these places. Finally, the results of the dynamic and static analysis are compared and the probability of gradual failure is assessed. Analytical results indicate that not taking panels into account during calculations can lead to errors in the evaluation of the probability of progressive failure of the structure [8].

In 2013, Tavakoli, V. and Kiakojouri, F proposed a new method to simulate dynamic column removal in steel structural systems.By using this method, they measured the structural response of a 5-story steel frame under different column removal scenarios. They also took into account the non-linear effects of materials and geometry in their analysis. Their results showed that the probability of progressive failure strongly depends on the location of column removal, and the proposed method has the characteristics of computational simplicity and practicality to simulate the removal of dynamic columns in frame structures [9].

Kandil, K. S. et al. In 2013, conducted a laboratory study on the progressive failure of steel frames. To this end, they designed two new experiments to strengthen sensitive points in multilayer steel structures. The frames studied have different geometries, different boundary conditions, different failure mechanisms, different damping ratios and different connections. The examined model was manufactured to a tenfold scale and has two openings 0.50 m long and 0.40 m high from the ground. The roof is welded to the beams and the beam-to-column connections are considered solid. To validate the model, the results of numerical finite element modeling performed by another researcher were used and showed good agreement with the software and laboratory results [10].

In 2015, F.Hashemi Rezvani studied the effect of span length on progressive failure in steel bending frames. For this purpose, nonlinear static and dynamic analyzes of the designed frame were performed in the highly seismic region using Opensee software. In 6 different cases the first floor columns were removed from the corner and central

columns. The results showed that the vertical displacement of the polarization point increases with the span length. The results showed that by doubling the span length, the vertical displacement increased by a factor of 5, and the vertical displacement of the corner column was 27% greater than that of the central column. Therefore, as the span of the length increases, the amount of DCR (desired supercapacitance ratio) increases and thus the risk of progressive failure increases [11].

In 2017, Bagheripourasil, M et al., in a numerical study, proposed a method to evaluate progressive failure caused by blast loads in steel-framed buildings. For this purpose, a 7-story steel building was exposed to blast loads, with the resulting blast stress on structural elements located in the vicinity of the blast under four different conditions. The results show that if failure initiation factors and blast loads are considered when assessing the potential for progressive damage, the structure will respond differently compared to the common method for assess the occurrence of progressive damage [12].

5. Research method

In this study, the author reviewed previous studies conducted in the field of collapse and tried to review all these studies and reach some important and acceptable conclusions in this field. With the appearance of this phenomenon in recent years, in several structures, the review of previous studies has become particularly important and necessary, and based on the results of these studies, the author tries to conduct a study more in-depth that explores this topic.

6. Findings

In this research, a literature review on the progressive collapse background of and types of it has been investigated.

In engineers' studies of the problem, they found that the types of occurrence of this phenomenon differ from one structure to another. Engineers are paying more attention to the problem after the partial collapse of Ronan Point tower, England, and the collapse of the building after the terrorist attacks on the World Trade Center.

Zhang et al. performed compressive column removal tests on bending steel frame structures, with a particular focus on how composite systems used in structural floors react during column removal.

Meanwhile Tavakoli, V. and Kiakojouri, F showed column removal tests in five different scenarios and found that the progressive collapse strongly depended on the sitution of column removal.

After reviewing the results of previous experiments, M. Bagheripour Asil et al. In 2017, a numerical study proposed a method to evaluate progressive failure caused by blast loads during bending of steel-framed buildings. For this purpose, they studied a 7-story steel building subjected to blast loads and concluded that the structural response of the method used is better if the blast loads are taken into account (i.e. the factors of 'initiation of failure) when assessing the development of rupture potential. progressive failures will vary in assessment.

Unlike previous tests on steel structures, in 2012 K. Qian and B. Li conducted progressive failure control tests on concrete structures and concluded that by changing the load displacement diagram and mechanism, the occurrence of cracks can effectively reduce the progressive collapse.

Since then, Song, B., Sezen,H et al have performed linear and nonlinear static analyzes of the Ohio Union Building, concluding that not accounting for the panels in the calculations could lead to errors in the assessment of possible progressive failure to the structure.

7. Conclusion

In this study, the previous literature and types of progressive collapse are reviewed. Since the number of reports of structures experiencing progressive failure is very small and over variable periods of time, it is important to consider the type of failure in the response of structures to this phenomenon when reviewing the results. For this reason, definitions of different types of progressive collapse are proposed by examining the results of previous research and reported mechanisms of structural collapse. It should help prevent this from happening. By reviewing the research results of engineers on various steel and concrete structures, these results can also be applied to structural design to reduce the progressive failure of structures. The types of loads such as explosion, wind, earthquake, terrorist attack, etc. are valid collapse types and should be considered during design. The importance of this problem is important to engineers trying to reduce the risk of progressive failure.

References

[1] Menchel Kfir, Progressive collapse: comparison of main standards, formulation and validation of new computational procedures, PHD thesis, 2009.

[2] National Institute of Standard and Technology (NIST). Best practices for reducing the potential for progressive collapse in buildings (Draft), 2006.

[3] Lew, H., “Best practices Guidelines For Mitigation of Building For progressive collapse”, 2003.

[4] Lew, H. and Ellingwood, B.R. and Smilowitz, R. and Carino, N., "Best Practices for Reducing the Potential for Progressive Collapse in Buildings", 2006.

[5] F.Z. Zhang and W.J. YI, 2010"Collapse experiment research and analysis of a RC flat plate," Journal of Hunan University (Natural Sciences), vol.37, no.4, pp.1-5, Apr.

[6] Zolghadr Jahromi, H.; Izzuddin, B.A.; Nethercot, D.A.; Donahue, S.; Hadjioannou, M.; Williamson, E.B.; Engelhardt, M.; Stevens, D.; Marchand, K.; Waggoner, M.2012, Robustness Assessment of Building Structures under Explosion. Buildings, , 2, 497-518.

[7] K. Qian and B. Li,2012, "Experimental and analytical assessment on rc interior beam-column subassemblages for progressive collapse," Journal of Performance of Constructed Facilities, vol.26, no.5, pp.576-589, Oct. 2012.

[8] Song, B., Sezen, H. 2013. Experimental and analytical progressive collapse assessment of a steel frame building. Engineering Structures .664–672.

[9] Tavakoli, V. and Kiakojouri, F., 2013, "Numerical Study of Progressive Collapse in Framed Structures: A New Approach for Dynamic Column Removal," International Journal of Engineering, Vol. 26, No. 7, 685-692.

[10] Kandil, K. S., Ellobody, E. A. E. F., & Eldehemy, H. (2013). Experimental Investigation of Progressive Collapse of Steel Frames. World Journal of Engineering and Technology, 1(03), 33.

[11] F.Hashemi Rezvani,A.M.Yousefi,H.R Ronagh,2015. Effect of span length on progressive collapse behaviour of steel moment resisting frames, Structures,2015,81-89

[12] Bagheripourasil, M., Mohammadi, Y., & Gholizad, A. (2017). A proposed procedure for progressive collapse analysis of common steel building structures to blast loading. KSCE Journal of Civil Engineering, 1-9.

[13] Abdollahzadeh,G.R. & Rashidi Alashti,A. & Tavakoli,H.R. ,2012, 3-D Nonlinear Static Progressive Collapse Analysis of Multi-story Steel Braced Buildings , International Journal of Engineering , ije transaction A: Basics Vol. 26, No. 7, (July 2013) 685-692.

[14] Hadi ,N. S. Muhammad & Saeed Alrudaini ,Thaer M ,(2011) ,A New Building Schem to Resist Progressive Collapse , Journal of Architectural Engineering , 1943-5568.0000088.

J-Researchers

Journal of Civil Engineering Researchers

Journal homepage: www.journals-researchers.com

Provisions Comparison of the National Building Regulations (The Eighth Topic) and Iranian Code of Practice for Seismic Resistant Design of Buildings (2800 Standard) for Masonry Buildings with Ring Beam

Hossein Nematian jelodar,[a,*] Negar Moloukaneh,[a] Ayda Khazaei Poul[a]

[a] *Department of civil Engineering, Chalous Branch, Islamic Azad University, Chalous, Iran*

ABSTRACT

Buildings with masonry materials are one of the weakest buildings against earthquakes, and the importance of proper design and correct construction of these buildings is not hidden. Among The buildings with masonry materials, the buildings with Ring beams are the most common of such buildings. Engineers use internal and external regulations and standards to design ring beam masonry buildings. The two main references for the design and construction of masonry buildings with Ring beams are the Code of Practice for Seismic Resistant Design of Buildings (Standard 2800, Fourth Edition) and the Eighth Topic of the National Building Regulations (2020 Edition) under the title of design and construction of buildings with masonry materials. The Provisions for masonry buildings with Ring beams are given in the fifth chapter of the Eighth Topic of the National Building Regulations and the Seventh Chapter of the 2800 Standard. In this research, an attempt has been made to examine the Provisions of masonry buildings with Ring beams of these two references and to identify the discrepancies and differences in the provisions. The investigation of these two references has shown that there were more than 66 cases of differences in Provisions regarding masonry buildings with Ring beams between the Eighth Topic of the National Building Regulations and the Seismic Resistant Design of Buildings. Most of the differences in the criteria were related to the sections of vertical and horizontal Ring beams, structural walls, and Non-structural walls with 34 cases and 51.5% compared to the total difference. Also, the type of soil is classified in the Eighth Topic of The National Construction Regulations with 3 types of soil and the 2800 Standard of Conduct is classified with 4 types of soil.

ARTICLE INFO

Received: June 11, 2024
Accepted: June 24, 2024

Keywords:
Masonry Buildings
structural walls
Non-structural walls
Ring Beams
Seismic Design

DOI: 10.61186/JCER.6.2.24
DOR: 20.1001.1.2538516.2024.6.2.3.4

1. Introduction

Masonry materials are one of the oldest man – made materials used in construction and be one of the most unknown [1]. Being unknown is confirmed by the fact that when the revisions of the references and specialized Codes in the field of materials and regulations of masonry buildings are examined, we will see many changes in it. In

* Corresponding author. Tel.: +989111120481; e-mail: hnematiyan@iauc.ac.ir .

Iran, there are two important references for the design and construction of masonry buildings, including The National Building Regulations (The Eighth Topic), under the title of design and construction of masonry buildings, 2019 Edition [2], and Iranian Code of Practice for Seismic Resistant Design of Buildings (2800 Standard, Fourth Edition) for Masonry Buildings with Ring Beam [3]. The Provisions for masonry buildings with ring beam are given in the fifth chapter of the eighth topic of the National Building Regulations and in the seventh chapter of Iran's 2800 Standard. The study and review of the previous editions of these two references have shown that there were many differences in the standards of masonry buildings [4]. Also, considering that in the 2018 edition of the 8th topic of the National Building Regulations, the Provisions and Regulations of the United States Uniform Code [5, 6] have been used, but there are still many contradictions and differences with the Building Design Code in different parts of the building, Against the earthquake, the 2800 Standard has been observed. Other references, such as books on seismic design of brick buildings [7], masonry buildings and a review of industrial buildings [8], and the design of earthquake-resistant structures [9], provide the Provisions and details of the design and construction of reinforced and unreinforced masonry building with examples and drawing shapes have been provided for better understanding of the reader.

In this research, it has been tried to determine the standards of masonry buildings with Ring beam in different sections, including the classification of masonry buildings, architectural requirements, structural requirements in the foundations, Seats, Structural walls and Non-structural walls, openings, lintel, ties, and roofs in the eighth topic of the National Building Regulations (edition of 2018) and the code of design of buildings against earthquakes, Standard 2800, edition 4, have been examined and compared, and the differences in the standards in these two references have been identified.

2. Provisions for masonry buildings with ring beam

2.1. Classification of masonry buildings

In the eighth topic of the National Building Regulations, masonry buildings are divided into two categories, including reinforced masonry building and masonry buildings with ring beams, and in Iran's Standard 2800, masonry buildings are divided into two categories under the headings of masonry buildings with horizontal and vertical Ring beams, and masonry buildings with Cohesive bars. In some other authorities, masonry buildings have been classified into four categories including non-reinforced, semi-reinforced, reinforced and framed [7].

2.2. Architectural requirements

Differences in standards in the section of architectural requirements of masonry buildings with ring beams between two review authorities and its summary are shown in table 1. Regarding the difference in the level of the roof on the floor or the difference in level, it is stated in the eighth topic of the national building regulations that if the difference in level is less than 600 mm, a separate horizontal Ring beam should be implemented in the boundary wall between the two parts that have a difference in level, or the two parts by means of Seismic seams separate from each other and in case it is more than 600 mm, it is necessary to separate the two parts of the building by means of a seismic joint. In the Standard 2800, only in the case that the difference in the level of the roof is more than 600 mm, they should be separated with additional Ring beams or construction joints. Also, the anchor of the cantilever in horizontal ring beams for the construction of a parapet on the projecting part of the building according to the Standard 2800 is shown in Figure 1.

2.3. Structural requirements

Structural requirements include excavation and foundation, base course, structural and non-structural walls, openings, lintel, parapet, ties, roofs and ridge. The difference between of provisions of the structural requirements section between the eighth topic of the National Building Regulations and the Standard 2800 has been investigated. The differences in provisions in the excavation and foundation section are shown in table 2, and the details of anchor of vertical ring beam in the masonry foundation base on Iran's Standard 2800 are shown in Figure 2.

In both references of the 8th topic of the National Building Regulations and the 2800 Standard of Iran, the base course width in masonry building with ring beam depends on the width of the wall, the height of the base course, the number of story and type of soil of the construction site. Investigations have shown that there are 3 types of soil classification in the 8th topic of the National Building Regulations, but in the 2800 Standard of Iran, 4 types of soil are classified. In the 2800 standard, soil type 4 is soil whose permissible strength is about 1 kg/cm2 and the width of the base course in this type of soil for 1, 2 and 3 story buildings is 500, 1000 and 1500 mm respectively, which is in the eighth topic of the National Building Regulation has not mentioned it. Sine both the eighth topic of the National Building Regulations and the Standard 2800 of Iran state the use of concrete foundations instead of masonry foundations, the differences in the provisions of this section in Table 3.

Table 1.
difference of Provisions in the architectural requirements section

Row	Title	Topic 8	2800 Standard
1	The maximum length of the masonry building ring beam	3 time the width of building with 25 m	3 time the width of the building
2	Basement height	Maximum 2.5 m	____
3	Projection of building (the upper story is ahead of the lower story)	____	Maximum 1 m
4	The use of steel ring beam in the projection	____	It is allowed
5	Construction of parapet on the front of projection	A maximum height of 500 mm is allowed	It is unobstructed in the case of anchor of cantilever in horizontal ring beams according to Figure 1

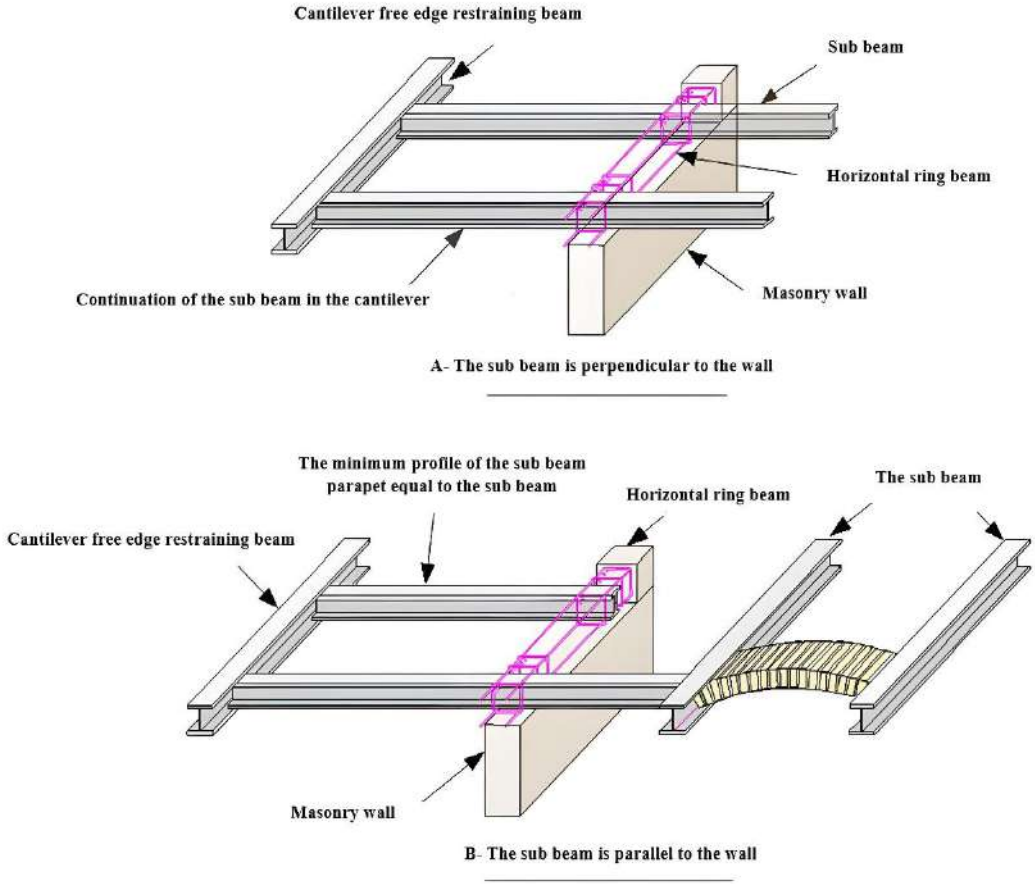

Figure 1: cantilever anchor in the horizontal ring beams of the building based on Iran's 2800 Standard

One of the most important parts of a masonry building with ring beams is its structural walls. Investigations have shown that in the section of structural wall, there are differences in provisions between these two references and there are 11 cases differences between the eighth topic and Iran's 2800 Standard. One of the differences is the maximum length of a structural wall between two vertical ring beams, which is equal to 5 m in the eighth topic of the National Building Regulations, but in Iran's 2800 Standard, the length of a structural wall is equal to the minimum value of 5 m and 30 times the thickness of the wall.

Another case is the thickness of structural wall in the stories and basement, which is stated in the eighth topic of the National Building Regulations for the first and second stories of the basement to be 350 mm, 320 mm, 200 mm respectively.

The next item, based on the eighth topic of the National Building Regulations, to determine the minimum amount of the relative wall, structural walls with conditions such as: the length of the wall should not be less than one-third of its height, the length of the wall should be more than 1 m, and the columns and piers on the side and between the

Table 2.
difference of Provisions in the excavation and foundations

Row	Title	Topic 8	2800 Standard
1	The depth of excavation	At least 800 mm	_____
2	The depth of foundation	at least 500 mm	It depends on the width of the base course minus the width of the horizontal ring beam
3	The width of foundation	It should not be less than 1.5 times the width of the base course	_____
4	Construction of the foundation in the form of dry	Not allowed	_____
5	Type of foundation	Paste with at least 350 lime kg/m^3,rubble stone immersed in concrete with 25 kg/m^3 cement, broken range work with sand-cement or sand-cement mortar, concrete with a cement 250 kg/m^3	Brick foundation, stone foundation, concrete foundation with minimum strength equal to 20 MPa

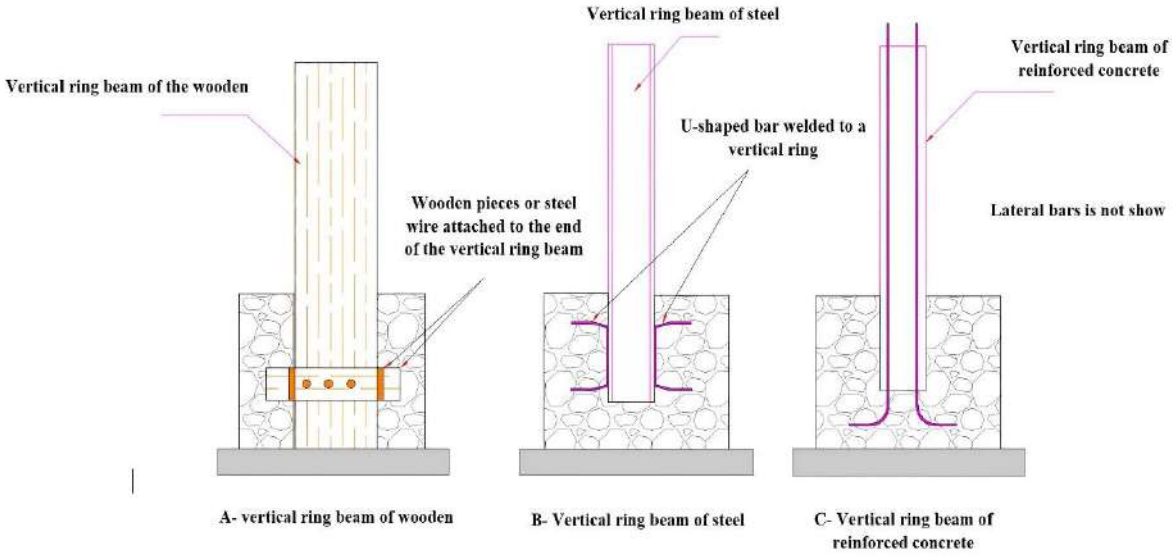

Figure 2: The details of vertical ring beam anchor in the foundation of masonry based on 2800 Standard

openings should be proportional their length to effective height should be more than one third, that these conditions are not included in Iran's 2800 Standard. Another point of difference, according to the eighth topic of the National Building Regulations, the structural walls on each story and in each direction must be spread evenly and symmetrically on the surface in such a way that the distance between the center of the story surface and the center of the surface of the relative walls of that story (eccentricity) in each extension, not more than 5% of the dimension of the building in that direction and if this distance is greater than the above value, its effect on the surface of the wall should be taken into account, and this case is not observed in Iran's 2800 Standard. The further investigation of these two references in this section has shown that there were other provisions differences in structural walls other than those mentioned, and these provisions differences are listed in Table 4.

Another one of the differences between the eighth topic of the National Building Regulations and Iran's 2800 Standard is the basement wall provisions. In the eighth topic of the National Building Regulations, the height of the basement wall is 2.5 m and the minimum thickness of the wall is 320 mm, and all lintels must be made of in situ concrete or masonry, and steel lintels should be avoided in the basement. While in the 2800 Standard of Iran, it is sufficient to mention only the minimum thickness of the basement wall equal to 350 mm and it is silent other cases.

Another difference between the 8th topic of the National Building Regulations and the 2800 Standard of Iran is the openings. The maximum dimensions of the opening are 2 m in the 8th topic of the National Building Regulations, and this length is 2.5 m in Iran's 2800 Standard. The cases of differences in standards in the implementation of non-structural walls and lintel are listed in Table 5.

Another case of difference between the 8th topic of the National Building Regulations and the 2800 Standard of Iran is the provisions for parapets. According to the requirements of the eighth topic of the National Building Regulations, the height of the parapet should not be more than 500 mm and its thickness should not be less than 200 mm. According to the 2800 Standard of Iran, if the

thickness of the wall is equal to 100 mm or 200 mm, the height of the parapet should not exceed 500 mm or 700 mm, respectively. The details of parapet anchor with a height of more than 700 mm according to Iran's 2800 Standard are shown in Figure 3. In the eighth topic of the National Building Regulations, no executive details have been provided like Iran's 2800 Standard.

One of the important parts of masonry buildings with ring beam is ties. The ties play an important role in the cohesion and integration of masonry building with ring beam. The ties include horizontal and vertical ring beams, and differences such as ribbed bar type, ribbed bar distance, use of steel and wooden section instead of concrete ring beams and double corner ring beams, etc. have been observed in the provisions of ties of two references. Differences in provisions for horizontal ring beam are shown in Table 6 and vertical ring beam in Table 7.

Another difference in this section is the width of the chimney in horizontal concrete ring beams, which the maximum diameter or width of the chimney in the eighth topic of the National Building Regulations is equal to one sixth and in The 2800 Standard of Iran, this size is equal to one half of the width of the horizontal concrete ring beam according to Figure 4.

Table 3.

difference of Provisions in the concrete foundation section

Row	Title	Topic 8	2800 Standard
1	The Width of concrete foundation	The Width of the foundation should not be more than 1.5 times the width of the wall or 600 mm.	The width of the foundation should match the width of the base course.
2	Concrete foundation depth	At least 500 mm	____
3	Maximum distance of bending	300 mm	300mm, but in another place, provided the number of bending ribbed bars, which is not consistent.
4	Longitudinal ribbed bars	Diameter 12 with a maximum distance of 300 mm	____
5	Lateral ribbed bar in concrete foundations whose width is more than 800 mm	____	It should be construction in two loops
6	Leveling on concrete foundation in cold regions with glaciers	At least 400 mm below the ground level	____
7	Classification of the soil of the construction site	3 type of soil	4 type of soil

Table 4.

difference of Provisions in the structural wall construction section

Row	Title	Topic 8	2800 Standard
1	Soaking of material units	It is necessary	_____
2	The distance between the vertical joint in the wall	At least a quarter of the length of the material unit	Do not put the vertical joint in the same direction
3	The thickness of the horizontal joints	It should not be less than 10 mm and more than 15 mm	_____
4	The thickness of the horizontal joints in case of bed joint reinforcement	Maximum to 20 mm	_____
5	The number of horizontal ribbed bars in the middle third of the wall	It is necessary for walls that are longer than 2.5 m	It is necessary for walls with shoulder length between 3 and 5 m
6	The number of horizontal ribbed bars in the middle third of the wall	In three levels of the middle of the wall, two ribbed bars with a diameter of at least 8 mm	In three levels of the middle of the wall, one ribbed bars with a diameter of at least 10 mm
7	Curing of wall	At least for 3 days with water	_____

Table 5.

difference of Provisions in the non-structural wall and lintel construction sections

Row	Title	Topic 8	2800 Standard
1	The free length of the non-structural wall	40 times the width of the wall and a maximum of 5 m	40 times the thickness of the wall and a maximum of 6 m
2	Anchor the edge of the non-structural wall	The vertical edge of the wall must be anchored with an vertical element	The vertical edge of the wall must be anchored with minimum size 6 steel channel section
3	Instead of using toothing, you can:	Two horizontal bars with a diameter of at least 8 mm and a distance of 500 mm are used in the height of the wall	It used an size 8 or 10 mm bar with a distance of 600 mm in the height of the wall
4	The length of the support of the lintel	At least 350 mm or one tenth of the length of the span, whichever is more	At least 200 mm

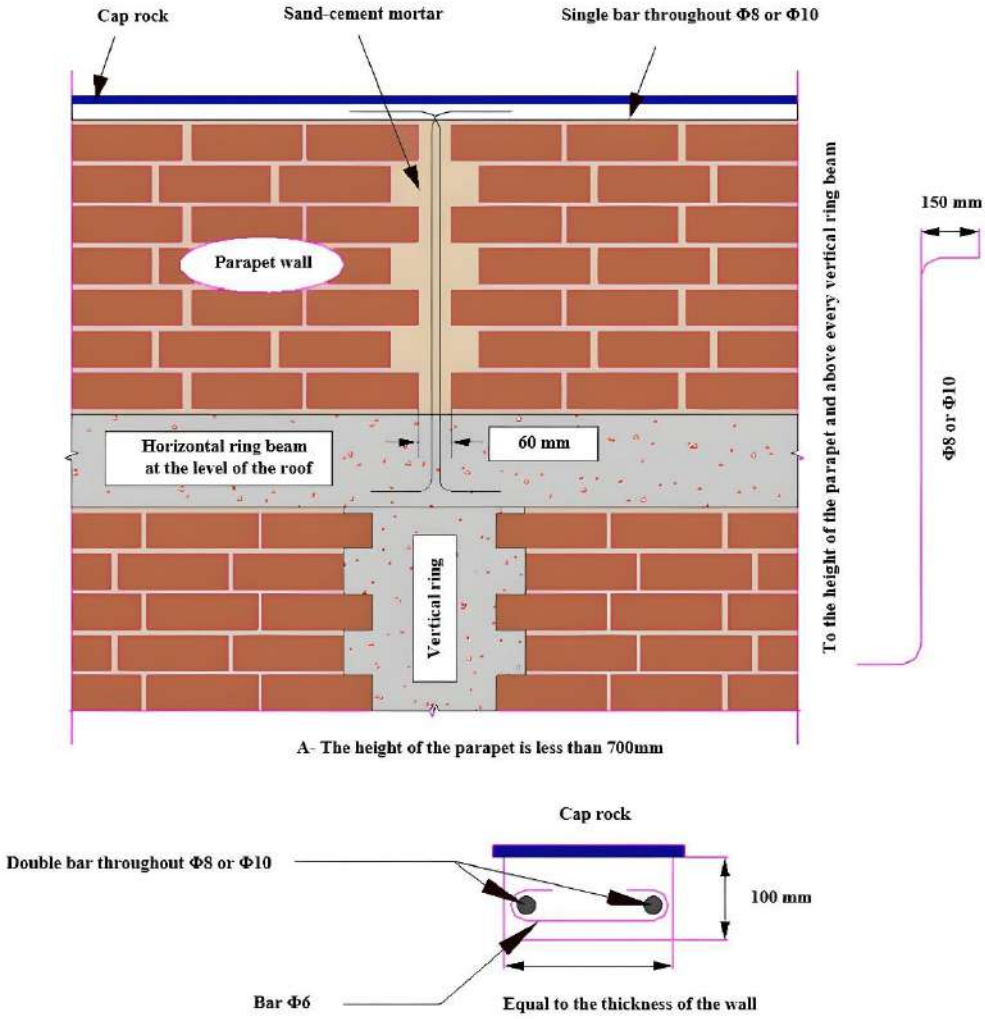

Figure 3: The details of parapet anchor with a height of more than 700 mm according to the 2800 Standard

Table 6.

Difference of Provisions in the horizontal ring beam sections

Row	Title	Topic 8	2800 Standard
1	The use of horizontal steel ring beam in the level on the wall	___	Size 10 Steel I-beam or equivalent steel profiles
2	Size of longitudinal bars in horizontal ring beam	At least size 12	At least size 10
3	The use of simple bars in horizontal concrete	___	It is allowed only in areas with medium and low relative risk
4	Minimum diameter of lateral bars in horizontal concrete ring beams	Size 8 bar with a maximum distance of 200 mm	Size 6 bar, its distance is equal to the smallest values of the ring beam height and 250 mm
5	The maximum distance of stirrup in the critical area	100 mm	150 mm
6	Minimum concrete cover in horizontal concrete ring beam	50 mm for the bottom of the wall and 30 mm for the top of the wall	50 mm for the bottom of the wall and 25 mm for the top of the wall
7	Maximum diameter and width of chimney in horizontal concrete ring beams	At most one sixth of the width of the ring beam	At most one half of the width of the horizontal ring beam (Figure 4)

Another difference between these two references in this section is the use of horizontal and vertical ribbed bars in the equivalent bar system, instead of imp vertical ring beams without providing design relationships, which is

given in the eighth topic of the National Building Regulations under the title of reinforced masonry building with providing of the design relationships. The details of vertical and horizontal ribbed bars in the equivalent bar system.

The cases of differences in regulations between topics 8 of the National Building Regulations and Iran's 2800 Standard are the construction of vertical steel ring beam. According to the provisions of Iran's 2800 Standard, steel vertical ring beams can be used instead of concrete vertical ring beams in building materials, and in this case, no provisions have been observed in the eighth topic of the National Building Regulations. The details of the construction of the vertical steel ring beam according to Iran's 2800 Standard are shown in Figure 6.

Differences and inconsistencies such as the integration of concrete beam-block roof, trusses and wooden roof, slanted roofs, curved roof, flat wooden roof, ridge, dome roof, false ceiling and boundary walls in the two references of the eighth topic of the National Building Regulations and 2800 Standard of Iran view has been.

3. Conclusion

In this research, the provisions of topics 8 of the National Building Regulations, 2018 edition, with the Iranian Code of Practice for Seismic Resistant Design of Buildings (2800 Standard, fourth edition), for masonry buildings with ring beam have been examined and compared. Differences in standards have been observed in building classification sections with masonry building, architectural requirements, structural requirements including excavation and foundation, concrete foundation, base course, structural and non-structural walls, openings, lintel, ties and roofs:

1-The results of the research have shown that there were more than 66 cases of provisions discrepancies in different sections.

2-The most difference of provisions between the standards of masonry building was respectively in the wrapping sections with 17 cases, structural and non-structural walls with 17 cases, excavation and concrete foundation with 12 cases.

3-The results of the investigation have shown that The 2800 Standard, contrary to the eighth topic of the National Building Regulations, has considered the use of simple bars in some areas of Iran as unobstructed.

4-In the design of foundations of masonry building with ring beam, investigations have shown that the classification of the soil type in the eighth topic of the National Building Regulations was based on 3 type of soil and in The 2800 Standard of Iran based on 4 type of soil.

Table 7.

Difference of Provisions in the vertical ring beam sections

Row	Title	Topic 8	2800 Standard
1	Using a vertical wooden ring beam	_____	It is unobstructed for one-story building located in areas with medium and low relative risk
2	The diameter of the longitudinal bars in a vertical concrete ring beam	At least size 12	At least size 10
3	Using a double vertical ring beam	In the outer corners of a two-story building or with a basement	_____
4	At least diameter of the lateral bars in the vertical concrete ring beam and its maximum distance	Size 8 bar with a maximum distance of 200 mm	Size 6 bar and its distance is equal to the minimum width of the ring beam and 250 mm
5	The distance of stirrup in the critical area	Maximum 100 mm	Maximum 150 mm
6	Concrete coating in vertical concrete ring beams	At least 30 mm	At least 25 mm
7	At least length of the vertical anchor of the longitudinal bars of the vertical concrete ring beam in the foundation	at least 250 mm	At least 400 mm
8	The use of equivalent vertical ring beams	_____	It can be made of Steel and wooden vertical ring beam
9	The use of vertical and horizontal bars in the equivalent bar system (instead of the vertical ring beam)	Reinforced masonry building	Construction details are given in Figure 5
10	Construction of reinforced concrete or steel ring beams around the openings	It is necessary for the openings whose dimensions are more than 2 m	_____

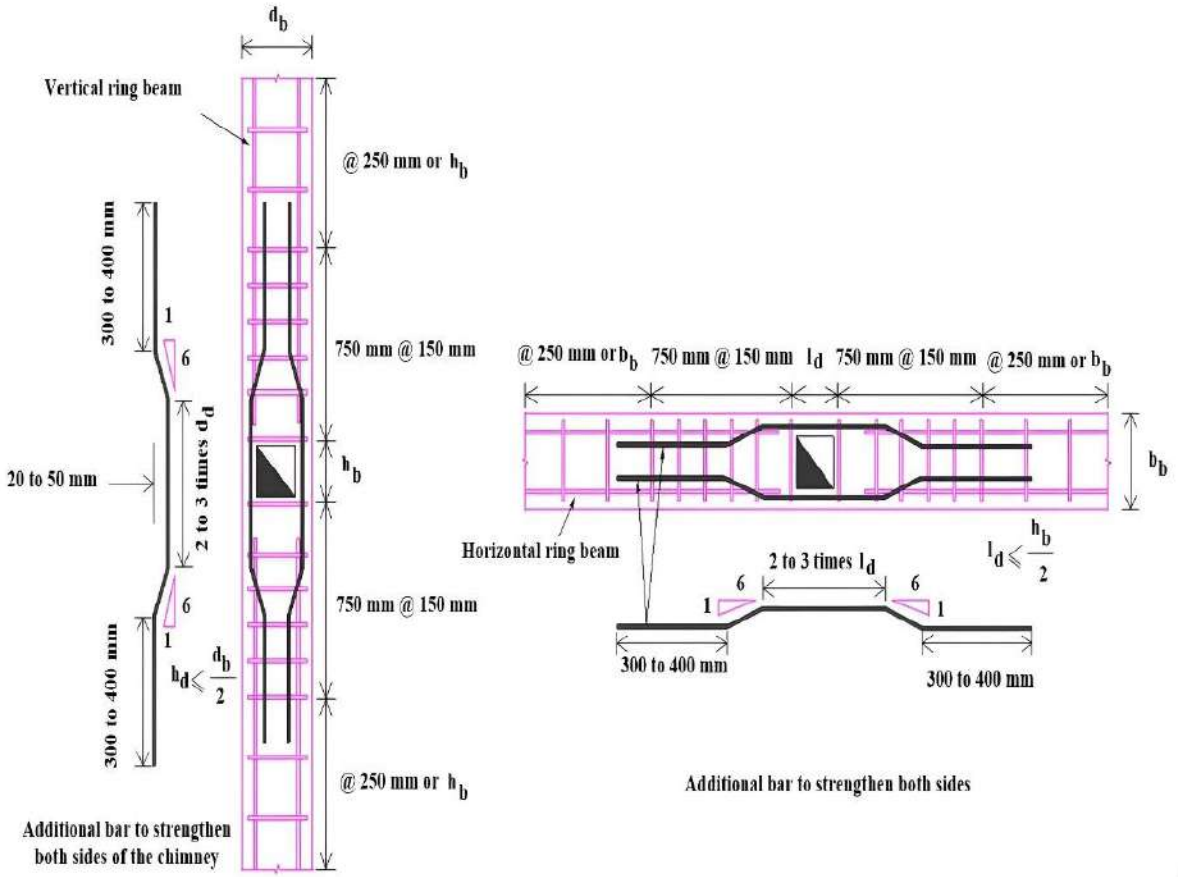

Figure 4: The maximum allowed width of chimney passing through horizontal and vertical ring beams along with reinforcement around them according to the 2800 Standard

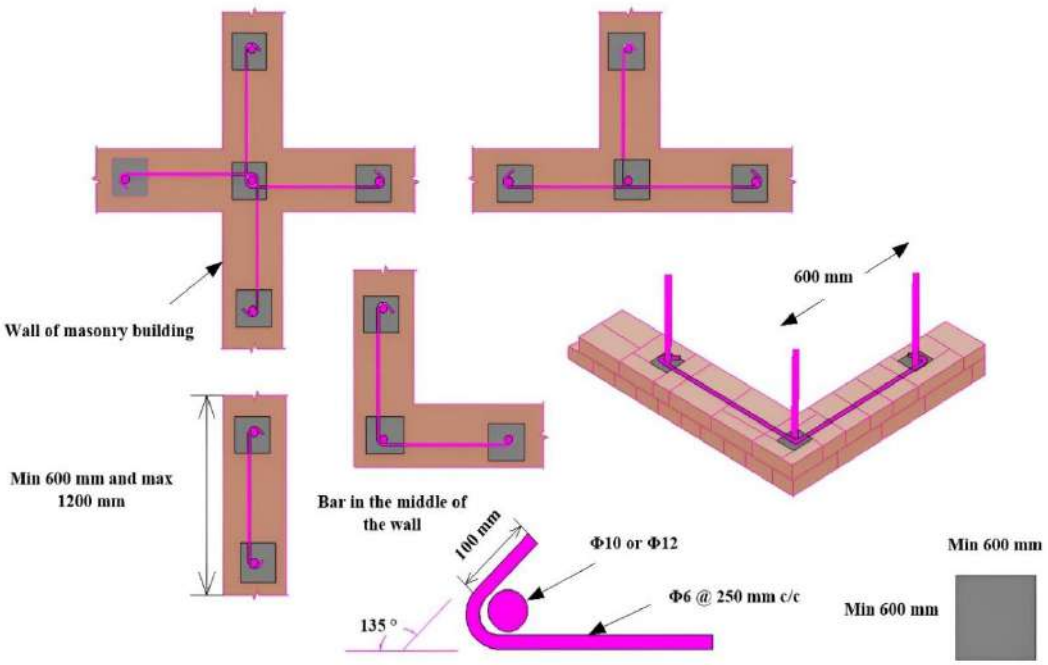

Figure 5: construction of vertical and horizontal bars in the equivalent bar system instead of vertical ring Beam according to the 2800 Standard

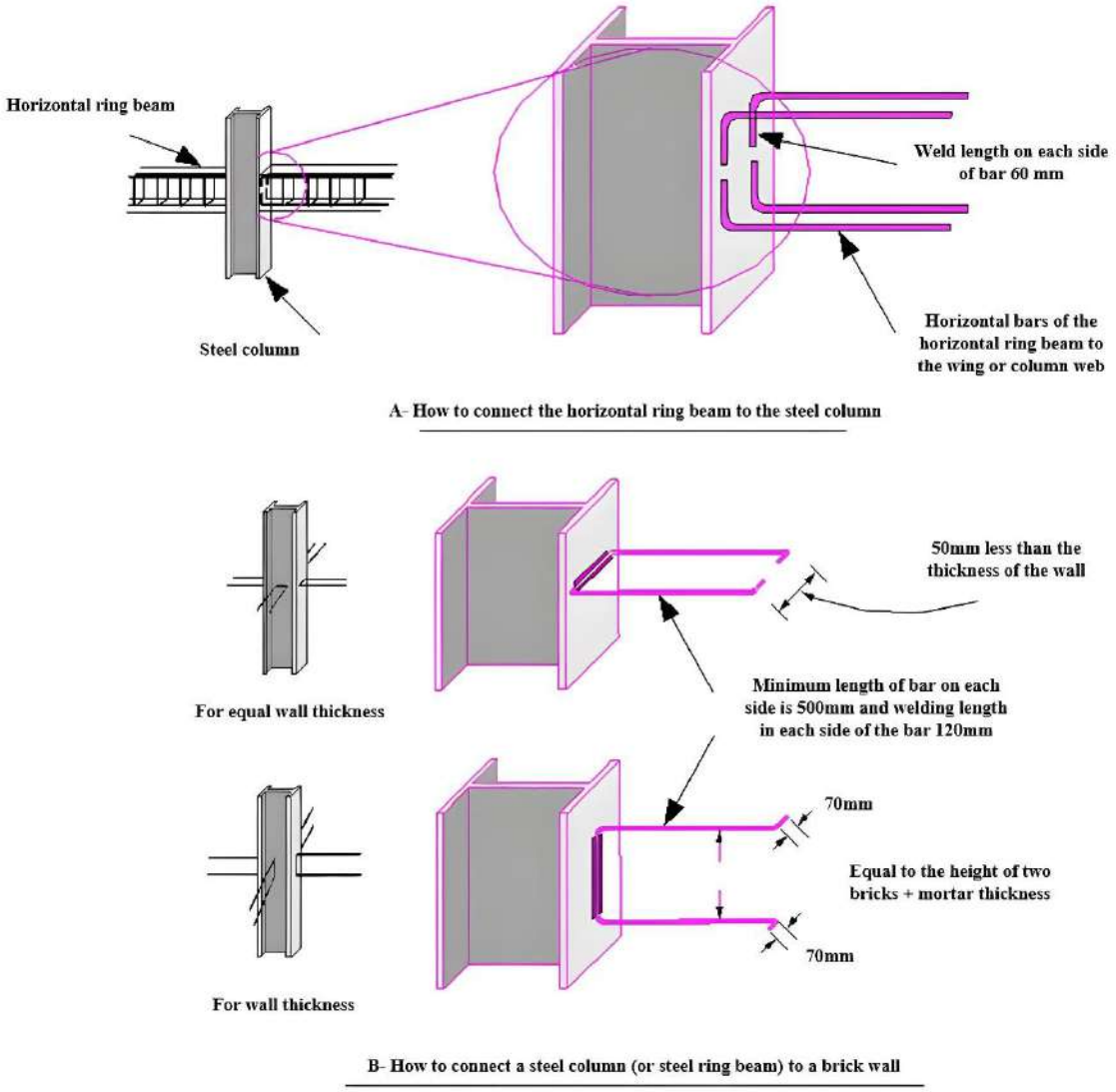

Figure 6: The details of connecting the horizontal ring beam and the brick wall to the steel column according to the 2800 Standard

References

[1] Schneider, R R. Dickey, W L. Reinforced Masonry Design. Second Edition. Tehran: Elm and Adab, (2009): Page (659).

[2] Road, Housing and Urban Development Research Center.The National Building Regulations: Design and Construction of Masonry Buildings, The Eighth Topic. Third Edition. Tehran: BHRC, (2020): Page (158).

[3] Road, Housing and Urban Development Research Center. Iranian Code of Practice for Seismic Resistant Design of Buildings: Standard No. 2800. 4th Edition. Tehran: BHRC, (2015): Page (232).

[4] Nematian, H J. Alborzy, H E. Comparison of the Third Chapter of Iranian Code of Practice for Seismic Resistant Design of Buildings (Standard No. 2800) and The National Building Regulations: Design and Construction of Masonry Buildings (The Eighth Topic). In: 14th Civil Students Conference Nationwde. Semnan: Semnan University, (2009): Page (8).

[5] Uniform Building Code. Structural Engineering Design Provisions. First Edition. California, (1991): Page (503).

[6] Tavakoli, M. Masonry Buildings. First Edition, Tehran: BHRC, (1995): Page (95).

[7] Moghaddam, H. Seismic Design of Brick Buildings. Sixth Edition, Tehran: SPI, (2015): Page (368).

[8] Moradi, M. jozani, A. Masonry Buildings and An Overview of Industrial Buildings. 15th Edition, Tehran: Serieomran, (2022): Page (380).

[9] Naeim, F. The Seismic Design Handbook. Fourth Edition, Tehran: Academic Publishing Center, (2018): Page (512).

J-Researchers

Journal of Civil Engineering Researchers

Journal homepage: www.journals-researchers.com

Structural Damage Identification Using a Multi-stage Gravitational Search Algorithm

Saeed Fallahian,[a] Seyed Mohammad Seyedpoor,[a,*] Eshagh Norouzi,[a] Sara Ghasemi[a]

[a] *Department of Civil Engineering, Shomal University, Amol, Iran*

ABSTRACT

A multi-stage gravitational search algorithm (MSGSA) is proposed here to solve the optimization-based damage detection of structural systems. Natural frequency changes of a structure are considered as a criterion for damage occurrence. Finite element method and structural dynamic principles are also employed to evaluate the required natural frequencies. The structural damage detection problem is first transformed into a standard optimization problem dealing with continuous variables, and then the MSGSA is utilized to solve the optimization problem for finding the site and severity of damage. In order to assess the performance of the proposed method for damage identification, an example with experimental data and two numerical examples with considering measurement noise are considered. All the results demonstrate the effectiveness of the proposed method for accurately determining the site and extent of multiple structural damage. Also, the performance of the MSGSA for damage detection compared to the standard gravitational search algorithm (GSA) is confirmed by examples.

ARTICLE INFO

Received: June 02, 2024
Accepted: June 25, 2024

Keywords:
Damage detection
Natural frequencies
Finite element analysis
Optimization method
Multi-stage gravitational search algorithm

DOI: 10.61186/JCER.6.2.33
DOR: 20.1001.1.2538516.2024.6.2.4.5

1. Introduction

Many structural systems may experience some local damage during their functional age. As the local damage is accurately detected and then rehabilitated within an appropriate time span, it will lead to increasing the total age of the system. Moreover, neglecting the local damage may cause to reduce the functional age of structural systems or even an overall failure of the structures. As a result, health monitoring and structural damage identification is a vital topic that has drawn wide attention from various engineering fields such as civil, mechanical, and aerospace engineering. The theoretical basis of damage detection lies in the fact that responses of a structure vary because of its inherent damage. This gives rise to the possibility of identifying the damage from the variation of structural responses before and after damage occurs. In particular, the damage detection formulates the relationship between the damage and modal parameter changes of a structure. A common practice is to obtain the fingerprint or baseline of modal parameters when a structure is in perfect health. Later, when the changes of these parameters occur, it is

* Corresponding author. Tel.: +981144203726; e-mail: s.m.seyedpour@shomal.ac.ir.

possible to investigate the structural damage which brings about the changes. During the last decades, many approaches have been introduced to determine the location and extent of eventual damage in the structural systems. One type of the methods employs the optimization algorithms for solving the damage detection problem.

Many successful applications of damage detection using an optimization algorithm have been reported in the literature. Mares and Surace used the genetic algorithm (GA) to maximize an objective function in order to identify macroscopic structural damage in elastic structures from measured natural frequencies and mode shapes [1]. A procedure for detecting the damage in beam-type structure based on a micro genetic algorithm using incomplete and noisy modal test data was proposed by Au et al. [2]. An application of GA for determining the damage site and extent of flexible bridge maximizing a correlation coefficient, named the multiple damage location assurance criterion (MDLAC) has been proposed by Koh and Dyke [3]. A fault diagnosis method in beam-like structures based on binary and continuous genetic algorithms and a model of the damaged structure has been proposed by Vakil-Baghmisheh et al. [4]. A two-stage method of determining the location and extent of multiple-beam-type structure damage by using the information fusion technique and micro-search genetic algorithm (MSGA) has been presented by Guo and Li [5]. Structural damage detection using an efficient correlation-based index (ECBI) and a modified genetic algorithm (MGA) has been introduced by Nobahari and Seyedpoor [6]. A self-adaptive multi-chromosome genetic algorithm (SAMGA) for localizing and quantifying the damage of truss structures was presented by Villalba and Laier [7]. An application of the bee algorithm (BA) to the problem of crack detection in beams was introduced by Moradi et al. [8]. A hybrid particle swarm optimization–simplex algorithm (PSOS) for structural damage identification using frequency domain data has been proposed by Begambre and Laier [9]. In order to find the location and extent of structural damage, a multi-stage particle swarm optimization (MSPSO) assuming a discrete nature for damage variables has been introduced by Seyedpoor [10]. Nouri Shirazi et al. used the modified particle swarm optimization (MPSO) to minimize an objective function (ECBI) in order to identify structural damage from changes of natural frequencies [11]. A mixed particle swarm-ray optimization together with harmony search (HRPSO) for localizing and quantifying the structural damage was presented by Kaveh et al. [12]. The differential evolution algorithm (DEA) for structural damage identification using natural frequencies has been proposed by Seyedpoor et al. [13]. The ant colony optimization (ACO) for structural damage identification has been proposed by Braunet al. [14]. An improved hybrid Pincus-Nelder-Mead optimization algorithm (IP-NMA) for structural damage identification using natural frequencies has been proposed by Nhamage et al. [15]. However, the performance of gravitational search algorithm (GSA) and its other versions for solving the damage detection problem have not been assessed seriously.

In this study, a multi-stage gravitational search algorithm (MSGSA) is introduced to identify multiple structural damage. For this, the problem of structural damage detection is first transformed into the standard form of an optimization problem dealing with real damage variables. The MSGSA is utilized as an optimization solver for finding the site and severity of damaged elements. Three illustrative test examples are considered to show the performance of the proposed method. The results show that the MSGSA can provide a robust tool for determining the site and extent of multiple damage precisely and quickly.

2. Optimization Based Damage Detection Method

Structural damage detection using non-destructive methods has received significant attention during the last years. The fundamental law is that damage will change the mass, stiffness, and damping properties of a structure. Such a change would lead to changes in the response data of the structure. This rule enables us to identify the damage by comparing the response data of the structure before and after damage. The damage detection problem can be interpreted to find a set of damage variables minimizing or maximizing a correlation index between response data of a structure before and after damage [1, 3-8, 10, 11, 13, 14]. Therefore, the problem can be transformed into an optimization problem as:

$$\begin{aligned} &\textit{Find: } X^T = \{x_1, x_2, \ldots, x_n\} \\ &\textit{Minimize: } Obj\ (X) \\ &\textit{Subject to: } X^l \le X \le X^u \end{aligned} \tag{1}$$

where $X^T = \{x_1, x_2, \ldots, x_n\}$ is a damage variable vector containing the location and size of n unknown damages; X^l and X^u are the lower and upper bounds of the damage vector and *Obj (X)* is an objective function that need to be minimized.

In many researches, various correlation indices were chosen as the objective function. In this study, an efficient correlation-based index (*ECBI*) introduced in [6] is used as the objective function for the optimization given by:

$$ECBI\ (X) = -\frac{1}{2}\left[\frac{|\Delta F^T .\ \delta F(X)|^2}{(\Delta F^T .\ \Delta F)(\delta F^T(X).\delta F(X))} + \frac{1}{n_f}\sum_{i=1}^{n_f}\frac{\min(f_i(X), f_{di})}{\max(f_i(X), f_{di})}\right] \tag{2}$$

In the objective function, ΔF is the change of frequency vector of damaged structure with respect to the frequency vector of healthy structure. The ΔF can be defined as:

$$\Delta F = \left\{\Delta f_i = \frac{f_{hi} - f_{di}}{f_{hi}}\right\}, i = 1,2,\dots,n_f \quad (3)$$

where f_{hi} and f_{di} are the i_{th} component of healthy frequency vector F_h and damaged frequency vector F_d of the structure, respectively. The number of total frequencies considered for damage detection is denoted by n_f.

Also, $\delta F(X)$ is the change of frequency vector of an analytical model with respect to the frequency vector of healthy structure. The $\delta F(X)$ can be defined as:

$$\delta F(X) = \left\{\Delta f_i(X) = \frac{f_{hi} - f_i(X)}{f_{hi}}\right\},\ i = 1,2,\dots,n_f \quad (4)$$

where $f_i(X)$ is the ith component of an analytical frequency vector $F(X)$ of the structure.

The $ECBI$ varies from a minimum value −1 to a maximum value 0. It will be minimal when the vector of analytical frequencies becomes identical to the frequency vector of the damaged structure, that is, $F(X) = Fd$.

In this study, the damage variables for truss and frame structures are defined via a relative reduction of elasticity modulus of an element as:

$$x_i = \frac{E - E_i}{E}, \quad i = 1,2,\dots,n \quad (5)$$

where E is the original modulus of elasticity and E_i is the final modulus of elasticity of ith element.

By solving the Eq. (1) using an optimization algorithm the damage variables can be determined. A non-zero value for the variable x_i represents that the ith element of the structure is damaged while a zero value denotes that the element is healthy.

3. The Proposed Optimization Algorithm

The selection of an efficient algorithm for solving the damage optimization problem is a critical issue, because the damage identification problem has many local solutions. In this study, a multi-stage gravitational search algorithm (MSGSA) is proposed to properly solve the damage detection problem. In the remaining part of this section, the original gravitational search algorithm (GSA) is briefly described at first and then the proposed MSGSA is discussed.

3.1. Gravitational Search Algorithm (GSA)

Gravitational search algorithm was introduced by Rashedi et al. [17] in 2009 to solve optimization problems. The population-based heuristic algorithm is based on the law of gravity and mass interactions. The algorithm is comprised of collection of searcher agents that interact with each other through the gravity force. The agents are considered as objects and their performance is measured by their masses. The gravity force causes a global movement where all objects move towards other objects with heavier masses. The agents are actually obeying the law of gravity as shown in Eq. (6) and the law of motion in Eq. (7).

$$F = G\left(\frac{M_1 M_2}{R^2}\right) \quad (6)$$

$$a = \frac{F}{M} \quad (7)$$

where F represents the magnitude of the gravitational force, G is gravitational constant, $M1$ and $M2$ are the mass of the first and second objects and R is the distance between the two objects. Eq. (6) shows that in the Newton law of gravity, the gravitational force between two objects is directly proportional to the product of their masses and inversely proportional to the square of the distance between the objects. Moreover, in Eq. (7), Newton's second law shows that when a force, F, is applied to an object, its acceleration, a, depends on the force and its mass, M.

In GSA, an agent has two parameters which are position and mass. The position of the agent represents the solution of the problem, while the mass of the agent is determined using a fitness function. Agents are attracted by the heaviest agent. Hence, the heaviest agent presents an optimum solution in the search space. The steps of GSA can be summarized as follows [17-19]:

Step 1) Agents initialization

The positions of the N number of agents are initialized randomly.

$$X_i = \left(x_i^1, \dots, x_i^d, \dots, x_i^n\right), \quad i = 1,2,\dots,N \quad (8)$$

where x_i^d represents the positions of the ith agent in the dth dimension, while n is the dimension of the problem.

Step 2) Fitness evolution and best fitness computation

For minimization problems, the fitness evolution is performed by evaluating the best and worst fitness of all agents at each iteration.

$$best(t) = \min fit_j(t) \quad , \quad j\epsilon\{1,2,\dots,N\} \quad (9)$$

$$worst(t) = \max fit_j(t) \quad , \quad j\epsilon\{1,2,\dots,N\} \quad (10)$$

where $fit_j(t)$ represents the fitness value of the jth agent at iteration t, $best(t)$ and $worst(t)$ represents the best and worst fitness at iteration t.

Step 3) Gravitational constant computation

In the algorithm, gravitational constant G is reduced with iteration to control the search accuracy and it is computed at iteration t as [18, 19]:

$$G(t) = G_0 . e^{\left(-\frac{\alpha t}{T}\right)} \quad (11)$$

where $G_0 = 100$ and $\alpha = 20$ are initialized at the beginning of the algorithm [19]. Also, T is the total number of iterations.

Step 4) Calculation of masses of the agents

Mass for each agent is calculated at iteration t as:

$$M_i(t) = \frac{m_i(t)}{\sum_{i=1}^{N} m_i(t)} \quad (12)$$

$$m_i(t) = \frac{fit_i(t) - worst(t)}{best(t) - worst(t)} \quad (13)$$

where $m_i(t)$ represents the compatibility of the *ith* agent at iteration t and $M_i(t)$ the mass of the *ith* agent at iteration t.

Step 5) Calculation of accelerations of agents

Acceleration of the *ith* agent at iteration t is computed using Eq. (14):

$$a_i^d(t) = \frac{F_i^d(t)}{M_i(t)} \quad (14)$$

where $F_i^d(t)$ is the total force acting on *ith* agent calculated as:

$$F_i^d(t) = \sum_{j \epsilon Kbest, j \neq i} \text{rand}_j . F_{ij}^d(t) \quad (15)$$

in which, *Kbest* is the set of first K agents with the best fitness value and biggest mass. *Kbest* will decrease linearly with iteration and at the end there will be only one agent applying force to the others. Also, $F_{ij}^d(t)$ is computed using Eq. (16):

$$F_{ij}^d(t) = G(t) . \frac{M_i(t) . M_j(t)}{R_{ij}(t) + \varepsilon} (x_j^d(t) - x_i^d(t)) \quad (16)$$

where $F_{ij}^d(t))$ is the force acting on agent i from agent j at dth dimension and tth iteration, $R_{ij}(t)$ is the Euclidian distance between two agents i and j at iteration t, $G(t)$ is the computed gravitational constant at the same iteration while ε is a small constant.

Step 6) Updating velocity and positions of agents:

Velocity and the position of the agents at next iteration *(t+1)* are computed based on the following equations:

$$v_i^d(t+1) = \text{rand}_i \, v_i^d(t) + a_i^d(t) \quad (17)$$

$$x_i^d(t+1) = x_i^d(t) + v_i^d(t+1) \quad (18)$$

where $V_i(t+1)$ represents the velocity of the ith agent at iteration $t+1$ and $X_i(t+1)$ indicates the mass of the ith agent at iteration $t+1$.

Step 7) Check the convergence

Steps 2 to 6 are repeated until the stop criteria are met. The best fitness value at the final iteration is considered as the global fitness while the position of the corresponding agent at specified dimensions is taken as the global solution of the problem. The flowchart of GSA can be simply shown in Fig. 1.

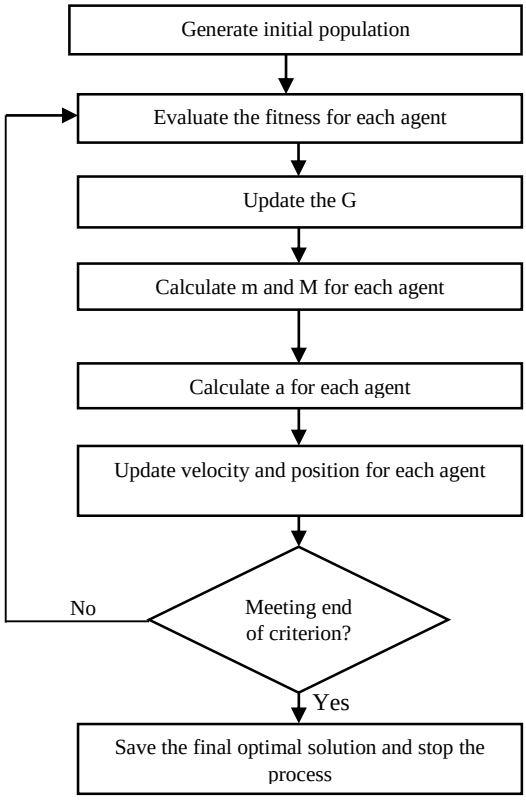

Figure 1. The flowchart of GSA

3.2. The multi-stage gravitational search algorithm (MSGSA)

A multi-stage gravitational search algorithm (MSGSA) is proposed here to accurately detect the multiple structural damages. Based on this algorithm, the location of damaged elements of a structure found in each optimization stage is imposed on the next optimization stage while the effects of healthy elements on the subsequent stage are neglected. By this approach, all healthy elements are successively eliminated during some stages and the algorithm converges to the correct locations and extents of flawed elements. During the optimization stages, the dimension of optimization problem are decreased gradually and this makes the time and total computational cost of the

optimization reduce. The step by step summary of the multi-stage gravitational search algorithm (MSGSA) is as follows:

Step 1) Set the initial number of damage variables, n to the total number of structural elements. Randomly generate the initial position vectors of agents distributed throughout the design space bounded by the specific limits: $X^l \leq X_i \leq X^u$, $i = 1, ..., N$.

Step 2) Employ the standard GSA to find the optimal solution, $X_{GSA}^T = \{x^1, x^2, \dots, x^n\}$

Step 3) Find the locations of healthy elements, that is, for all components of damage vector X_{GSA} find i: $x^i = 0$, and also determine the total number of healthy elements, *m*.

Step 4) Remove the healthy elements from the set of damage variables and reduce the dimension of optimization problem from n to *n-m*.

Step 5) Employ a new GSA stage to find the optimal solution of current stage, i.e. $X_{GSA}^T = \{x^1, x^2, \dots, x^{n-m}\}$.

Step 6) Check the convergence by comparing the optimal solutions of two sequential optimization stages. If two vectors are identical go to step 7, otherwise go to step 3.

Step 7) Save the final optimal solution and stop the optimization process. According to steps 1 to 7, the flowchart of the MSGSA can be simply shown in Fig. 2.

4. Test examples

In order to demonstrate the capabilities of the proposed approach for identifying the damage, three illustrative test examples selected from the literature are considered. The first example is a 16-element cantilevered beam with experimental data, the second example is a 47-bar planar truss and the last example is a 45-element frame (A five-story and four-span frame). In 47-bar planar truss and 45-element frame, the effect of measurement noise on the efficiency of the method is studied.

4.1. Sixteen-element cantilevered beam with experimental data

The proposed method is validated using experimental data obtained from test on the 16-element cantilevered beam by Sinha et al [16]. Table 1 gives details of the geometric and material properties of the beam. The modal test was conducted by Sinha et al. on the beam without any crack and also with a single crack at 275mm (element 5) with the crack depths 8 mm (damage extent 0.32) and 12 mm (damage extent 0.48). Table 2 gives the identified experimental natural frequencies.

A finite element model of the cantilever beam was constructed using Euler-Bernoulli beam elements including translational and rotational springs to simulate the boundary conditions at the clamped end of the beam. The finite element model, shown schematically in Fig. 3 has 16 elements and 34 degrees of freedom. The boundary stiffnesses, $k_t = 26.5\ MN/m$ and $k_\theta = 150\ kN.m/rad$, are required to simulate the translation and rotation flexibility of the clamped support [16].

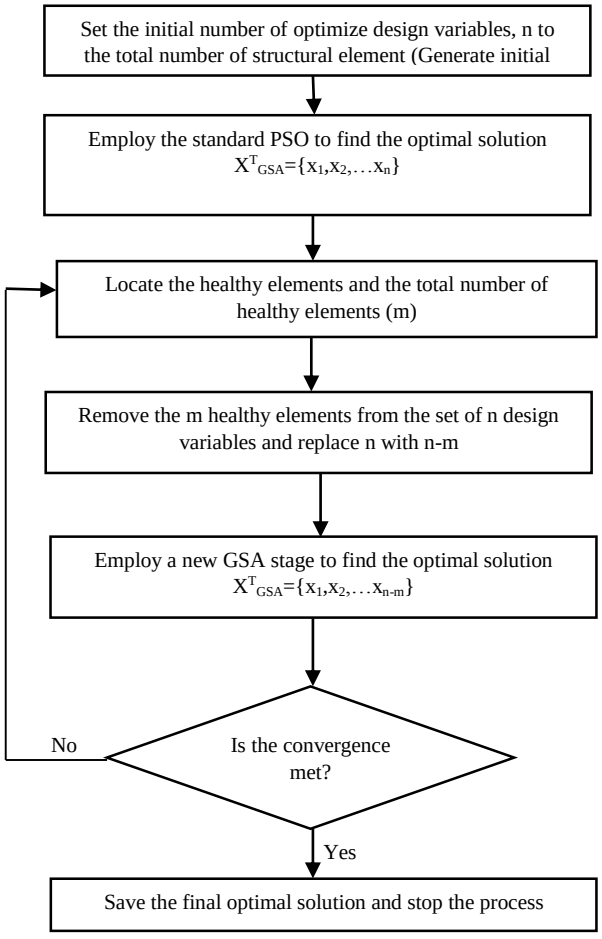

Figure 2. The flowchart of the MSGSA

For this example, two damage scenarios of experimental test [16], listed in Table 3, are studied and the first four natural frequencies are used for damage detection.

Table 1.
The properties of 16-element cantilevered beam

Boundary conditions	Cantilever
Material	Aluminum
Young's modulus (*E*)	69.79 GN/m^2
Mass density (ρ)	2600 kg/m^2
The Poisson Ratio (v)	0.33
Beam length (*L*)	996 mm
Beam width (w)	50 mm
Beam depth (d)	25 mm
Boundary stiffnensses	$k_t = 26.5\ MN/m^2$ $k_\theta = 150\ kN.m/rad$

Table 2.
The natural frequencies of the beam without any crack and with one crack [16]

Mode	No crack	d_{c1}=8 mm x_1=275 mm	d_{c1}=12 mm x_1=275 mm
	Experimental natural frequencies (Hz)	Experimental natural frequencies (Hz)	Experimental natural frequencies (Hz)
1	20	19.75	19
2	124.5	124.063	123
3	342.188	336.875	326.563
4	664.375	662.313	660.313

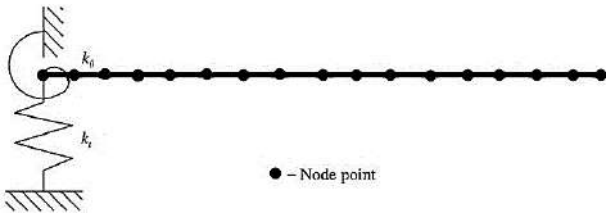

Figure 3. The finite element model for the 16-element cantilevered beam

Table 3.
Two different experimental damage scenarios induced in a 16-element beam

Scenario 1		Scenario 2	
Element number	Damage extent	Element number	Damage extent
5	0.32	5	0.48

The specifications of standard GSA and the proposed MSGSA for applying to the damage detection problem are also given in Table 4.

Table 4.
The specifications of GSA and MSGSA

Algorithm	Parameter	Description	Value
GSA	npop	The number of agents	50
	maxiter	The maximum number of iterations	1000
	G_0	The primal value of the gravitational constant	100
	α	The exponent coefficient of gravitational constant equation	20
MSGSA	npop	The number of GSA agents	40
	maxiter	The maximum iterations performing by GSA	100
	max_stage	The maximum number of optimization stages	2

The convergence of the GSA is met when the objective function does not considerably change after 150 successive iterations or the maximum number of iterations is attained. Also, the convergence of the MSGSA is met when the all optimization stages are attained. The reason why the convergence conditions are different in two algorithms is that each of the algorithms has been considered in the best possible conditions to achieve a completely correct answer with the most minimal number of analyses. In order to consider the stochastic nature of the optimization process using two algorithms, 10 independent sample runs are made for each damage scenario. The damage identification results of damage scenario 1 using two algorithms are given in Tables 5a and 5b, respectively. The average damage ratios for scenario 1 using two algorithms are also shown in Figs. 4a and 4b, respectively. The damage identification results of damage scenario 2 are given in Tables 6a and 6b, respectively. The average damage ratios for scenario 2 are also shown in Figures 5a and 5b, respectively.

Table 5a.
The damage detection results of 16-element beam for scenario 1 via GSA

Run numbers	Element numbers								Required modal analyses	*ECBI*
	1	...	5	...	11	12	...	16		
1	0		0.338		0.086	0.04		0	23850	-0.978
2	0		0.338		0.086	0.04		0	25200	-0.978
3	0		0.338		0.086	0.04		0	24050	-0.978
4	0		0.338		0.086	0.04		0	24650	-0.978
5	0		0.338		0.086	0.04		0	22850	-0.978
6	0		0.338		0.086	0.04		0	23600	-0.978
7	0		0.338		0.086	0.04		0	23800	-0.978
8	0		0.338		0.086	0.04		0	24600	-0.978
9	0		0.338		0.086	0.04		0	25800	-0.978
10	0		0.338		0.086	0.04		0	26000	-0.978
Average	0		0.338		0.086	0.04		0	24440	-0.978
Actual damage	0		0.32		0	0		0	-	-1

Table 5b.

The damage detection results of 16-element beam for scenario 1 via MSGSA

Run numbers	Element numbers								Required modal analyses	*ECBI*
	1	...	5	...	11	12	...	16		
1	0		0.348		0.057	0.06		0	8080	-0.978
2	0		0.429		0.065	0.054		0	8080	-0.978
3	0		0.348		0.042	0.079		0	8080	-0.978
4	0		0.442		0.073	0.065		0	8080	-0.978
5	0		0.359		0.044	0.074		0	8080	-0.978
6	0		0.383		0.064	0.062		0	8080	-0.978
7	0		0.373		0.052	0.061		0	8080	-0.978
8	0		0.351		0.061	0.058		0	8080	-0.978
9	0		0.386		0.072	0.055		0	8080	-0.978
10	0		0.361		0.043	0.063		0	8080	-0.978
Average	0		0.376		0.057	0.063		0	8080	-0.978
Actual damage	0		0.32		0	0		0	-	-1

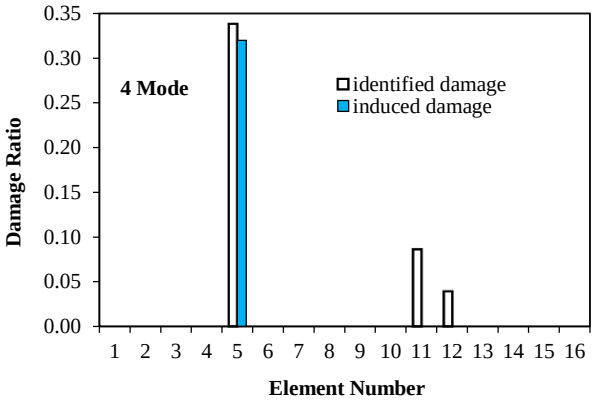

Figure 4a. Final damage ratios of the 16-element beam for scenario 1 via GSA

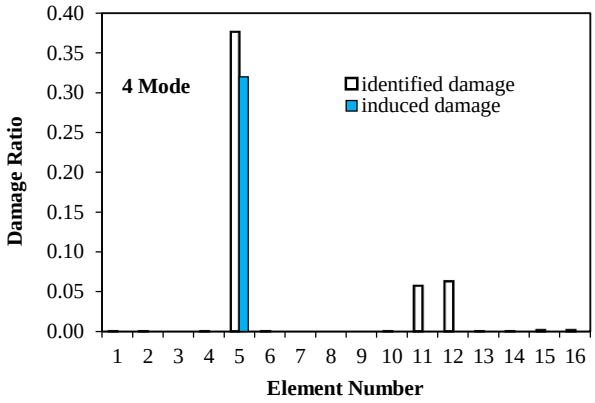

Figure 4b. Final damage ratios of the 16-element beam for scenario 1 via MSGSA

Table 6a.

The damage detection results of 16-element beam for scenario 2 via GSA

Run numbers	Element numbers							Required modal analyses	*ECBI*
	1	...	5	...	11	...	16		
1	0		0.431		0.062		0	22900	-0.992
2	0		0.431		0.062		0	23650	-0.992
3	0		0.431		0.062		0	24300	-0.992
4	0		0.431		0.062		0	25150	-0.992
5	0		0.431		0.062		0	22250	-0.992
6	0		0.431		0.062		0	23150	-0.992
7	0		0.431		0.062		0	22050	-0.992
8	0		0.431		0.062		0	26600	-0.992
9	0		0.431		0.062		0	24200	-0.992
10	0		0.431		0.062		0	24450	-0.992
Average	0		0.431		0.062		0	23470	-0.992
Actual damage	0		0.48		0		0	-	-1

Table 6b.
The damage detection results of 16-element beam for scenario 2 via MSGSA

Run numbers	Element numbers							Required modal analyses	*ECBI*
	1	...	5	...	11	...	16		
1	0		0.525		0.031		0	8080	-0.9945
2	0		0.525		0.038		0	8080	-0.9945
3	0		0.566		0.037		0	8080	-0.9946
4	0		0.53		0.038		0	8080	-0.9945
5	0		0.604		0.015		0	8080	-0.994
6	0		0.527		0.032		0	8080	-0.9944
7	0		0.561		0.036		0	8080	-0.9944
8	0		0.56		0.037		0	8080	-0.9946
9	0		0.556		0.048		0	8080	-0.9945
10	0		0.519		0.044		0	8080	-0.9946
Average	0		0.547		0.036		0	8080	-0.9945
Actual damage	0		0.48		0		0	-	-1

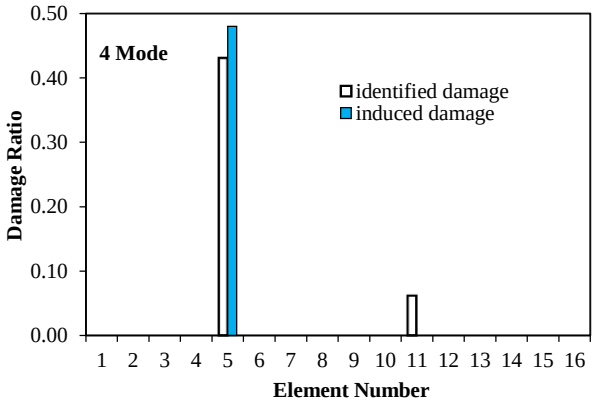

Figure 5a. Final damage ratios of the 16-element beam for scenario 2 via GSA

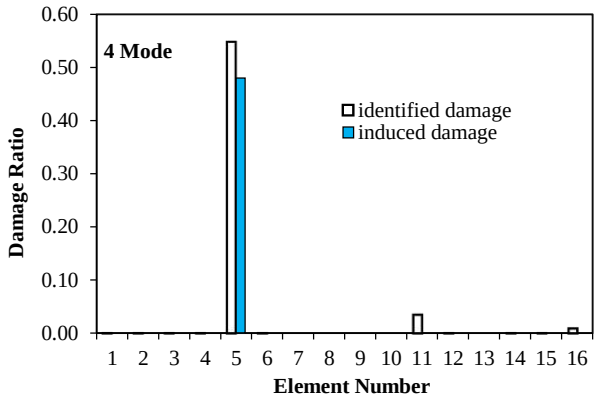

Figure 5b. Final damage ratios of the 16-element beam for scenario 2 via MSGSA

All of the results shown in the tables and figures demonstrate that the best solutions in terms of actual damage identification and the total number of finite element analyses (FEAs) required are obtained by the MSGSA. The average number of FEAs requiring for scenarios 1 and 2 of MSGSA are 8080, while the average number of FEAs needing for GSA is 23440 and 23470, respectively. It is revealed that the MSGSA has a better performance when compared to the GSA.

4.2. Forty-seven-bar planar truss

The 47-bar planar power line tower [11], shown in Fig. 6, is considered to show the robustness of the proposed method. The structure has 47 members and 22 nodes. The truss is modeled using the conventional finite element method without internal nodes, leading to 41 degrees of freedom. All members are made of steel, and the material density, modulus of elasticity and area of each element are 0.3 lb/in^3, 30000 ksi and 2 in^2, respectively. Damage in the structure is simulated as a relative reduction in the elasticity modulus of individual elements. Therefore, the optimization problem of damage identification has 47 damage variables. Four different damage scenarios, given in Table 7, are induced in the structure, and the MSGSA and the GSA are tested for each scenario. For identifying the damage scenarios 1 and 2, the first 10 natural frequencies and for identifying the damage scenarios 3 and 4, the first 15 natural frequencies of the structure are considered. In order to investigate the noise effect on the performance of the proposed method, measurement noise is considered here by polluting the natural frequencies using a standard error of ±0.15 % [3, 4, 11 and 12]. For identifying the damage scenarios 1 and 2, agent numbers and the maximum numbers of GSA iterations are set to 40 and 1000, respectively. Also, for identifying the damage scenarios 3 and 4, agent numbers and the maximum numbers of GSA iterations are set to 50 and 2000, respectively. For identifying the damage scenarios 1 and 2, agent numbers, the maximum numbers of MSGSA

iterations and the maximum number of optimization stages are set to 25, 700 and 20, respectively. Also, for identifying the damage scenarios 3 and 4, agent numbers and the maximum numbers of MSGSA iterations and the maximum number of optimization stages are set to 20, 200 and 20, respectively.

The convergence of the GSA is met when the objective function reaches -0.995 or the maximum number of iterations is attained. For identifying the damage scenarios 1 and 2, the convergence of the MSGSA is met when the objective function reaches -0.967. Also, for identifying the damage scenarios 3 and 4, the convergence of the MSGSA is met when the objective function reaches -0.994. In order to consider the stochastic nature of the optimization process using GSA and MSGSA ten independent sample runs are made for each damage scenario. The solutions of GSA and MSGSA for damage scenarios 1 to 4 are given in Tables 8–15 and Figs. 7-14.

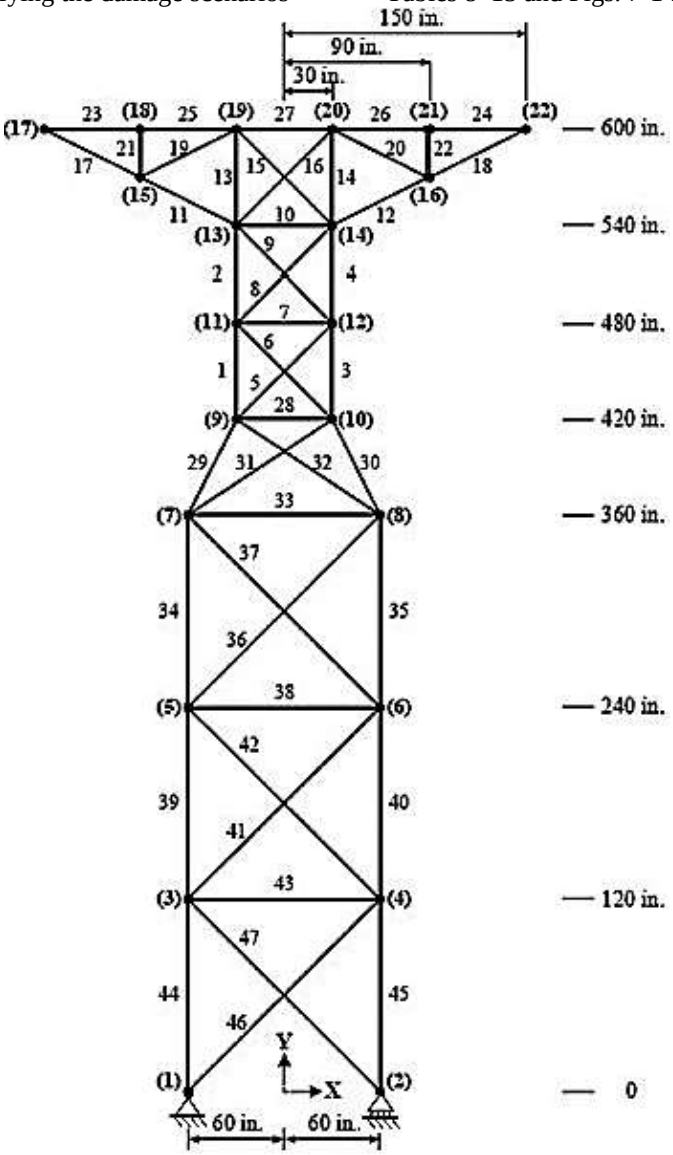

Figure 6. The finite element model for the 47-bar planar truss

Table 7.

Four different damage scenarios induced in 47-bar planar truss

Scenario 1		Scenario 2		Scenario 3		Scenario 4	
Element number	Damage extent	Element number	Damage extent	Element number	Damage extent	Element number	Damage extent
10	0.30	30	0.30	10	0.30	40	0.30
-	-	-	-	30	0.30	41	0.20

Table 8.
The damage detection results of 47-bar planar truss for scenario 1 via GSA

Run numbers	Element numbers					Required modal analyses	*ECBI*
	1	...	10	...	47		
1	0		0.295		0	40040	-0.9858
2	0		0.158		0	40040	-0.9722
3	0.016		0.263		0	40040	-0.9681
4	0		0.204		0	40040	-0.9707
5	0		0.244		0	40040	-0.9733
6	0		0.252		0	40040	-0.9726
7	0.01		0.256		0	40040	-0.9647
8	0		0.185		0	40040	-0.9791
9	0		0.323		0	40040	-0.9858
10	0		0.14		0	40040	-0.9725
Average	0.0026		0.232		0	40040	-0.9749
Actual damage	0		0.3		0	-	-1

Table 9.
The damage detection results of 47-bar planar truss for scenario 1 via MSGSA

Run numbers	Element numbers					Required modal analyses	*ECBI*
	1	...	10	...	47		
1	0		0.284		0	17525	-0.9922
2	0		0.279		0	17525	-0.99
3	0		0.146		0	17525	-0.9821
4	0		0.108		0	17525	-0.9871
5	0		0.276		0	17525	-0.9909
6	0		0.267		0	17525	-0.9932
7	0		0.255		0	17525	-0.9725
8	0		0.116		0	17525	-0.974
9	0		0.136		0	17525	-0.9881
10	0		0.161		0	35050	-0.968
Average	0		0.203		0	19278	-0.9838
Actual damage	0		0.3		0	-	-1

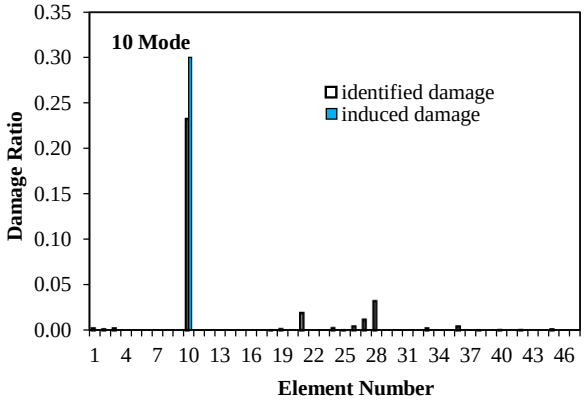

Figure 7. Final damage ratios of the 47-bar planar truss for scenario 1 via GSA

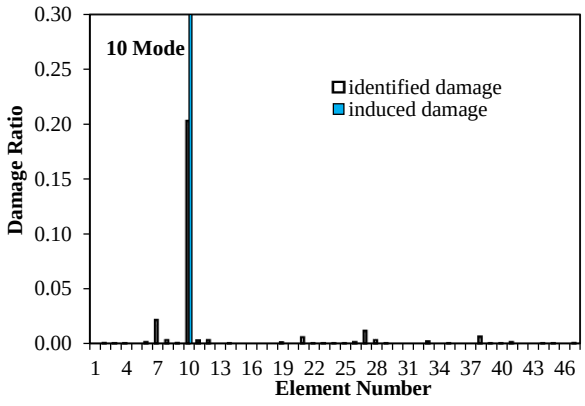

Figure 8. Final damage ratios of the 47-bar planar truss for scenario 1 via MSGSA

Table 10.
The damage detection results of 47-bar planar truss for scenario 2 via GSA

Run numbers	Element numbers					Required modal analyses	*ECBI*
	1	...	30	...	47		
1	0		0.28		0	40040	-0.9929
2	0.042		0.246		0	12160	-0.9951
3	0		0.304		0	5520	-0.9983
4	0		0.337		0	8128	-0.9955
5	0		0.323		0	8000	-0.9972
6	0.028		0.286		0	12840	-0.995
7	0.013		0.268		0	40040	-0.9948
8	0		0.273		0	40040	-0.9926
9	0		0.272		0	8720	-0.9954
10	0		0.278		0	10760	-0.9951
Average	0.008		0.287		0	18624	-0.9952
Actual damage	0		0.3		0	-	-1

Table 11.
The damage detection results of 47-bar planar truss for scenario 2 via MSGSA

Run numbers	Element numbers					Required modal analyses	*ECBI*
	1	...	30	...	47		
1	0		0.306		0	17525	-0.9955
2	0		0.299		0	17525	-0.9975
3	0.024		0.272		0	17525	-0.9965
4	0.033		0.171		0	17525	-0.9986
5	0.026		0.297		0	17525	-0.9965
6	0		0.289		0	17525	-0.995
7	0		0.272		0	17525	-0.9955
8	0		0.262		0	17525	-0.9957
9	0		0.181		0	17525	-0.998
10	0		0.261		0	17525	-0.9987
Average	0.008		0.261		0	17525	-0.9968
Actual damage	0		0.3		0	-	-1

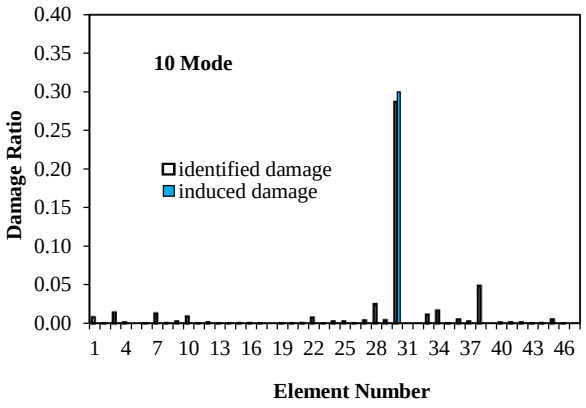

Figure 9. Final damage ratios of the 47-bar planar truss for scenario 2 via GSA

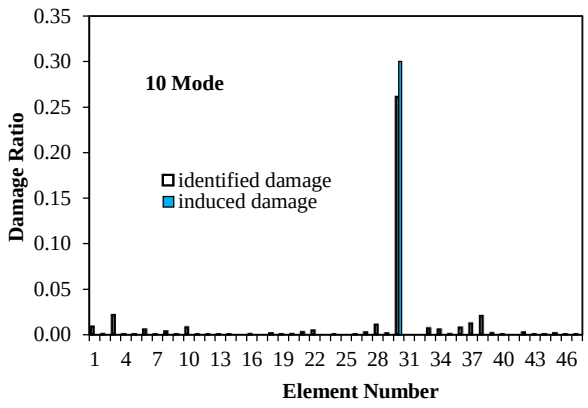

Figure 10. Final damage ratios of the 47-bar planar truss for scenario 2 via MSGSA

Table 12.
The damage detection results of 47-bar planar truss for scenario 3 via GSA

Run numbers	Element numbers							Required modal analyses	*ECBI*
	1	...	10	...	30	...	47		
1	0		0.306		0.276		0	24700	-0.9955
2	0		0.32		0.323		0	24650	-0.9951
3	0.022		0.345		0.344		0	23350	-0.9954
4	0.043		0.317		0.334		0	24000	-0.9951
5	0.045		0.27		0.261		0	21750	-0.9955
6	0.011		0.307		0.316		0	25000	-0.9956
7	0		0.209		0.31		0	22100	-0.9951
8	0		0.35		0.288		0	22000	-0.9952
9	0.012		0.328		0.336		0	24700	-0.9954
10	0		0.35		0.332		0	24200	-0.9957
Average	0.014		0.31		0.312		0	23645	-0.9953
Actual damage	0		0.3		0.3		0	-	-1

Table 13.
The damage detection results of 47-bar planar truss for scenario 3 via MSGSA

Run numbers	Element numbers							Required modal analyses	*ECBI*
	1	...	10	...	30	...	47		
1	0		0.304		0.283		0	16080	-0.9992
2	0		0.285		0.254		0	20100	-0.9982
3	0		0.352		0.395		0	16080	-0.9989
4	0.032		0.264		0.197		0	12060	-0.9991
5	0		0.286		0.281		0	4020	-0.9994
6	0		0.276		0.297		0	8040	-0.9991
7	0		0.293		0.227		0	16080	-0.9983
8	0		0.265		0.267		0	4020	-0.9988
9	0		0.281		0.238		0	4020	-0.9992
10	0		0.289		0.291		0	4020	-0.999
Average	0.0032		0.289		0.273		0	10452	-0.9989
Actual damage	0		0.3		0.3		0	-	-1

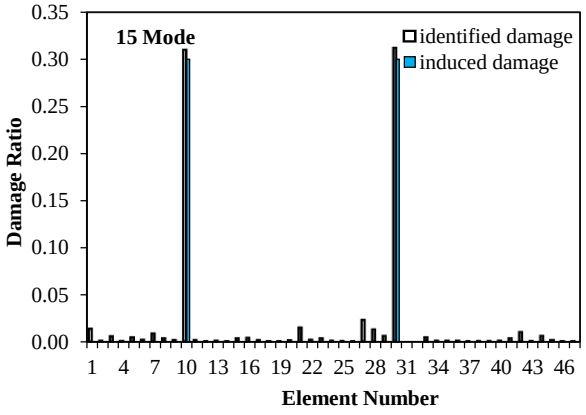

Figure 11. Final damage ratios of the 47-bar planar truss for scenario 3 via GSA

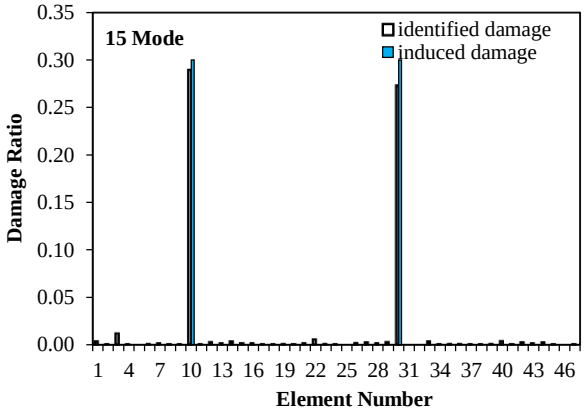

Figure 12. Final damage ratios of the 47-bar planar truss for scenario 3 via MSGSA

Table 14.
The damage detection results of 47-bar planar truss for scenario 4 via GSA

Run numbers	Element numbers							Required modal analyses	*ECBI*
	1	...	40	...	41	...	47		
1	0		0.279	0		0	100050	-0.9946	0.279
2	0		0.338	0.251		0	23400	-0.9955	0.338
3	0		0.359	0.247		0	23300	-0.9957	0.359
4	0		0.303	0.201		0	23450	-0.9953	0.303
5	0		0.345	0.245		0	21400	-0.9952	0.345
6	0		0.358	0.235		0	23900	-0.9953	0.358
7	0		0.365	0.232		0	23700	-0.9951	0.365
8	0		0.381	0.305		0	21450	-0.9959	0.381
9	0		0.34	0.215		0	24650	-0.9951	0.34
10	0		0.264	0.174		0	26050	-0.995	0.264
Average	0		0.333	0.21		0	31105	-0.9953	0.333
Actual damage	0		0.3	0.3		0	-	-1	0.3

Table 15.
The damage detection results of 47-bar planar truss for scenario 4 via MSGSA

Run numbers	Element numbers							Required modal analyses	*ECBI*
	1	...	40	...	41	...	47		
1	0		0.274	0.164		0	4020	-0.9944	0.274
2	0		0.258	0.155		0	8040	-0.9981	0.258
3	0		0.271	0.181		0	4020	-0.997	0.271
4	0		0.254	0.146		0	32160	-0.9945	0.254
5	0		0.277	0.164		0	4020	-0.9953	0.277
6	0		0.225	0.153		0	4020	-0.9953	0.225
7	0		0.207	0.141		0	12060	-0.9949	0.207
8	0		0.239	0.108		0	4020	-0.9946	0.239
9	0		0.277	0.213		0	4020	-0.9948	0.277
10	0		0.264	0.179		0	8040	-0.9976	0.264
Average	0		0.255	0.162		0	8424	-0.9957	0.255
Actual damage	0		0.3	0.3		0	-	-1	0.3

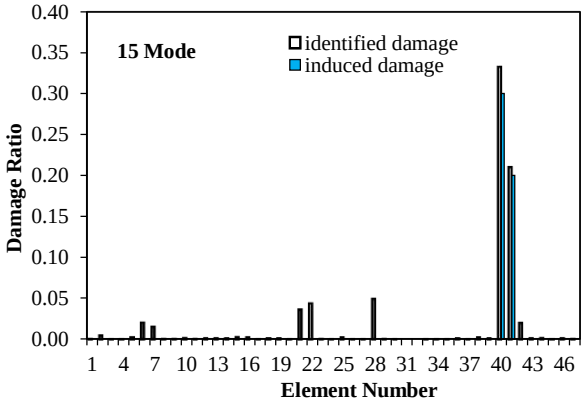

Figure 13. Final damage ratios of the 47-bar planar truss for scenario 4 via GSA

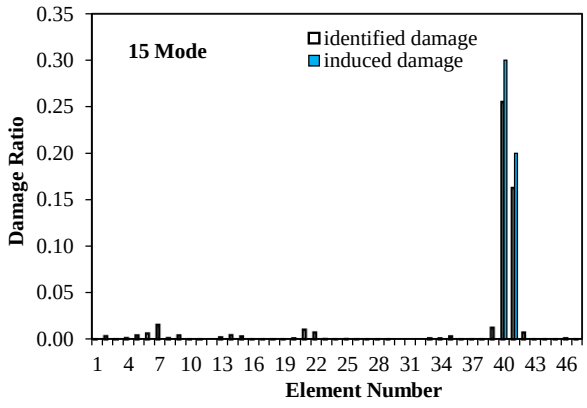

Figure 14. Final damage ratios of the 47-bar planar truss for scenario 4 via MSGSA

All of the results shown in the tables and figures demonstrate that the best solutions in terms of actual damage identification and the total number of FEAs required are obtained by means of the MSGSA. The average number of FEAs requiring for scenarios 1, 2, 3 and 4 of MSGSA are 19278, 17125, 10452 and 8442, respectively, while the average number of FEAs needing for GSA are 40040, 18628, 23645 and 31105, respectively. It is revealed that the MSGSA has a better performance when compared to the GSA.

4.3. Forty-five-element planar frame

A five-story and four-span frame [12] as depicted in Fig. 15 is considered as the last example. The structure has 45 members and 30 nodes. This frame is modeled using the finite element method, leading to 75 degrees of freedom. The sections used for the beams and columns are (W14×145). The area and inertia moment of each element are 0.0276m2 and 0.000712 m4, respectively. The modulus of elasticity is 210 GPa and the material density is 7780 kg/m3.Damage in the structure is also simulated as a relative reduction in the elasticity modulus of individual elements. Two different damage scenarios are considered as listed in Table 16. For identifying the damage scenarios 1 and 2, the first 12 and 14 natural frequencies of the structure are considered, respectively. The measurement noise is considered here by polluting the natural frequencies using a standard error of ±0.15 % [3, 4, 11 and 12].

In this example, the GSA could not converge to an appropriate solution, accordingly only the results of MSGSA have been reported here. For identifying the damage scenario 1 using MSGSA, agent numbers, the maximum numbers of iterations and the maximum number of optimization stages are set to 50, 500 and 10, respectively. Also, for identifying the damage scenario 2 using MSGSA, agent numbers and the maximum numbers of iterations and the maximum number of optimization stages are set to 40, 300 and 5, respectively. The convergence of the MSGSA is met when all optimization stages is attained. In order to consider the stochastic nature of the optimization process, ten independent sample runs are made for each damage scenario. The damage identification results for damage scenarios 1 and 2 using MSGSA are given in Tables 17 and 18, respectively. The average damage ratios for scenarios 1 and 2 are also shown in Figs. 16 and 17, respectively.

As can be seen in the tables and figures, the MSGSA proposed here can accurately detect the damage sites and extent for most of the simulations. It is observed that the optimization process can achieve to the site and extent of actual damage truthfully. The average number of FEAs requiring for scenarios 1 and 2 of MSGSA are 250500 and 60200, respectively.

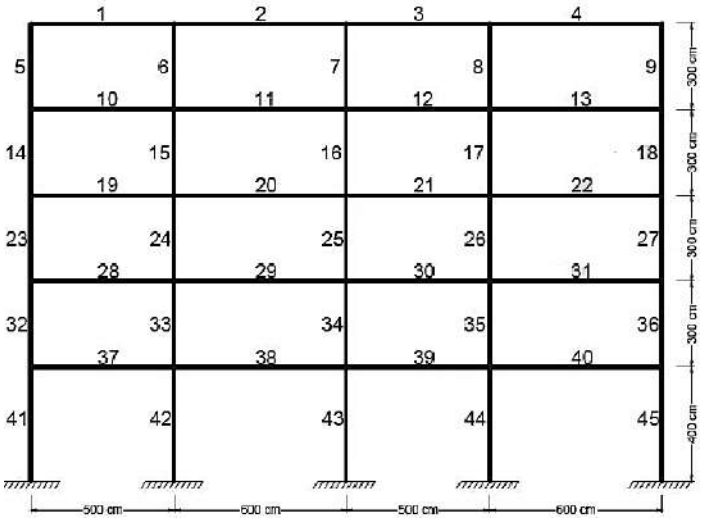

Figure 15. The finite element model for the 45-element frame

Table 16.

Different damage scenarios for planar frame

Scenario 1		Scenario 2	
Element number	Damage extent	Element number	Damage extent
14	0.35	9	0.30
28	0.30	18	0.20
38	0.35	36	0.25

Table 17.
The damage detection results of 45-element frame for scenario 1 via MSGSA

Run numbers	Element numbers 1	...	14	...	28	...	38	...	45	Required modal analyses	*ECBI*
1	0		0.33		0.28		0.07		0	250500	-0.9974
2	0		0.32		0.28		0.3		0	250500	-0.9981
3	0		0.27		0.09		0.34		0	250500	-0.9993
4	0		0.3		0.29		0.04		0	250500	-0.999
5	0		0		0.21		0		0	250500	-0.9996
6	0		0.19		0.17		0.19		0	250500	-0.9995
7	0		0.3		0.2		0		0	250500	-0.9975
8	0		0.31		0.12		0.4		0	250500	-0.9983
9	0		0.32		0.08		0		0	250500	-0.9977
10	0		0.34		0.02		0.17		0	250500	-0.9976
Average	0		0.27		0.17		0.15		0	250500	-0.9984
Actual damage	0		0.35		0.3		0.35		0	-	-1

Table 18.
The damage detection results of 45-element frame for scenario 2 via MSGSA

Run numbers	Element numbers 1	...	9	...	18	...	36	...	45	Required modal analyses	*ECBI*
1	0		0.32		0.14		0.22		0	60200	-0.9994
2	0		0.27		0.2		0.23		0	60200	-0.9985
3	0		0.23		0.31		0.19		0	60200	-0.9992
4	0		0.28		0.24		0.25		0	60200	-0.9985
5	0		0.3		0		0.13		0	60200	-0.9989
6	0		0.3		0.21		0.23		0	60200	-0.9977
7	0		0.31		0.14		0.26		0	60200	-0.9993
8	0		0.33		0.15		0.25		0	60200	-0.9986
9	0		0.29		0.14		0.25		0	60200	-0.9991
10	0		0.28		0.21		0.25		0	60200	-0.9986
Average	0		0.29		0.17		0.23		0	60200	-0.9988
Actual damage	0		0.3		0.2		0.25		0	-	-1

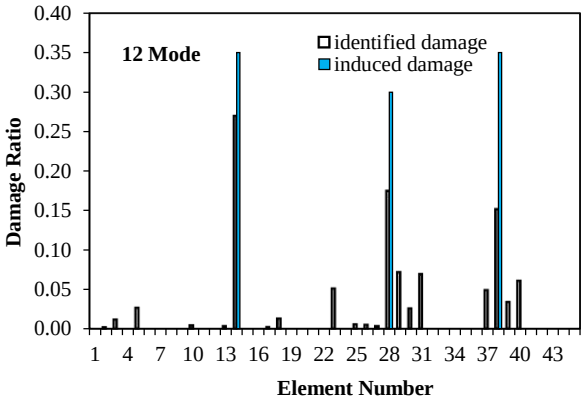

Figure 16. Final damage ratios of the 45-element frame for scenario 1 via MSGSA

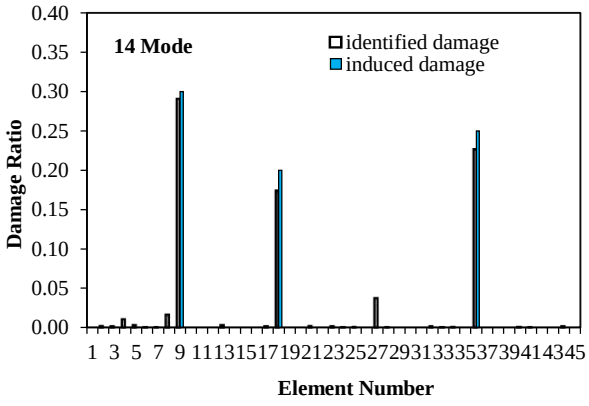

Figure 17. Final damage ratios of the 45-element frame for scenario 2 via MSGSA

5. Conclusions

An efficient optimization procedure has been introduced to solve the problem of structural damage detection that is a highly nonlinear problem with a great number of local solutions. The structural damage detection problem is firstly formulated as a standard optimization problem aiming to minimize an ECBI for finding real damage variables. The MSGSA is proposed to properly solve the optimization problem. In order to assess the competence of the proposed approach for structural damage detection, three illustrative examples are tested. The results demonstrate that the combination of ECBI and MSGSA can provide a robust tool for damage detection. The results of the proposed approach have shown a high performance for the method when compared with actual damage induced and those of standard GSA.

References

[1] Mares, C., and Cecilia Surace. "An application of genetic algorithms to identify damage in elastic structures." Journal of sound and vibration 195.2 (1996): 195-215.

[2] Au, F. T. K., et al. "Structural damage detection based on a micro-genetic algorithm using incomplete and noisy modal test data." Journal of Sound and Vibration 259.5 (2003): 1081-1094.

[3] Koh, B. H., and S. J. Dyke. "Structural health monitoring for flexible bridge structures using correlation and sensitivity of modal data." Computers & structures 85.3-4 (2007): 117-130.

[4] Vakil-Baghmisheh, Mohammad-Taghi, et al. "Crack detection in beam-like structures using genetic algorithms." Applied soft computing 8.2 (2008): 1150-1160.

[5] Guo, H. Y., and Z. L. Li. "A two-stage method to identify structural damage sites and extents by using evidence theory and micro-search genetic algorithm." Mechanical Systems and Signal Processing 23.3 (2009): 769-782.

[6] Nobahari, Mehdi, and Seyed Mohammad Seyedpoor. "Structural damage detection using an efficient correlation-based index and a modified genetic algorithm." Mathematical and Computer modelling 53.9-10 (2011): 1798-1809.

[7] Villalba, J. D., and José Elias Laier. "Localising and quantifying damage by means of a multi-chromosome genetic algorithm." Advances in Engineering Software 50 (2012): 150-157.

[8] Moradi, S., P. Razi, and L. Fatahi. "On the application of bees algorithm to the problem of crack detection of beam-type structures." Computers & Structures 89.23-24 (2011): 2169-2175.

[9] Begambre, O., and José Elias Laier. "A hybrid Particle Swarm Optimization–Simplex algorithm (PSOS) for structural damage identification." Advances in Engineering Software 40.9 (2009): 883-891.

[10] Seyedpoor, S. M. "Structural damage detection using a multi-stage particle swarm optimization." Advances in Structural Engineering 14.3 (2011): 533-549.

[11] Nouri Shirazi, M. R., H. Mollamahmoudi, and Seyed Mohammad Seyedpoor. "Structural damage identification using an adaptive multi-stage optimization method based on a modified particle swarm algorithm." Journal of Optimization Theory and Applications 160 (2014): 1009-1019.

[12] Kaveh, A., S. M. Javadi, and M. Maniat. "Damage assessment via modal data with a mixed particle swarm strategy, ray optimizer, and harmony search." (2014): 95-106.

[13] Seyedpoor, S. M., S. Shahbandeh, and O. Yazdanpanah. "An efficient method for structural damage detection using a differential evolution algorithm-based optimisation approach." Civil Engineering and Environmental Systems 32.3 (2015): 230-250.

[14] Braun, Carlos E., Leonardo D. Chiwiacowsky, and Arthur T. Gomez. "Variations of Ant Colony Optimization for the solution of the structural damage identification problem." Procedia Computer Science 51 (2015): 875-884.

[15] Nhamage, Idilson António, Rafael Holdorf Lopez, and Leandro Fleck Fadel Miguel. "An improved hybrid optimization algorithm for vibration based-damage detection." Advances in Engineering Software 93 (2016): 47-64.

[16] Sinha, Jyoti K., M. I. Friswell, and S. Edwards. "Simplified models for the location of cracks in beam structures using measured vibration data." Journal of Sound and vibration 251.1 (2002): 13-38.

[17] Rashedi, Esmat, Hossein Nezamabadi-Pour, and Saeid Saryazdi. "GSA: a gravitational search algorithm." Information sciences 179.13 (2009): 2232-2248.

[18] Sabri, Norlina M., Mazidah Puteh, and Mohamad Rusop Mahmood. "A Review of Gravitational Search Algorithm. " International Journal of Advances in Soft Computing and its Applications 5.3 (2013): 1-39.

[19] Chatterjee, A., G. K. Mahanti, and Priya Ranjan Sinha Mahapatra. "Generation of phase-only pencil-beam pair from concentric ring array antenna using gravitational search algorithm." 2011 International Conference on Communications and Signal Processing. IEEE, 2011.

J-Researchers

Journal of Civil Engineering Researchers

Journal homepage: www.journals-researchers.com

Solar Energy Application for Erbil Municipal Wastewater Treatment and Reusing

Sarwah Othman Ismael,[a,*] Shuokr Qarani Aziz [a]

[a] *Department of Civil Engineering, College of Engineering, Salahaddin University-Erbil, Erbil, Kurdistan Region, Iraq*

ABSTRACT

Up to now, there is no central wastewater treatment plant (WWTP) in Erbil City, Kurdistan Region Iraq. Erbil Municipal waste water (EMWW) discharges directly to the environment, or sometimes it used for irrigation, without treatment. This research focused on the EMWW characteristics, treatment using solar energy technique and reusing. Data were collected from published works since 1994 and visiting the site. Some EMWW quality parameters such as total suspended solids (TSS), chemical oxygen demand (COD), and five-day biochemical oxygen demand (BOD5) topped the effluent standards. Accordingly, treatment process like solar energy is essential. Quantity of solar energy in Erbil City is A Unit. Application of solar energy for EMWW treatment led to removal of (80-98) % of BOD, (75-95) % COD, and (85-98) % of TSS. Treaded WW is safe for irrigation. Solar energy can be used for EMWW treatment and it regards as efficient and economic technique.

ARTICLE INFO

Received: May 29, 2024
Accepted: June 26, 2024

Keywords:
Erbil
Municipal
Solar Energy
Treatment
Wastewater

DOI: 10.61186/JCER.6.2.49
DOR: 20.1001.1.2538516.2024.6.2.5.6

1. Introduction

Erbil Municipal wastewater (EMWW) comprises of domestic, industrial, commercial, washing, institutional etc. WWs. EMWW collects in the main channel near Tooraq Quarter in Erbil City, Kurdistan Region, Iraq. Due to investment projects in Erbil City, population increase, refuges and internally displaced persons (IDPs), and development of the city, tourist etc., the discharge of EMWW has been increased from 0.85 m3/s - 1.7 m3/s in 2001 to 5.56 m3/s in 2020 [1, 2]. Up to now in Erbil City, there's no principal WW treatment plants (WWTP). As a result, produced MWW from Erbil City discharges directly to the natural environment, mixes with the Greater-Zab River at Guer Area, infiltrate to groundwater, and sometimes it uses for irrigation by farmers [2,3,4]. Untreated EMWW causes problems for the environment, water sources and the population. Accordingly, treatment is crucial for the EMWW.

In literature, researchers tried to treat WWs in Erbil City. Aziz and Ali [5] treated dairy and EMWWs by using biological trickling filter. Aziz and Ali [5] published a work on quality and treatment using different methods for WWs. Industrial WW and reusing were studied by [6]. Oil

* Corresponding author. Tel.: +9647504537531; e-mail: srwa.ismail@su.edu.krd.

refinery WW at Kawergosk arae treated by sequencing batch reactor and adsorption [7]. Firstly, moving bed biofilm reactor (MBBR), the sequencing batch reactor (SBR), and conventional activated sludge were designed for residential WW treatment and reusing in Erbil City [8]. But to date, there is no application of solar energy for treatment of EMWW.

Regarding solar energy application for WW treatment, Ugwuishiwu et al. [9] estimated the use of solar energy in solid waste and wastewater treatment such as in pyrolysis, solar ignition, and desalination for wastewater treatments, solar distillation, solar photocatalytic degradation, solar pathogenic organic destruction, and gasification for solid wastes treatments. Additionally, Zhang et al. [10] provided reviewed main solar based water treatment methods and technologies, and evaluated the applicability and economic and technical feasibility of various technologies in the real world. Also Guo et al. [11] investigated biomass energy and the available green energy (Solar Energy, Wind Energy, Heat Energy) that can be used in wastewater treatment plants. As a result, a comprehensive description of energy efficient technologies for wastewater treatment plants was provided. Kretschmer et al. [12] presented a new concept of adjusting the internal heat supply of (WWTP) to support the efficient usage of thermal energy and make available additional heat for (WWTP) external supply.

The current research focused on the characteristics, treatment via solar energy, and reusing of EMWW. Previously, this kind of research has not been carried out in Erbil City.

2. MATERIALS AND METHODS

2.1. Study Area and Data Collection

Erbil Province is the capital of Iraqi Kurdistan, which has a population of approximately 2 million. Erbil Province is situated in northeast Iraq. Its boundaries extend from longitude 43° 15′ E to 45° 14′ E and from latitude 35° 27′ N to 37° 24′ N. EMWW comes from domestic sewage, including wastewaters from bathrooms and kitchens, public commercial buildings and industrial regions, and storm water. All generated wastewaters from Erbil City are discharged into a valley near Turaq village, which is located at 36° 10′ 14” N to 43° 56′ 12” E and 371 m a.s.l, Figures 1 and 2. The effluent stream extends for more than 50 km, passing through several farmlands and villages, until discharging into the Greater Zab River. The quantity of discharged EMWW ranges from 0.85 m3/sec to 1.7 m3/sec [7].

2.2. Solar Energy

Solar energy is a kind of energy that is obtained from the sun. The sun acts as a fusion reactor. The continuous fusion reaction of the sun is responsible for the heat energy from which it radiates. This energy can travel infinite distances to planets millions of light-years away. The use of sunlight power for a broad range of industrial, lighting, and heating applications has been a goal of scientific researches. The exact inception date of solar energy and system science is not known.

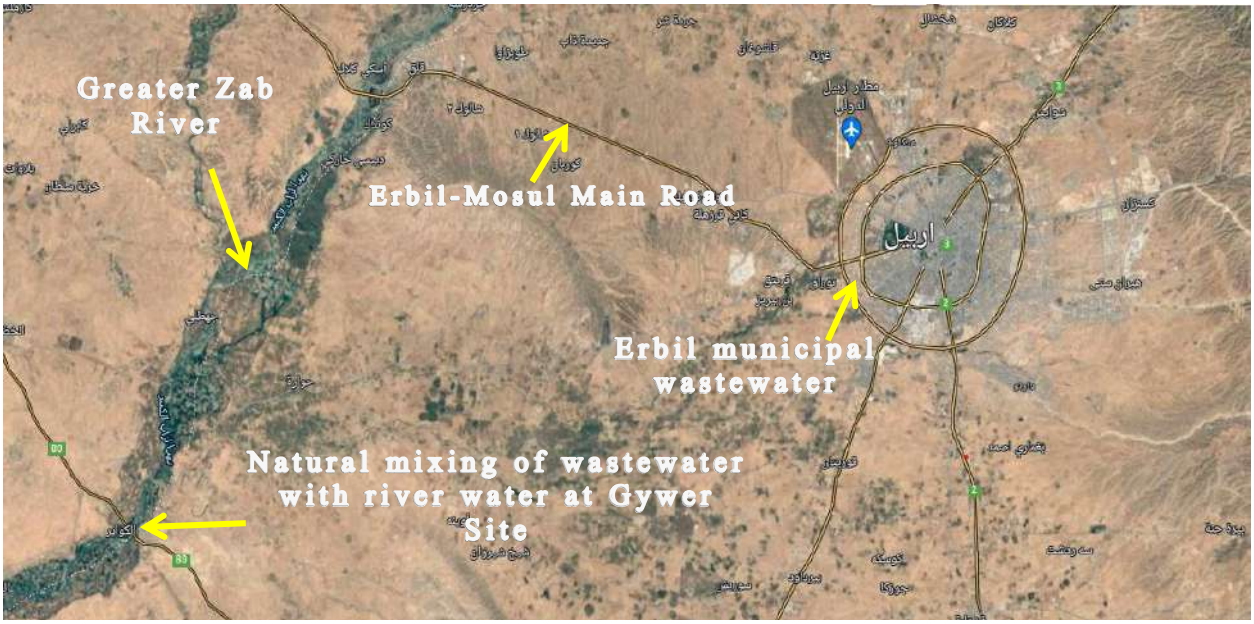

Figure 1. Satellite image (https://www.google.iq/maps/@36.1593852,43.8110409,38506m/data=!3m1!1e3

Date: December 9, 2020

Date: March 2,2021

Figure 2. EMWW main channel at Tooraq Area.

Greeks made the first attempts in the 2nd century, to explain the solar system kinematics. They developed the Ptolemaic or geocentric scheme for the solar system [13].

3. RESULTS AND DISCUSSION

3.1. EMWW Characteristics

Table 1 illustrates characteristics of EMWW in Erbil City from 1994 to 2020. It can be seen from the table some wastewaters parameters, like BOD, COD, TSS, NH_3, NO_3, NO_2, PO_4, Mg, Cd, Cu, Zn, color, Pb, Mn, oil and grease, and phenols, surpassed the principles for removal of WW. Therefore, treatment techniques are necessary earlier removal to the herbal surroundings or blending with water sources. Published works discovered that various treatment strategies which include sequencing batch reactor, adsorption, lagoons, oxidation ditch, wetland, and trickling filter had been studied for remedy of wastewaters in Erbil City [2]. Of course, every remedy approach has benefits and disadvantages. Further, preliminary cost, construction, process, and renovations are different problems of the cited treatment process. Subsequently in the extant research, treatment of EMWW via solar energy was examined. Normally, EMWW considered as weak WW [2, 5, 14].

3.2. Applied Treatment Techniques on EMWW

MSWW includes both residential and commercial wastewater, as well as wastewater discharged from industry, municipal, and similar establishments. The goal of the wastewater treatment method is to kill pathogenic microorganisms and remove or decrease toxic substances, organic and inorganic components [17, 18]. As a result, the feature of treated wastewater is improved to fulfill the criteria of WW disposal standards [2]. WW treatment commonly consists of three stages including primary, secondary and tertiary treatment (Figure 3) [19]. Removing the largest particles and organic matter happens in the primary and secondary treatment process, respectively. Then, several unfavorable substances remain in the treated water. Therefore, the tertiary treatment is applied as a polishing unit to remove these substances. These treatments usually include a combination of various biological, chemical, and physical processes. In Literature, various treatment techniques (such as wetlands, aerated lagoon, oxidation ditch, trickling biological filter, conformist activated sludge, sequencing batch reactor,

Table 1
Characteristics of EMWW from 1994 to 2020 Aziz [2].

No.	Parameter	Range	Standards
1	pH	6.1-8.85	6-9.5**
2	Temp. (ºC)	10-31.5	35**, 40*
3	EC (µs/cm)	284-2300	
4	T. Salts (mg/L)	236.8-1800	
5	TS (mg/L)	300-10000	
6	TSS (mg/L)	40-1800	60**, 35*
7	TDS (mg/L)	100-8200	
8	Turbidity (NTU)	0.41-1000	
9	Chloride (mg/L)	0.86-165	750 *
10	T. Acidity (mg/L)	0.18-60	
11	T. Hardness (mg/L)	120-590	
12	$BOD_{5\,(}$mg/L)	6.3-304	40**
13	COD (mg/L)	12.2-901	100**
14	NH_3-N (mg/L)	0.004-11.4	Nil**, 1 *
15	NO_{2-}N (mg/L)	0.001-26	1 *
16	NO_3 –N (mg/L)	0.003-47	50**, 10*
17	SO_4 (mh/L)	0.008-1220	1500*
18	DO (mg/L)	0-10.4	
19	PO_4 (µg/L)	0.0015-6.97	3**
20	Na (%)	6.1-73	
21	SAR (%)	0.19-16	
22	otal coliform cell/100 ml X 1(	0.34-380	
23	Na (mg/L)	0.38-62	
24	Ca (mg/L)	1..8-85	
25	Mg (mg/L)	0.1-30.8	0.5**
26	Cd (mg/L)	0- 46.73	0.01**
27	Cu (mg/L)	0-18.69	0.2**
28	Zn (mg/L)	0-76.92	0.2**
29	Pb (mg/L)	0-61.76	0.1**
30	TVS (mg/L)	100-300	
31	TnVS (mg/L)	100-600	
32	BOD_5/COD	0.487-0.830	
33	Color (Pt.Co,)	186-379	Nil **
34	Mn (mg/L)	1.3-4.6	0.2 **
35	TOC (mg/L	19-180	

Continued from pervious page

No.	Parameter	Range	Standards
36	Phenols (mg/L)	0.044-0.102	0.01-0.05**
37	Oil & grease (mg/L)	0.04-1.05	Nil*, 10 **
38	ORP (Mv)	-107.4 - (-33.2)	
39	Salinity	0.26-057	
40	T. Alkalinity (mg/L)	157.3-340	
41	Alkalinity (%)	8.93-40.15	
42	TVC Bacteria (Cfu/mL)	$110*10^5$-$176*10^5$	
43	Phytoplankton density (Cells/L)	21787.5	
44	Total Bacteria Count ($X10^8$)	0.002-0.74	
45	Total bacteria cell/L x $l0^5$	0.047-193	
46	Total fungi cells/L X 10^4	0.035-240	
47	Discharge (m^3/s)	0.85-5.56	

* (EPA) Environment Protection Agency (EPA), Standards for effluent discharge, Regulations, 2003 [15].
** Iraqi Environmental Standards, Contract No.: W3QR-50-M074, Rev. No.: 03 Oct 2011 [16].

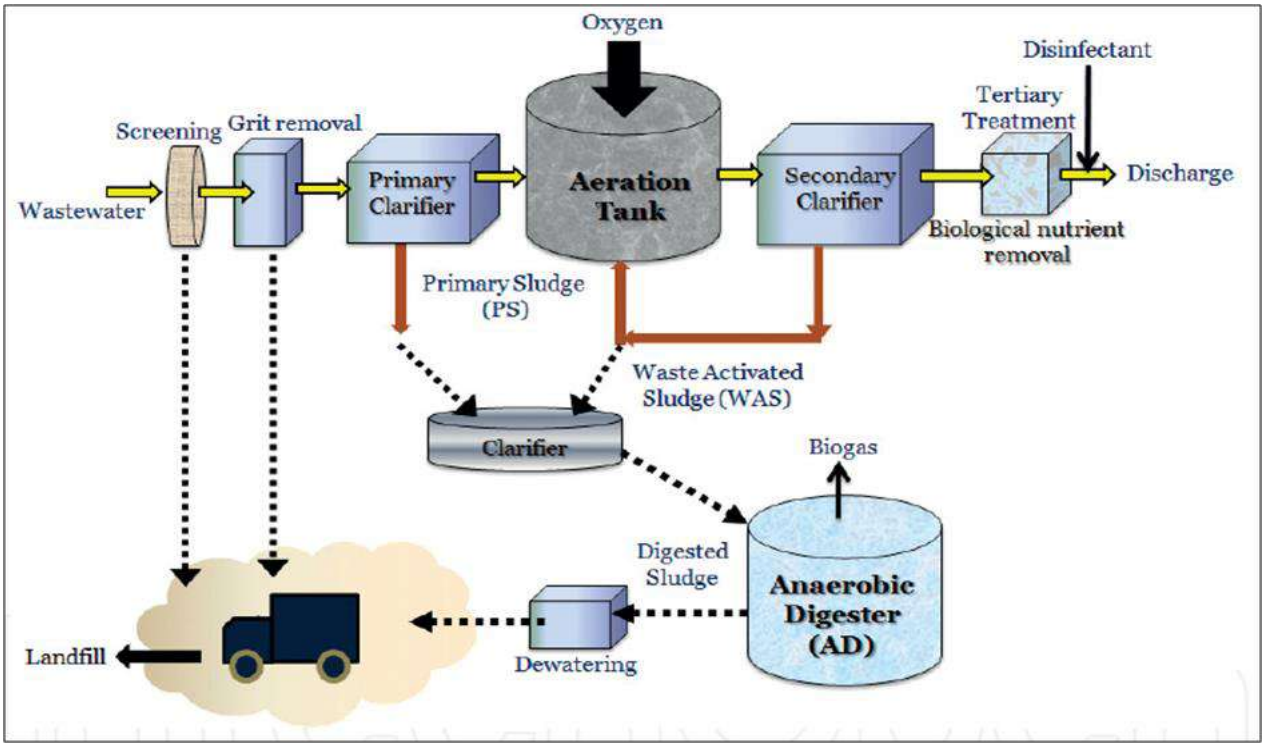

Figure 3. Typical municipal WW treatment processes Elbeshbishy and Okoye [22].

moving bed biofilm reactor, and dilution technique) were studied for treatment of EMWW [2, 8, 20, 21]. To date, treatment of EMWW using solar energy was not studied in Erbil City.

3.3. EMWW Treatment Using Solar Energy

WW treatment methods could be categorized into three groups: biological, chemical, and mechanical. They are

applied in different combinations based on the concentration and type of pollutants. The most abundant renewable energy source is solar energy, which can be introduced into WWTPs. The use of solar thermal energy in WW treatment mostly consists of three aspects: (a) the solar heat is accumulated by a heat collector to improve the treatment efficiency and enhance the reaction temperature [23]; (b) In industrial WW treatment, solar thermal is being used to dewater sludge or lowering water contents of particular unique effluent [24, 25]; and (c) the solar heat can be applied for desalination and evaporation of specific wastewater in industrial WW treatment [26].

3.3.1. Solar Distillation and Desalination of WW

Water distillation is a common physical or mechanical separation technique that is obtained through condensation and evaporation processes. Solar distillation includes using solar energy to obtain distillation. A solar collector in simple solar water stills traps the solar radiation and converts it to heat. Then it is applied to evaporate the water contained in the distillation chamber of the still. As a result of saturation in the chamber, the evaporated water condenses on the trapping side. On this side, the condensed water goes through a funnel-shaped hopper to the distillate storage tank. Solar distillation can be applied to make salty water potable [9].

3.3.2. Photoelectric or Photovoltaic (PV) Energy

Solar PV power generation is a technique to convert light energy into electric energy using semiconductor materials. Solar energy conversion efficiency improvement and the decreasing the solar panel cost, PV can be used more. Various WWTPs apply PV to supply electricity to the treatment plant due to their aeration tanks [27].

Solar energy disinfection mostly employs ultraviolet (UV) rays of sunlight for killing bacteria in wastewater. It should be noticed that PV power generation mostly employs visible light. Therefore, some WWTPs combine PV power generation with UV disinfection. In artificial solar wetlands that are powered by solar heat or PV, wastewater is discharged into the wetland for biological and physical treatment [28].

3.3.3. Photocatalytic energy (UV)

Another usage of solar energy in WW treatment is using solar UV radiation for photocatalytic oxidation. Photocatalysis is the combination of catalysis and photochemistry. It is a procedure that catalysis and light is applied to accelerate or promote a chemical reaction at the same time. It can be defined as the acceleration caused by the catalyst of a light-induced reaction [29]. Photocatalysis appears as a great tool for final treatments of samples including persistent organic pollutants. The view of a typical solar photo Reactor is shown in Figure 4.

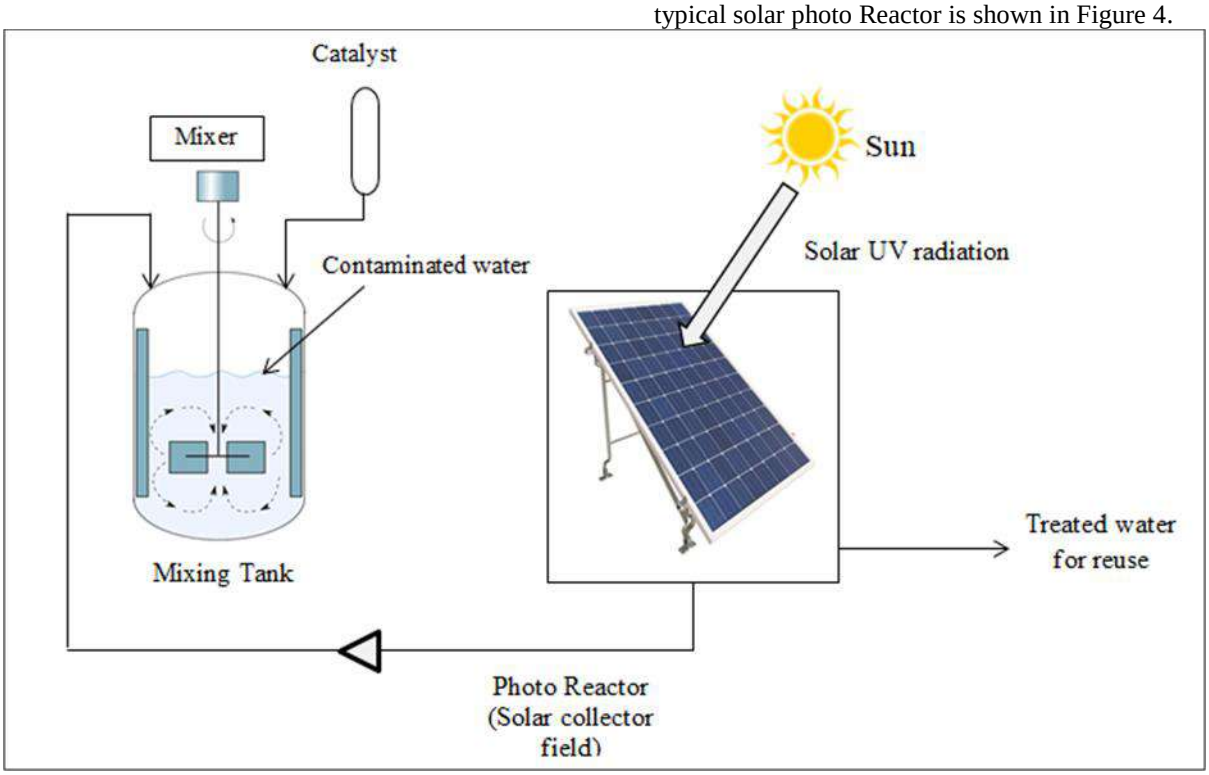

Figure 4. solar photocatalytic plants for the treatment of wastewater taken from Ugwuishiwu et al. [9].

Table 2.
WW treatment by solar energy process

No.	Type of WW	Removal Efficiency (%)	References	years
1	grey water	80 – 90 %	Mahdi et al. [30]	2021
2	WW containing chlorophenol	91 %	Jbari and Abderafi [31]	2020
3	Municipal WW	60 – 90 %	Sun et al. [27]	2019
4	Municipal WW	87 %	Sacco et al. [32]	2018
5	Municipal WW	80 %	Gurung et al. [33]	2018
6	Sewer WW	80 %	Vaccari et al. [34]	2018
7	Municipal WW	85 - 99 %	Taha and Al-Sa'ed [35]	2017
8	Municipal WW	84 %	Xu et al. [36]	2017
9	Municipal WW	79.5 %	Yan et al. [37]	2017
10	Sewer WW	56–72 %	Ni et al. [38]	2016
11	Winery WW	80 %	Velegraki and Mantzavinos [39]	2015
12	Municipal WW	96 %	Shen et al. [40]	2015
13	subsurface agricultural drainage water	85 %	Stuber et al. [41]	2015
14	Olive mill WW	87.3 %	Michael et al. [42]	2014
15	Synthetic wool dying WW	75 - 79 %	Hernandez- Rodriguez et al. [43]	2014
16	Municipal WW	75 %	Sobańtka, and Rechberger [44]	2013
17	Municipal WW	97 %	Mo and Zhang [45]	2013
18	Municipal WW	93.5 %	Chae and Kang[46]	2013
19	Municipal WW	35 - 77 %	Sousa et al. [47]	2012
20	Drinking water with pesticides spike	90 %	Fenoll et al. [48]	2012
21	Municipal WW	85 %	Miranda-Garcia et al. [49]	2011
22	Commercial azo dye Solution WW	80 %	Zayani et al. [50]	2009

3.3.4. WWs treatment by solar energy process

In literature, solar energy was applied for treatment of various types of WWs. Table 2 illustrates WWs treatment by solar energy process.

3.4. Application of solar energy for EMWW treatment

Kurdistan's geographical function on this planet gave it the proper state of affairs concerning the sun's electricity

Table 3.
Results of WW treated by solar energy system Mahdi et al. [30]

Parameters	Concentration before treatment mg/l	Concentration after treatment mg/l	Concentration range for irrigation mg/l
Chemical oxygen demand (COD)	900-1330	30-90	100
Biochemical oxygen demand(BOD_5)	270-390	11-30	40
Total nitrogen (TN)	50-65	5-9	
total natural carbon (TOC)	170-200	10-30	19-180
Ammonia (NH_3)	40-45	Nil	5
total suspended solids (TSS)	310-380	Nil	30-60

potential. The province located between 34° 42' N and 37° 22' N latitudes, which is highly rich in solar energy and utilizing solar energy applications reduce the dependence on fossil fuels and protects the environment from pollution and keeps it clean [51]. Solar energy capacity for the place may be evaluated via way of means of annual sun radiation as the common for Kurdistan place is 6318.83 MJ/ m2 / year and equal to 1755.23 kWh/m²/year, which is '4.81 kWh/m²/day' [52].

In the last years a research has been published in Iraq and they have benefited from solar energy for WW treatment, like Mahdi et al. [30] consider the overall performance of recycling solar-powered grey water treatment machines for the intent of irrigation, used to reduce the quantity of waste grey water and decrease power intake and decrease the fees of constructing huge-scale water treatment plants. Maximum efficiency values got at the stages treatment are COD (90%-97%), BOD5 (89%-97%), TOC (80%-94%), and TN (84%-92%) and the concentration of pollution materials before and after treatment are shown in Table 3, that's why they appear that this system will reuse almost 70% of the water that can be released into the drains that can be utilized after being treated for irrigation, car wash, and in bathrooms.

3.5. Reusing

WW reuse after proper treatment can successfully help resolve the emergency situations that may occur in areas with inadequate water resources. Industrial, municipal, and household drains can be recycled. Reuse is permitted, provided that complete environmental safety is ensured (without harm to the existing cultural plants, soil, and ecosystem), and that any health hazards to the local population are eliminated. This needs strict adherence to existing health and safety regulations and also current laws for agriculture and industry [53]. Generally, reusing municipal WW can be categorized as indirect and direct reuse. Direct reuse of treated wastewater for drinking water is not currently a viable option because of health risks. Indirect reuse is using treated wastewater after returning it to natural water sources (i.e. aquifer, lake, and river) for dilution and purification. It consists of natural buffers for further spatial and temporal separation of treatment [54].

Investigators described that Erbil City's wastewater became now no longer secure for all kinds of irrigation earlier than treatment. They found that EMWW is proper for cooked vegetables and for irrigating green areas and [3]. Also, Aziz et al. [6] investigated on fresh wastewater samples had been gathered from Yörüksüt Dairy Factory and Erbil Steel Company and evaluated for 21 water pleasant parameters like COD, BOD5, TSS, etc. were surpassed the standards for removal of wastewater. Therefore, treatment methods are vital for the previous disposal of wastewater to the surroundings or the use for irrigation objectives. Assembled at the functions of the wastewaters, the treatment methods together with primary, secondary and tertiary have been examined. Also, the great of uncooked wastewater samplings and suggested handled business wastewater have been in comparison with the irrigation recommendations (WHO, 2005) so it can be suitable for irrigation aim. Additionally, Aziz [2] aimed to study features variants of EMWW, suitable treatment the usage of separate methods, and the suitability of the handled wastewater WW for disposal to the herbal surroundings or use for irrigation objectives. Treatment of EMWW the usage of each number one gadgets and wetland brought about elimination performance of 94.75 %, 93.07 %, 89.47 %, 96.72 %, and 57.68 % for BOD5, COD, NH3-N, TSS and PO4, respectively which resulted the disposed discharges features to be within WW criteria. Hence, handled EMWW may be used for cooked greens and watering inexperienced areas.

3.6. Sustainably and Management of EMWW

Waste management and sustainably are the procedure and practice or the administration of activities that provide for the disposal, treatment, processing, transfer, transportation, storage, separation, and collection of waste [55]. The generation of waste cannot be totally eliminated; neither can waste recycling be achieved completely. So there is always the need for waste management. The concept of waste management becomes very important

because of the need to prohibit the contact between waste and humans and protect the immediate environment and safeguard community, families, and individual health. Suitable management of waste adds to the aesthetic value of the environment which is very vital for psychological, social and emotional well-being. The concept of waste management is highly dependent on the form of waste. Many researches have been done on sustainably and management in Iraq for WW, for instant Mustafa et al. [56] assessed the sustainability of the amount and great of water reassess for Erbil City and maintain security and steady primarily based totally on the evaluation with the usual limitations. In addition, Omran et al. [57] demonstrated that the sustainability of wastewater treatment is directly associated with the four dimensions in Iraq (technical, economic, social, environmental). Also, Alanbari and Muter [58] by using software programs designed to assess environmental sustainability indicators for any WW treatment plant.

4. CONCLUSION

This research highlights using of solar energy WW treatment as in Photovoltaic (PV) Energy, photocatalytic energy (UV), solar desalination and distillation for WW treatments. The application of solar energy in the management of WW guarantee the water availability for different industrial and agricultural goals and decreases pathogenicity through deactivating disease causing organisms in water for domestic purposes.

EMWW contains parameters such as BOD_5, COD, TSS etc. surpassed the WW disposal standards. Accordingly, Treatment is crucial before disposal to the environment, water resources, or reusing. EMWW regarded as weak WW. Solar energy method was effectual in removal of (80-98) % of BOD_5, (75-95) % COD, and (85-98) % of TSS. It is economic and easy method for treatment and reusing EMWW.

Conflicts of Interest

The authors declare that there are no conflicts of interest regarding the publication of this paper.

Acknowledgement

The authors would like to acknowledge Salahaddin University-Erbil for providing the grant of the research grant to conduct this work.

References

[1] Mustafa, Basil Y., and Shahin Sabir. "Reuse of Erbil city sewage for irrigation purposes." Sci. Conf. of Water-Erbil. J. Brayeti-Cent. Vol. 18. 2001.

[2] Aziz, Shuokr Qarani. "Variation of Erbil municipal wastewater characteristics throughout 26 years (1994-2020) with possible treatments and reusing: A review." IOP Conference Series: Materials Science and Engineering. Vol. 978. No. 1. IOP Publishing, 2020.

[3] Amin, K. N., and Sh Q. Aziz. "Feasibility of Erbil wastewater reuse for irrigation." Zanco 17.2 (2005): 63-77.

[4] Shekha, Yahya Ahmed. "The effect of Erbil city wastewater discharge on water quality of Greater Zab river, and the risks of irrigation." PhD, university of Baghdad (2008).

[5] Aziz, S. Q., and S. M. Ali. "Characteristics and potential treatment technologies for different kinds of wastewaters." Zanco Journal of Pure and Applied Science 30.1 (2018).

[6] Aziz, Shuokr Qarani, Shawnm Mudhafar Saleh, and Imad Ali Omar. "Essential treatment processes for industrial wastewaters and reusing for irrigation." Zanco Journal of Pure and Applied Sciences 31.s3 (2019): 269-275. http://dx.doi.org/10.21271/zjpas

[7] Aziz, Shoukr Qarani, and Enas Sa'ad Fakhrey. "Optimization of aeration style and cycle time for treatment of oil refinery wastewater using powdered activated carbon and sequential batch reactor." ZANCO Journal of Pure and Applied Sciences 29.1 (2017).

[8] Aziz, Shuokr Qarani, et al. "Stage by stage design for primary, conventional activated sludge, SBR and MBBR units for residential wastewater treatment and reusing." Advances in environmental research 9.4 (2020): 233-249. https://doi.org/10.12989/aer.2020.9.4.233

[9] Ugwuishiwu, B. O., I. P. Owoh, and I. J. Udom. "Solar energy application in waste treatment-a review." Nigerian Journal of Technology 35.2 (2016): 432-440. http://dx.doi.org/10.4314/njt.v35i2.27

[10] Zhang, Ying, et al. "Application of solar energy in water treatment processes: A review." Desalination 428 (2018): 116-145. https://doi.org/10.1016/j.desal.2017.11.020

[11] Guo, Ziyang, et al. "Integration of green energy and advanced energy-efficient technologies for municipal wastewater treatment plants." International journal of environmental research and public health 16.7 (2019): 1282. https://doi.org/10.3390/ijerph16071282

[12] Kretschmer, Florian, et al. "Wastewater treatment plants as local thermal power stations—modifying internal heat supply for covering external heat demand." Processes 9.11 (2021): 1981. https://doi.org/10.3390/pr9111981

[13] Nwokoye, A. O. C., and L. Ezenwaka. "A functional 1.5 kva electricity power generation using solar photovoltaic system." UNIZIK Journal of Engineering and Applied Sciences 4.1 (2008): 52-57.

[14] Metcalf, E., & Eddy, E., Wastewater engineering: treatment and reuse. McGrawHill. Inc., London, (2014),

[15] Environment Protection Agency (EPA) (2003), Standards for effluent discharge, Regulations. General Notice No.44. The Environmental Protection Act 2002. Regulations made by the Minster under section 39 and 96 of the Environmental Protection Act 2002.

[16] Iraqi Environmental Standards, Contract No.: W3QR-50-M074, Rev. No.: 03Oct. Morning Star for General Services, LLC Iraq, West Qurna I Project, EXHIBIT Eight, (2011).

[17] Zhou, Guang-Jie, et al. "Simultaneous removal of inorganic and organic compounds in wastewater by freshwater green microalgae." Environmental Science: Processes & Impacts 16.8 (2014): 2018-2027.

[18] Gedda, Gangaraju, et al. "Antibacterial effect of calcium oxide nano-plates fabricated from shrimp shells." Green Chemistry 17.6 (2015): 3276-3280.
[19] Chan, Yi Jing, et al. "A review on anaerobic–aerobic treatment of industrial and municipal wastewater." Chemical engineering journal 155.1-2 (2009): 1-18. https://doi.org/10.1016/j.cej.2009.06.041
[20] Aziz, Shuokr Qarani, and Sazan Mohammed Ali. "Characterization of municipal and dairy wastewaters with 30 quality parameters and potential wastewater treatment by biological trickling filters." International Journal of Green Energy 14.13 (2017): 1156-1162. https://doi.org/10.1080/15435075.2017.1370594
[21] Aziz, Shuokr Qarani A., and Sardar Mamand B. Bruska. "Applying mass balance dilution technique for wastewater disposal to Greater-Zab river in Erbil, Kurdistan region-Iraq." Recycling and Sustainable Development 14.1 (2021): 31-39.
[22] Elbeshbishy, Elsayed, and Frances Okoye. "Improper disposal of household hazardous waste: Landfill/municipal wastewater treatment plant." Municipal Solid Waste Management 183 (2019).
[23] Mahmoodi, Vahid, Tahereh Rohani Bastami, and Ali Ahmadpour. "Solar energy harvesting by magnetic-semiconductor nanoheterostructure in water treatment technology." Environmental Science and Pollution Research 25 (2018): 8268-8285. https://doi.org/10.1007/s11356-018-1224-y
[24] Rodríguez, R., et al. "Life cycle assessment and techno-economic evaluation of alternatives for the treatment of wastewater in a chrome-plating industry." Journal of Cleaner Production 172 (2018): 2351-2362. https://doi.org/10.1016/j.jclepro.2017.11.175
[25] Qarani, Aziz Shuokr, and Mustafa Jwan Sabah. "Wastewater sludge characteristics, treatment techniques and energy production." Recycling and Sustainable Development 15.1 (2022): 9-26. https://doi.org/10.3390/su142215398
[26] Deng, Yaocheng, et al. "Facile fabrication of mediator-free Z-scheme photocatalyst of phosphorous-doped ultrathin graphitic carbon nitride nanosheets and bismuth vanadate composites with enhanced tetracycline degradation under visible light." Journal of colloid and interface science 509 (2018): 219-234. https://doi.org/10.1016/j.jcis.2017.09.016
[27] Sun, Yongteng, et al. "Application and evaluation of energy conservation technologies in wastewater treatment plants." Applied Sciences 9.21 (2019): 4501. https://doi.org/10.1016/j.jcis.2017.09.016
[28] Drouiche, Nadjib, et al. "Photovoltaic solar cells industry wastewater treatment." Desalination and Water Treatment 51.31-33 (2013): 5965-5973. https://doi.org/10.1080/19443994.2012.763217
[29] Oliveira, Anabela, et al. "Solar photochemistry for environmental remediation-advanced oxidation processes for industrial wastewater treatment." Molecular Photochemistry-Various Aspects. Rijeka: InTech (2012): 195-223.
[30] Mahdi, Hashim A., et al. "Design and Performance Investigation of a Solar-Powered Biological Greywater Treatment System in the Iraqi Climate." Baghdad Science Journal 19.3 (2022): 0670-0670.
[31] Jbari, Yousra, and Souad Abderafi. "Parametric study to enhance performance of wastewater treatment process, by reverse osmosis-photovoltaic system." Applied Water Science 10.10 (2020): 1-14. https://doi.org/10.1007/s13201-020-01301-4
[32] Sacco, Olga, et al. "Photocatalytic activity of a visible light active structured photocatalyst developed for municipal wastewater treatment." Journal of Cleaner Production 175 (2018): 38-49.
[33] Gurung, Khum, Walter Z. Tang, and Mika Sillanpää. "Unit energy consumption as benchmark to select energy positive retrofitting strategies for Finnish wastewater treatment plants (WWTPs): a case study of Mikkeli WWTP." Environmental Processes 5.3 (2018): 667-681. https://doi.org/10.1007/s40710-018-0310-y
[34] Vaccari, M., et al. "Benchmarking of energy consumption in municipal wastewater treatment plants–a survey of over 200 plants in Italy." Water Science and Technology 77.9 (2018): 2242-2252. https://doi.org/10.2166/wst.2018.035
[35] Taha, Manal, and Rashed Al-Sa'ed. "Potential application of renewable energy sources at urban wastewater treatment facilities in Palestine: three case studies." (2017). http://hdl.handle.net/20.500.11889/5310
[36] Xu, Jin, et al. "Exploring the feasibility of energy self-sufficient wastewater treatment plants: a case study in eastern China." Energy Procedia 142 (2017): 3055-3061. https://doi.org/10.1016/j.egypro.2017.12.444
[37] Yan, Peng, et al. "Net-zero-energy model for sustainable wastewater treatment." Environmental science & technology 51.2 (2017): 1017-1023. https://doi.org/10.1021/acs.est.6b04735
[38] Ni, Long, et al. "Experimental study of the separation performance of a novel sewage hydrocyclone used in sewage source heat pump." Applied Thermal Engineering 106 (2016): 1300-1310. https://doi.org/10.1016/j.applthermaleng.2016.06.093
[39] Velegraki, T., and D. Mantzavinos. "Solar photo-Fenton treatment of winery effluents in a pilot photocatalytic reactor." Catalysis Today 240 (2015): 153-159. https://doi.org/10.1016/j.cattod.2014.06.008
[40] Shen, Yanwen, et al. "An overview of biogas production and utilization at full-scale wastewater treatment plants (WWTPs) in the United States: challenges and opportunities towards energy-neutral WWTPs." Renewable and Sustainable Energy Reviews 50 (2015): 346-362. https://doi.org/10.1016/j.rser.2015.04.129
[41] Stuber, Matthew D., et al. "Pilot demonstration of concentrated solar-powered desalination of subsurface agricultural drainage water and other brackish groundwater sources." Desalination 355 (2015): 186-196. https://doi.org/10.1016/j.desal.2014.10.037
[42] Michael, I., et al. "Utilizing solar energy for the purification of olive mill wastewater using a pilot-scale photocatalytic reactor after coagulation-flocculation." Water research 60 (2014): 28-40. https://doi.org/10.1016/j.watres.2014.04.032
[43] Hernández-Rodríguez, M. J., et al. "Treatment of effluents from wool dyeing process by photo-Fenton at solar pilot plant." Journal of Environmental Chemical Engineering 2.1 (2014): 163-171. https://doi.org/10.1016/j.jece.2013.12.007
[44] Sobańtka, A., and H. Rechberger. "Extended statistical entropy analysis (eSEA) for improving the evaluation of Austrian wastewater treatment plants." Water Science and Technology 67.5 (2013): 1051-1057. https://doi.org/10.2166/wst.2013.665
[45] Mo, Weiwei, and Qiong Zhang. "Energy–nutrients–water nexus: Integrated resource recovery in municipal wastewater treatment plants." Journal of environmental management 127 (2013): 255-267. https://doi.org/10.1016/j.jenvman.2013.05.007
[46] Chae, Kyu-Jung, and Jihoon Kang. "Estimating the energy independence of a municipal wastewater treatment plant incorporating green energy resources." Energy Conversion and Management 75 (2013): 664-672. https://doi.org/10.1016/j.enconman.2013.08.028
[47] Sousa, M. A., et al. "Suspended TiO2-assisted photocatalytic degradation of emerging contaminants in a municipal WWTP effluent using a solar pilot plant with CPCs." Chemical Engineering Journal 198 (2012): 301-309. https://doi.org/10.1016/j.cej.2012.05.060
[48] Fenoll, José, et al. "Photodegradation of eight miscellaneous pesticides in drinking water after treatment with semiconductor materials under sunlight at pilot plant scale." Chemical engineering journal 204 (2012): 54-64. https://doi.org/10.1016/j.cej.2012.07.077
[49] Miranda-García, Norma, et al. "Photocatalytic degradation of emerging contaminants in municipal wastewater treatment plant effluents using immobilized TiO2 in a solar pilot plant." Applied

Catalysis B: Environmental 103.3-4 (2011): 294-301. https://doi.org/10.1016/j.apcatb.2011.01.030

[50] Zayani, Ghanem, et al. "Solar photocatalytic degradation of commercial textile azo dyes: Performance of pilot plant scale thin film fixed-bed reactor." Desalination 246.1-3 (2009): 344-352. https://doi.org/10.1016/j.desal.2008.03.059

[51] Qadir, Karwan Wasman, and Mohammed Aziz Saeed. "Study and analysis of global and extraterrestrial solar radiation over Kurdistan Region-Iraq." 3rd International Scientific Conference of Salahaddin University-Erbil. 2011.

[52] Abdul-Wahid, Sahib Neamh, Ali Mahdy, and Hassan Abbas Godu. "Calculation and applications of net solar radiation in Iraq." Journal of Al-Qadisiyah for Pure Science 15.1 (2010): 1-30.

[53] Abdelrahman, Rasha M., Sameh E. Khamis, and Zeinelabidin E. Rizk. "Public attitude toward expanding the reuse of treated wastewater in the United Arab Emirates." Environment, Development and Sustainability 22.8 (2020): 7887-7908. https://doi.org/10.1007/s10668-019-00551-w

[54] Cirelli, Guiseppe L., et al. "Treated municipal wastewater reuse in vegetable production." Agricultural Water Management 104 (2012): 163-170. https://doi.org/10.1016/j.agwat.2011.12.011

[55] Pradhan, Upendra Mani. "Sustainable solid waste management in a mountain ecosystem: Darjeeling, West Bengal, India." (2009).

[56] Omran, Isam I., et al. "Sustainability assessment of wastewater treatment techniques in urban areas of Iraq using multi-criteria decision analysis (MCDA)." Water Practice & Technology 16.2 (2021): 648-660.

[57] Al-anbari, Mohammad Ali, and Mais Salim Muter. "Evaluation of Environmental Sustainability Indicators of Northern Rustimeh Wastewater Treatment Plant in Baghdad, Iraq, Using Simapro7. 1 Program." Journal of Engineering and Sustainable Development 22.5 (2018): 188-199. https://doi.org/10.2166/wpt.2021.013

[58] Mustafa, Basil Y., and Shahin Sabir. "Reuse of Erbil city sewage for irrigation purposes." Sci. Conf. of Water-Erbil. J. Brayeti-Cent. Vol. 18. 2001. https://doi.org/10.31272/jeasd.2018.5.14

J-Researchers

Journal of Civil Engineering Researchers

Journal homepage: www.journals-researchers.com

Numerical Investigation of the Beam Web Weakening Pattern Impact On the Seismic Behavior of the Steel Beam-Column Connection

Reza Molavi,[a,*]

[a] *Department of Civil Engineering, Chalous Branch, Islamic Azad University , Chalous, Iran*

ABSTRACT

Due to the damage that occurred in the unreinforced welded flange (WUF) connections during the 1994 Northridge earthquake, the use of reduced beam section (RBS) connections and subsequently the reduced web section (RWS) connections became common to prevent premature brittle failure in the welded connections. The RWS connections are created to provide a controlled weak point for the formation of a plastic hinge, which can prevent stress concentrations in the groove welds of the connection. This method, where the transfer of the plastic hinge is achieved by weakening the beam web and without the need to remove the concrete slab, is proposed as a suitable solution for the rehabilitation of connections. In this paper, the effect of different beam web weakening patterns on the seismic performance of the connection is investigated analytically and numerically. Seven beam web weakening designs were studied and compared with the uniform web slotting pattern, and the seismic behavior of the mentioned connections was simulated using the Abaqus software, and the effect of using each of them on the distribution of equivalent plastic strains and the moment-rotation curve was examined. The results showed that the appropriate beam web weakening pattern plays an effective role in reducing the plastic strain in the penetration weld of the direct beam-to-column connection and preventing their premature tearing and failure, so that one of the perforation designs studied can reduce the maximum equivalent plastic strain in the upper penetration weld of the direct beam-to-column connection by an average of 48% compared to the uniform web slotting pattern as the reference connection.

ARTICLE INFO

Received: May 29, 2024
Accepted: June 26, 2024

Keywords:
Beam-to-column connection
Seismic rehabilitation
Reduced beam section
Reduced web section connection
Finite element method

DOI: 10.61186/JCER.6.2.60
DOR: 20.1001.1.2538516.2024.6.2.6.7

1. Introduction

The Northridge earthquake that occurred on January 17, 1994, in California, led to brittle and premature failures and lack of ductility in the welded unreinforced flange (WUF) beam-to-column connections, as shown in Figure 1. The most common damage originated from fractures in the complete joint penetration (CJP) weld of the beam flange to the column or in the vicinity of the connection. Consequently, after the Northridge earthquake, research progressed towards increasing the ductility of rigid connections, and the post-Northridge connections were developed. In these connections, the main objective is to transfer the plastic hinge into the beam and at a certain distance from the column face, as this transfer of the plastic hinge from the column face reduces the concentration of

* Corresponding author. Tel.: +989123889252; e-mail: reza.molavi22@gmail.com.

strain in the weld region, thereby reducing the degree of weld cracking and brittle failure in the connection.

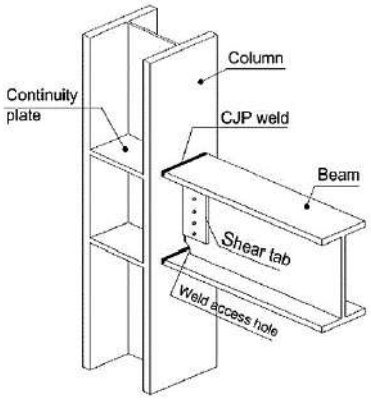

Figure 1. Example of conventional connection in Northrich [1]

Various methods have been proposed for the transfer of the plastic hinge, which are generally classified into two main categories: connection reinforcement and beam weakening. In the connection reinforcement method, with the aim of preventing premature failures, by adding components to the existing connection, a stronger connection than the beam is created, and the plastic hinge is formed in the beam and away from the column face, preventing the beam rotation relative to the column to reduce the stress in the weld region. Examples of this category include the use of local flange reinforcement, reinforcing the connection joint by adding components such as various stiffeners [2-7]. The use of the connection reinforcement method can significantly reduce the stress in the connection and is an effective rehabilitation technique for increasing the ductility of rigid connections. However, despite the mentioned advantage, it often requires costly and difficult welding operations.

The second category is the reduced beam section (RBS) method, where the beam section is weakened at a specific and predetermined location with the aim of forming a plastic hinge in that region, to reduce the stress levels in the vicinity of the beam flange-to-column groove welds. This method has been able to address the deficiencies of the pre-Northridge connections to a considerable extent. Given that this method can reduce the stress demand in the areas near the weld and connection components, including the connection source, weld, bolts, and so on, it has received much attention and research, and various methods have been proposed for its implementation, mainly through the creation of different shapes of cuts, slots, and holes in the beam flange at a suitable distance from the column face or the use of various replaceable reduced sections [7-19].

Another method of beam weakening to improve the performance of steel connections is the heat-treated beam section (HBS) method, which was recently proposed by Morrison et al. in 2015. This method involves the application of a specific heat treatment process to a defined range of the beam flanges using specialized pads. This heat treatment process reduces the yield strength of the steel and, consequently, the strength in the heat-affected zone, leading to the transfer of the plastic hinge onto the beam [20-23]. Another method for creating a reduced beam section is the slotted-flange (DF) connection, where a series of holes are created on the beam flanges instead of cutting the flanges, creating a controlled weak zone for the formation of the plastic hinge to reduce the stress concentration in the beam flange-to-column welds [24-28].

Since the flanges are the main components of the beam for resisting bending, some researchers have proposed the reduced web section (RWS) method, which is generally achieved through web cutting and creating holes in the web with different geometric shapes, such as circular, elliptical, semi-circular, or rectangular [29-36], replacing the flat web with different sections such as accordion-like or tubular [37-39], or using replaceable reduced sections [40-42], as an alternative approach to reducing the beam section. The use of RWS connections has recently gained particular attention, especially for steel moment frames in existing buildings, as the reduction of the beam section through flange cutting is accompanied by the difficulty of cutting the upper part of the beam flange due to its location in the floor slab. Therefore, in this aspect, RWS connections are more practical when used as a rehabilitation technique [41-42].

In the present study, with the aim of investigating the cyclic behavior and performance of other RWS connection designs, after the validation of the finite element model, seven non-uniform beam web weakening patterns are proposed and compared against the uniform vertical slotting pattern (RWS-1) to evaluate their influence on the cyclic behavior of the beam-to-column connection through analytical and finite element modeling.

2. Beam Web Weakening Patterns Investigated

Figure 2 shows the details of the non-uniform RWS-2 to RWS-8 beam web weakening patterns studied to evaluate their impact on the seismic behavior and performance of the beam-to-column connection compared to the uniform web slotting pattern (RWS-1). All these designs result in an equal reduction of the beam cross-section area by 7189 mm².

3. Finite Element Model Validation and Modeling

3.1. Finite Element Modeling of the Connection

To evaluate the impact of the different web reduction patterns on the seismic performance of the connection, the

Abaqus software was used for the three-dimensional modeling and nonlinear analysis of the direct beam-to-column connection with complete joint penetration (CJP) welds. The beam section was taken as 270 IPE with a free span of 1500 mm, and the column section was IPB200 with a free span of 1500 mm. To obtain accurate stress and strain conditions close to the actual conditions, the finite element model components, including the column, beam, doubler plate, and continuity plates, were modeled using shell elements, which have the capability to consider large deformations, nonlinear behavior, and the simulation of buckling and its effects on the reduction of the analytical model's strength. Additionally, the "NLGEOM" option was activated to consider the geometric nonlinearity effects. Rigid shell elements were also used to model the support plates at the two ends of the column and the beam. The steel material was ST37 with the nominal mechanical properties listed in Table 1, with a nonlinear behavior using a combined hardening model that can consider both isotropic and kinematic hardening behavior of the steel.

The loading was applied according to Figure 3, based on the displacement history protocol following the SAC loading protocol [43, 44], through the gradual application of a series of cyclic pseudo-static incremental displacements at the beam tip. To simulate the boundary conditions in the finite element model, including the supports and load application points, a reference point (RP) was first defined on the rigid end plates of the column and beam, and then the corresponding boundary conditions were assigned to this point, as shown in Figure 3.

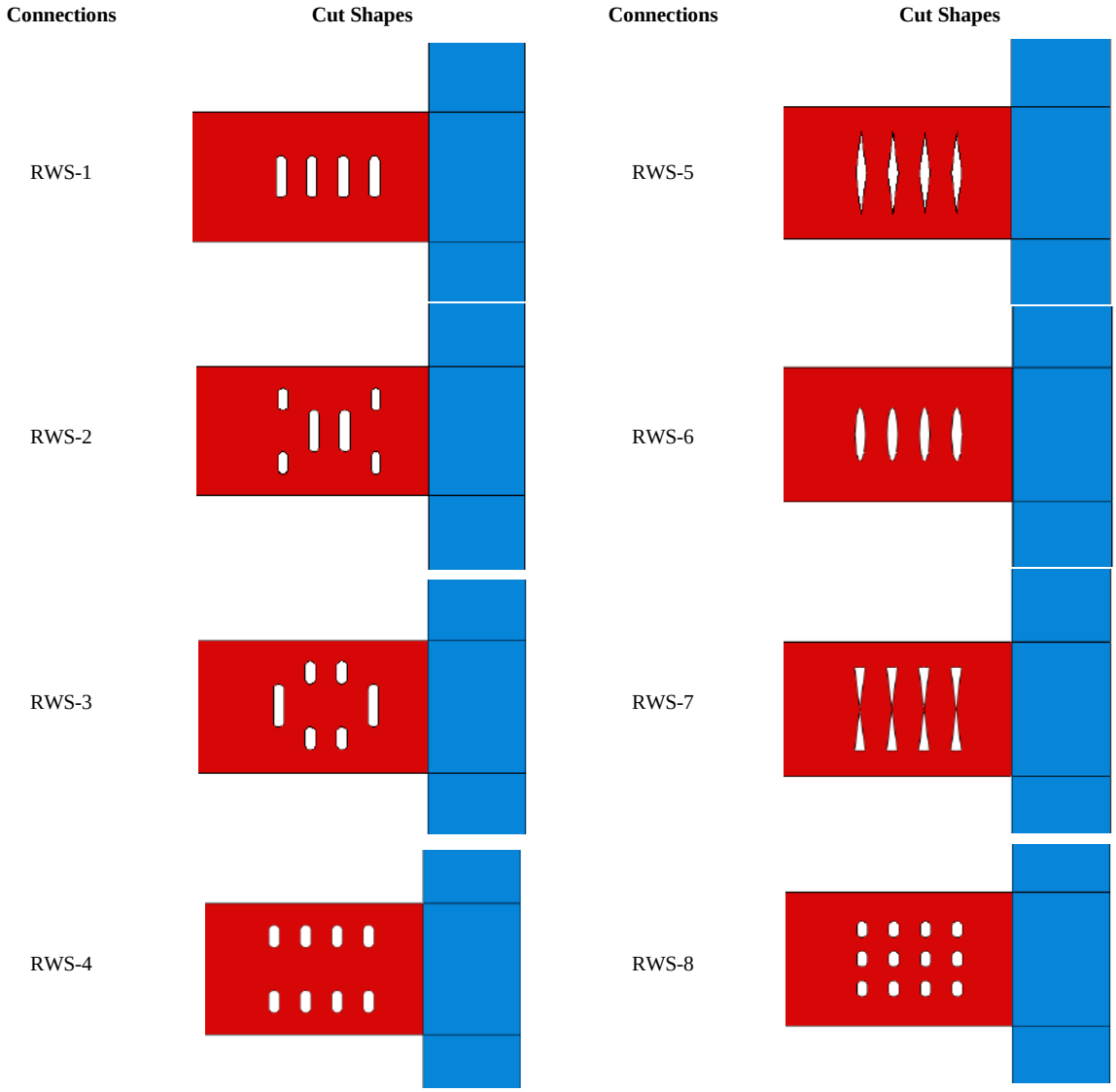

Figure 2. Details of the different web reduction patterns

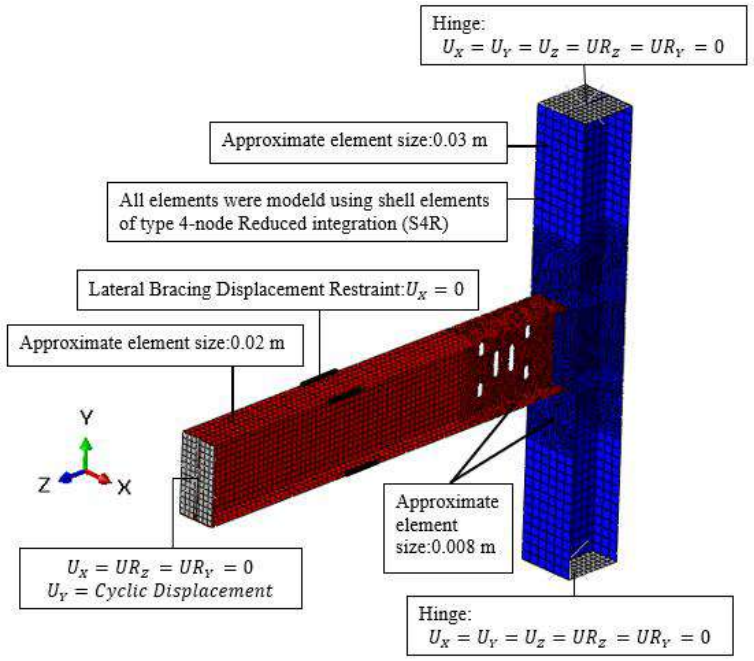

Figure3. 3D FE model for Specimen B3

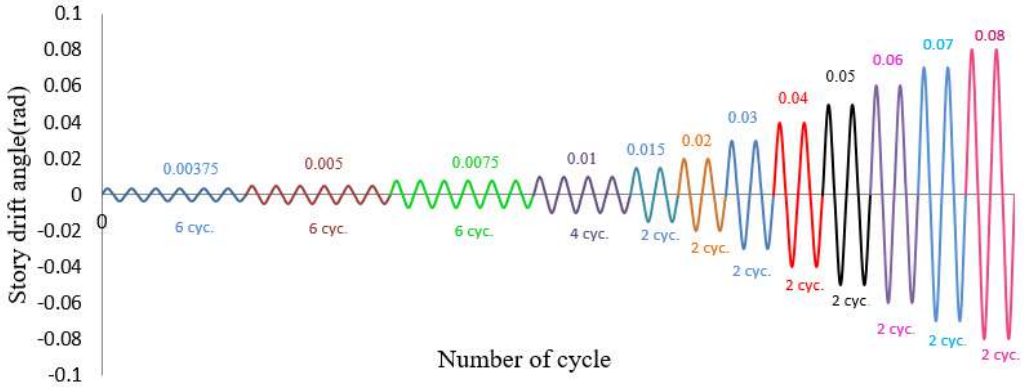

Figure 4. Loading protocol based on FEMA 351 [43, 44]

Additionally, lateral bracing of the beam was modeled to prevent out-of-plane buckling. The meshing of each connection component was performed separately using S4R elements, and a finer mesh was used in the vicinity of the connection, the connection joint, and the web weakened region to provide a more accurate representation of the buckling behavior and the high stress and strain rates in these critical areas. Figure 3 shows a three-dimensional view of the finite element model and the meshing details and boundary conditions for the RWS-1 connection. It should be noted that in this study, the modeling and the influence of factors such as the concrete slabs were neglected, and only the modeling of the steel beam-to-column connection was performed, assuming high-quality complete joint penetration (CJP) welding of the beam to the column, and the weld modeling was not considered, and the beam-to-column connection was modeled directly.

Table2.
Mechanical Properties of Structural Steel – St37[45]

$\sigma_y^{nominal}$	$\sigma_u^{nominal}$	Elongation(%)	E	υ
240 Mpa	360 Mpa	30.8	210 Gpa	0.03

3.2. Model Validation

The overall validity of the finite element modeling approach in Abaqus and the accuracy of the numerical analysis results in predicting the seismic behavior, strength degradation, and stiffness reduction due to the formation of the plastic hinge and the buckling of the connection components are evaluated by comparing the numerical analysis results of the experimental specimen DB700-SW, whose seismic behavior under the SAC loading protocol was investigated in the studies by Lee et al. [46, 47]. Figure 5 shows the geometric details, and Table 2 presents the

material properties used for the construction of the aforementioned model.

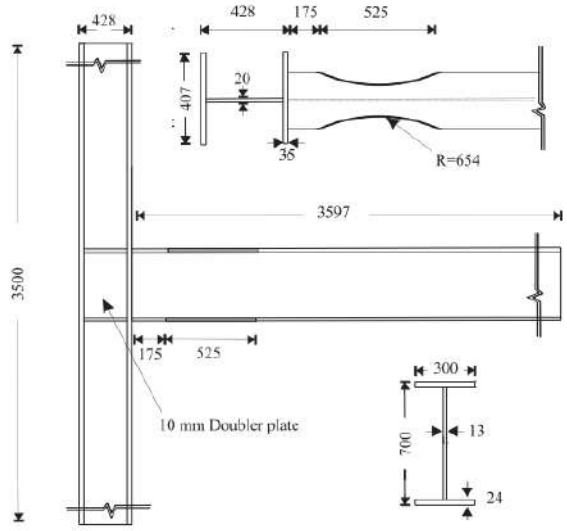

Figure 5. Specimen DB700-SW tested by lee et al(units in mm) [46,47]

Table 2.
Physical properties of the DB700-SW connection materials [47]

Member	Coupon	σ_y	σ_u
Beam (SS400)	Flange	304 Mpa	455 Mpa
	Web	364 Mpa	480 Mpa
Column(SM490)	Flange	343 Mpa	512 Mpa
	Web	358 Mpa	520 Mpa

3.3. Validation Model Analysis Results

After the finite element analysis under cyclic loading, the accuracy of the results is compared with the experimental and numerical results of the DB700-SW connection. As shown in Figure 6, the cyclic response, Bauschinger effect, strain hardening, and strength degradation due to local and torsional buckling obtained from the finite element model of the DB700-SW specimen in the present study show acceptable agreement with the seismic response and deformation of the experimental and finite element reference specimen [44].

4. Finite Element Analysis Results

4.1. Moment-Rotation and Hysteresis Curves

Accepting the von Mises criterion as the basis for evaluating the performance and ultimate failure of the steel, to assess the impact of the different web cutting patterns on the seismic behavior of the connection, the normalized moment-rotation hysteresis curves of the studied connections are compared in Figure 7 up to the end of the loading (6% rotation). The total beam rotation is calculated by dividing the tip displacement at the load application point by the distance to the column center (1600 mm).

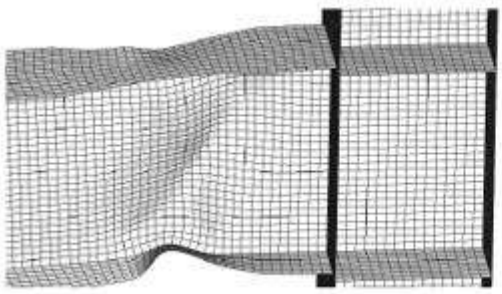

(a) FE[46]

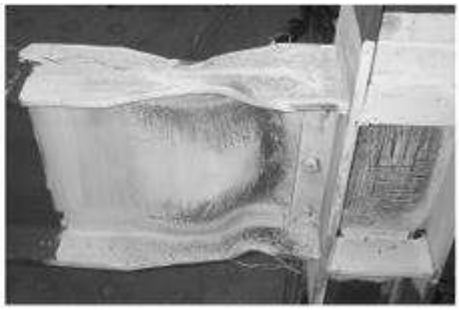

(b) DB700-SW at 6% drift [46]

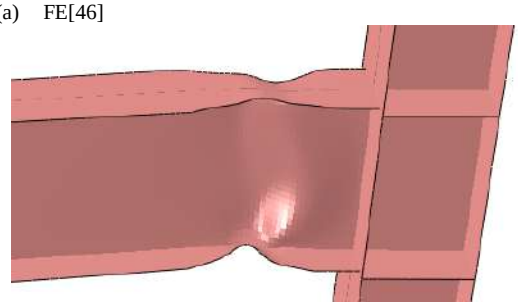

(c) Local buckling of the beam at 6% drift

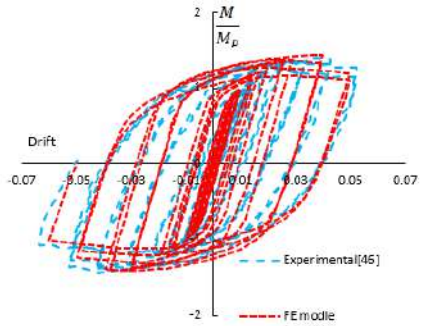

(d) hysteresis response

Figure 6. Comparison of the FE model and test results of specimen DB700-SW tested by lee et al[46].

As observed, although all models exhibit suitable hysteretic behavior, some of these curves are significantly influenced by the beam web weakening patterns. The hysteresis curves show that the connection strength in all models decreases due to the local buckling of the beam. However, this strength reduction is not significant, as the connection strength in all models is still greater than 80% of the beam plastic moment at 4% rotation.

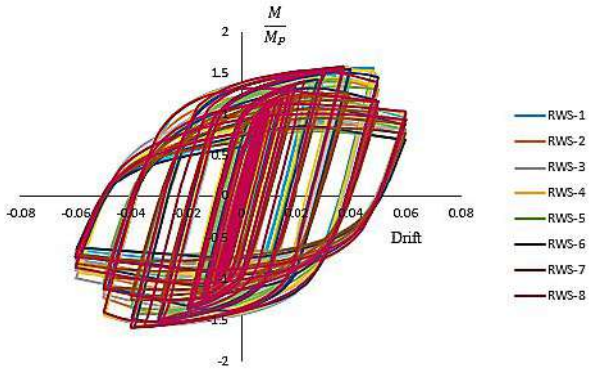

Figure 7. Cyclic moment-rotation curves of the specimens

4.2. Investigation of the Equivalent Plastic Strain Distribution

In the seismic analysis of connections, parameters should be used to identify the potential failure or crack initiation locations. One of the damage indicators used to evaluate the potential for failure and fracture in fillet welds and steel elements is the equivalent plastic strain (PEEQ), which is defined as:

$$PEEQ = \sqrt{\frac{2\epsilon_{ij}^{pl}\epsilon_{ij}^{pl}}{3}} \quad (1)$$

where ϵ_{ij}^{pl} are the plastic strain components in the *i* and *j* directions.

This indicator of energy dissipation during cyclic loading and as a measure of the extent of residual strains in the materials and locations in the connection that are susceptible to tearing and fracture is considered, and it directly represents the degree of progression and expansion of plastic deformations in the connection during cyclic loading. Therefore, in the evaluation and comparison of the changes in plastic strain in different regions of the connection, particularly in the vicinity of the complete joint penetration (CJP) weld to the column, considering the different beam web weakening patterns can also be useful.

In Figures 8 and 9, the distribution of the equivalent plastic strain (PEEQ) for two critical and determinant parts of the connection behavior, namely the fillet welds connecting the beam flanges to the column flanges and the weakened region of the studied connections, were investigated at the end of the loading cycle corresponding to 6% rotation. The selection criteria for the mentioned sections are based on the failure location in the Northridge earthquake connections and the evaluation of the ability of each weakening pattern to transfer and reduce the strain from the column surface to the weakened region.

The results shown in Figure 8 indicate that in terms of reducing the plastic strains in the fillet welds and the potential for connection failure, the weakening pattern (RWS-7) can reduce the equivalent plastic strain in the CJP weld of the direct beam-to-column connection by an average of 48% compared to the uniform web slotting pattern (RWS-1) as the reference connection. In contrast, the (RWS-2) pattern has resulted in an average 42% increase in the equivalent plastic strain in the CJP weld compared to the (RWS-1) connection. The asymmetry of the PEEQ values at the two ends of the weld line in the (RWS-2) connection is also due to the significant increase in beam buckling compared to the other patterns studied. Therefore, the appropriate performance of this type of connection can be expected by selecting a suitable beam web weakening pattern.

Figure 9 also shows that, in terms of the ability of each weakening pattern to transfer and reduce the strain from the column surface to the weakened region, the (RWS-3) pattern has the best performance among the studied patterns in concentrating the plastic strains in the weakened region.

5. Conclusion

Due to the inaccessibility of the top beam flange, which is usually embedded in the concrete slab, and the high cost of slab demolition to cut the top flange, one of the methods for the rehabilitation of existing moment-resisting frame connections is the use of beam web weakening. This research describes the numerical investigation of the cyclic performance of steel beam-to-column connections rehabilitated by the web section reduction method with different patterns. To provide a preliminary evaluation of the behavior of the mentioned connections, seven new web section reduction patterns were considered for finite element modeling in Abaqus, and the effect of their implementation on the changes in the equivalent plastic strain, moment-rotation curves, and the potential for failure were investigated, disregarding the influence of factors such as the presence of concrete slabs. A summary of the results of this study is as follows:

1. The research results showed that the creation of beam web weakening with a suitable pattern can shift the strain concentration region from the CJP weld near the column to the weakened region.

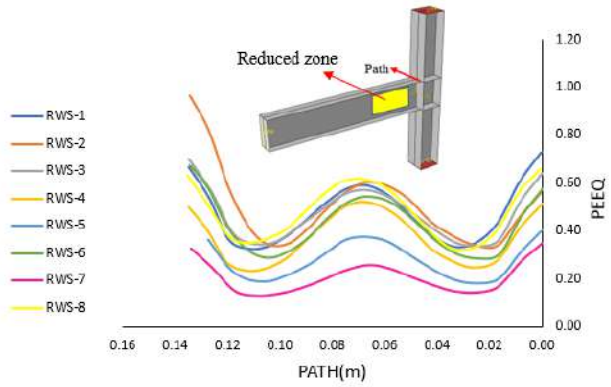

Figure 8. PEEQ strain changes at the end of the loading cycle corresponding to 6% rotation above the weld line

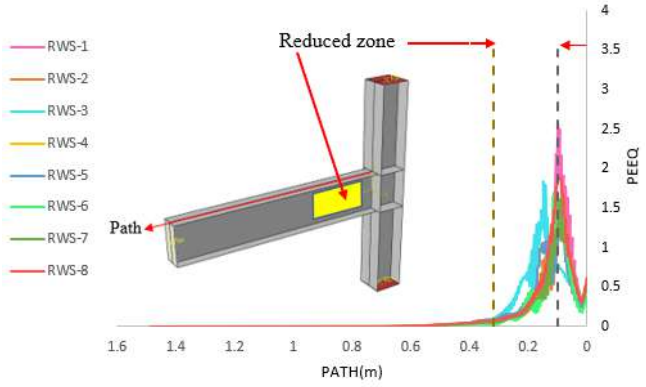

Figure 9. PEEQ strain changes at the end of the loading cycle corresponding to 6% rotation along the central axis of the beam wing

2. The investigations showed that the connection with the web weakened in a suitable pattern can reduce the equivalent plastic strain in the beam-to-column CJP weld by 48% compared to the reference analytical specimen.

Despite the above results, it should be noted that further research and studies are necessary to identify the behavior of the mentioned connections.

References

[1] Oh, Sang-Hoon, Young-Ju Kim, and Hong-Sik Ryu. "Seismic performance of steel structures with slit dampers." Engineering structures 31.9 (2009): 1997-2008. https://doi.org/10.1016/j.engstruct.2009.03.003

[2] Shi, Gang, et al. "Experimental study of cyclic behavior of retrofitted beam-to-column joints with welded haunches." Journal of Constructional Steel Research 171 (2020): 106146. https://doi.org/10.1016/j.jcsr.2020.106146

[3] Zhao, Huatian, et al. "Numerical simulation and mechanical model of steel beam-to-column joints retrofitted by haunches." Journal of Constructional Steel Research 185 (2021): 106858. https://doi.org/10.1016/j.jcsr.2021.106858

[4] Zhao, Huatian, et al. "Finite element analysis and design of retrofitted beam-to-column joints with welded haunches." Journal of Constructional Steel Research 186 (2021): 106924. https://doi.org/10.1016/j.jcsr.2021.106924

[5] Tonidis, Margaritis, and Akanshu Sharma. "Detailed 3D FE modeling approach for 2D and 3D beam-column joints retrofitted with fully fastened haunch retrofit solution including anchor behavior." Engineering Structures 294 (2023): 116769. https://doi.org/10.1016/j.engstruct.2023.116769

[6] Richards, Paul W., and Hooseok Lee. "Special moment frame connections with shear-yielding haunches." Engineering Structures 304 (2024): 117635. https://doi.org/10.1016/j.engstruct.2024.117635

[7] Feng, Yulong, et al. "Design and numerical analysis of steel frame joints with replaceable buckling-restrained links." Journal of Constructional Steel Research 196 (2022): 107415. https://doi.org/10.1016/j.jcsr.2022.107415

[8] Arunkumar, C., and N. Umamaheswari. "Numerical study on the behaviour of resilient beam-column end plate connection with dual structural fuse." Innovative Infrastructure Solutions 7.3 (2022): 222. https://doi.org/10.1007/s41062-022-00807-x

[9] He, Xiuzhang, et al. "Development of a connection equipped with fuse angles for steel moment resisting frames." Engineering Structures 265 (2022): 114503. https://doi.org/10.1016/j.engstruct.2022.114503

[10] Lin, Xuchuan, et al. "Experimental study on seismic behavior of the damage-control steel plate fuses for beam-to-column connection." Engineering Structures 270 (2022): 114862. https://doi.org/10.1016/j.engstruct.2022.114862

[11] Chen, Peng, et al. "Numerical investigation on seismic resilient steel beam-to-column connections with replaceable buckling-restrained fuses." Journal of Constructional Steel Research 199 (2022): 107598

[12] Mousavi, S. E., H. A. Mosalman Yazdi, and M. Mosalman Yazdi. "Optimization design of reduced beam section using genetic algorithm." International Journal of Steel Structures 22.3 (2022): 805-815.

[13] Indupriya, G., and B. Anupriya. "Simulation of RBS moment connections using the Finite Element Method for Indian profiles." Materials Today: Proceedings 64 (2022): 1023-1028. https://doi.org/10.1016/j.matpr.2022.05.091

[14] Özkılıç, Yasin Onuralp, and Mehmet Bakır Bozkurt. "Numerical validation on novel replaceable reduced beam section connections for moment-resisting frames." Structures. Vol. 50. Elsevier, 2023. https://doi.org/10.1016/j.istruc.2023.02.027.

[15] Feng, Yulong, et al. "Experimental Study on a Single-Sided Column–Tree Connection with a Replaceable Buckling-Restrained Cover Plate at a Bottom Flange." Journal of Structural Engineering 149.11 (2023): 04023155. DOI: 10.1061/JSENDH.STENG-11710.

[16] Abar, Bahram Mirzaie, et al. "A new energy-dissipating RBS connection with double-nut-bolts: Seismic performance assessment and design methodology." Engineering Structures 293 (2023): 116596.

[17] Casita, Cintantya Budi, Budi Suswanto, and Masahide Matsumura. "Numerical Investigation to Assess the Cyclic Performance of RBS Connection using Cover Plates." E3S Web of Conferences. Vol. 434. EDP Sciences, 2023. https://doi.org/10.1051/e3sconf/202343402017.

[18] Tarighi, Payam, Mohammad Ali Kafi, and Reza Vahdani. "Experimental and numerical investigation of the performance of replaceable-rigid connection." Structures. Vol. 53. Elsevier, 2023. https://doi.org/10.1016/j.istruc.2023.04.047

[19] Lu, Shengcan, et al. "Seismic behavior of reduced beam section joints considering concrete floor effect." The Structural Design of Tall and Special Buildings (2024): e2092. https://doi.org/10.1002/tal.2092

[20] M. Morrison, D. Schweizer and T.Hassan. An innovative seismic performance enhancement technique for steel building moment resisting connections. Journal of constructional steel research. 109, 34–46 , 2015.

[21] Bahirai, Mohammad, and Mohsen Gerami. "Seismic rehabilitation of steel frame connections through asymmetrically weakening the beam." International Journal of Steel Structures 19 (2019): 1209-1224.

[22] Hamed, Arash Akbari, and Mohammad Charkhtab Basim. "Experimental-numerical study on weakened HSS-to-HSS connections using HBS and RBS approaches." Structures. Vol. 28. Elsevier, 2020. https://doi.org/10.1016/j.istruc.2020.09.076.

[23] Bahirai, Mohammad, and Mohsen Gerami. "An experimental and numerical investigation on seismic retrofit of steel moment frame connections." Journal of Earthquake Engineering 25.10 (2021): 2085-2105.

[24] Peyman Shadman Heidari, Armin Aziminejad, A.S. Moghadam, Mohammad Ali Jafari. Experimental and analytical investigation of drilled flange connections (DFCs) with radial drilling patterns. Journal of Building Engineering .52 , 104493,2022.

[25] P. Shadman Heidari , A. Aziminejad , A.S. Moghadam , M. A. Jafari .Investigation of seismic behavior of drilled flange connection with inclined arrangement of holes.Amirkabir Journal Civil Engineering. 54(1) , 67-70,2022.

[26] Bahram Mirzaie Abar, Yashar Bakhshayesh, Reyes Garcia, Iman Hajirasouliha. A new energy-dissipating RBS connection with double-nut-bolts: Seismic performance assessment and design methodology. Engineering Structures .293,116596,2023.

[27] Subhra Paul , Sajal K. Deb, Abhay H. Rangoonwala Seismic performance of bidirectional bolted drilled cut RBS-CFT connections under cyclic loads. Journal of Building Engineering. 77 , 107185,2023.

[28] Mehrdad Hejazi , Ashkan Shoushtarian, Maryam Daei .Cyclic performance welded steel reduced beam section moment connections using longitudinal slots in flanges. Structures .57 , 105328,2023.

[29] Boushehri, Kavoos, Konstantinos Daniel Tsavdaridis, and Gaochuang Cai. "Seismic behaviour of RWS moment connections to deep columns with European sections." Journal of Constructional Steel Research 161 (2019): 416-435. https://doi.org/10.1016/j.jcsr.2019.07.009

[30] Davarpanah, Mohammad, et al. "Cyclic behavior of welded elliptical-shaped RWS moment frame." Journal of Constructional Steel Research 175 (2020): 106319. https://doi.org/10.1016/j.jcsr.2020.106319

[31] Nazaralizadeh, Hamidreza, et al. "Cyclic performance of bolted end-plate RWS connection with vertical-slits." Journal of Constructional Steel Research 173 (2020): 106236. https://doi.org/10.1016/j.jcsr.2020.106236

[32] Nazaralizadeh, Hamidreza, et al. "Design Approach To Bolted End-Plate Vertical-Slits RWS Connection." (2021). https://doi.org/10.21203/rs.3.rs-308954/v1

[33] Tsavdaridis, Konstantinos Daniel, Chun Kit Lau, and Andres Alonso-Rodríguez. "Experimental behaviour of non-seismical RWS connections with perforated beams under cyclic actions." Journal of Constructional Steel Research 183 (2021): 106756. https://doi.org/10.1016/j.jcsr.2021.106756

[34] Tabar, Afshin Moslehi, Andres Alonso-Rodriguez, and Konstantinos Daniel Tsavdaridis. "Building retrofit with reduced web (RWS) and beam (RBS) section limited-ductility connections." Journal of Constructional Steel Research 197 (2022): 107459. https://doi.org/10.1016/j.jcsr.2022.107459

[35] Nazaralizadeh, Hamidreza, et al. "A practical design approach to bolted end-plate vertical-slits RWS connection." Bulletin of Earthquake Engineering (2022): 1-40. https://doi.org/10.1007/s10518-021-01238-2

[36] Chang, Heui-Yung, et al. "Seismic performance of RWS moment connections to steel box-columns and H-beams with general sections." Journal of Constructional Steel Research 201 (2023): 107691. https://doi.org/10.1016/j.jcsr.2022.107691

[37] Vahedi, Masood, Reza Ardestani, and Seyed Mehdi Zahrai. "Sensitivity analysis of tubular-web reduced beam section connections under cyclic loading." International Journal of Steel Structures 21 (2021): 100-117. DOI:10.1007/s13296-020-00418-1

[38] Mansouri, Ali, Mohammad Reza Shakiba, and Ehsan Fereshtehpour. "Two novel corrugated web reduced beam section connections for steel moment frames." Journal of building engineering 43 (2021): 103187. https://doi.org/10.1016/j.jobe.2021.103187.

[39] Khalilpourazar, Yasaman, and Ahmad Maleki. "Thermal and seismic performance evaluation of the innovative cylindrical RBS connection using numerical modelling." Structures. Vol. 50. Elsevier, 2023. https://doi.org/10.1016/j.istruc.2023.02.045

[40] Vesmawala, Gaurang, and Rudradatta Mehta. "Numerical analysis of steel beam–column connection under cyclic loading with dog bone type fuses." Asian Journal of Civil Engineering 25.1 (2024): 115-122. https://doi.org/10.1007/s42107-023-00761-8.

[41] Vesmawala, Gaurang, and Rudradatta Mehta. "Analysis of steel beam column connection under cyclic loading with reduced web opening type fuses." Asian Journal of Civil Engineering 25.3 (2024): 2587-2597. https://doi.org/10.1007/s42107-023-00930-9.

[42] Tartaglia, Roberto, et al. "Retrofit of non-code conforming moment resisting beam-to-column joints: A case study." Journal of Constructional Steel Research 189 (2022): 107095. https://doi.org/10.1016/j.jcsr.2021.107095.

[43] AISC, Seismic Provisions for Structural Steel Buildings, AISC/ANSI 341-16, American Institute of Steel Construction (AISC), Chicago, IL, 2016.

[44] FEMA, Recommended Seismic Design Criteria for newSteelMoment Frame Buildings, FEMA 350, Federal Emergency Management Agency (FEMA),Washington, DC, 2000.

[45] Nia, Z. Saneei, M. Ghassemieh, and A. Mazroi. "WUF-W connection performance to box column subjected to uniaxial and biaxial loading." Journal of Constructional Steel Research 88 (2013): 90-108.

[46] Lee, Cheol-Ho, et al. "Effects of panel zone strength and beam web connection method on seismic performance of reduced beam section steel moment connections." Journal of Structural Engineering 131.12 (2005): 1854-1865

[47] Lee, Cheol-Ho, and Jae-Hoon Kim. "Effect of PZ Strength on Cyclic Seismic Performance of RBS Steel Moment Connections." Journal of the Earthquake Enginerring Society of Korea 10 .3(2006):149-158. DOI:10.5000/EESK.2006.10.3.149

Author Guidelines EditEdit Author Guidelines

GENERAL GUIDELINES FOR AUTHORS

Journal of civil engineering researches invites unsolicited contributions of several forms: articles, reviews and discussion articles, translations, and fora. Contributions should fall within the broad scope of the journal, as outlined in the statement of scope and focus. Contributors should present their material in a form that is accessible to a general anthropological readership. We especially invite contributions that engage with debates from previously published articles in the journal.

Submissions are double-blind peer-reviewed in accordance with our policy. Submissions will be immediately acknowledged but due to the review process, acceptance may take up to three months. Submissions should be submitted via our website submission form (see links above for registration and login). Once you login, make sure your user profile has "author" selected, then click "new submission" and follow the instructions carefully to submit your article. If problems arise, first check the FAQ and Troubleshooting guide posted below. If you are still experiencing difficulty, articles can be submitted to the editors as email attachments.

Each article should be accompanied by a title page that includes: all authors' names, institutional affiliations, address, telephone numbers and e-mail address. Papers should be no longer than 10,000 words (inclusive of abstract 100-150 words, footnotes, bibliography and notes on contributors), unless permission for a longer submission has been granted in advance by the Editors. Each article must include a 100 words "note on contributor(s)" together will full institutional address details, including email address. We request that you submit this material (title page and notes on the contributors) as "supplementary files" rather than in the article itself, which will need to be blinded for peer-review.

We are unable to pay for permissions to publish pieces whose copyright is not held by the author. Authors should secure rights before submitting translations, illustrations or long quotes. The views expressed in all articles are those of the authors and not necessarily those of the journal or its editors. After acceptance, authors and Special Issue guest editors whose institutions have an Open Access library fund must commit to apply to assist in article production costs. Proof of application will be requested. Though publication is not usually contingent on the availability of funding, the Journal is generally under no obligation to publish a work if funding which can be destined to support open access is not made available.

Word template and guidelines

Our tailored Word template and guidelines will help you format and structure your article, with useful general advice and Word tips.

(La)TeX template and guidelines

We welcome submissions of (La)TeX files. If you have used any .bib files when creating your article, please include these with your submission so that we can generate the reference list and citations in the journal-specific style

Artwork guidelines

Illustrations, pictures and graphs, should be supplied with the highest quality and in an electronic format that helps us to publish your article in the best way possible. Please follow the guidelines below to enable us to prepare your artwork for the printed issue as well as the online version.

Format: TIFF, JPEG: Common format for pictures (containing no text or graphs).

EPS: Preferred format for graphs and line art (retains quality when enlarging/zooming in).

Placement: Figures/charts and tables created in MS Word should be included in the main text rather than at the end of the document.

Figures and other files created outside Word (i.e. Excel, PowerPoint, JPG, TIFF, EPS, and PDF) should be submitted separately. Please add a placeholder note in the running text (i.e. "[insert Figure 1.]")

Resolution: Rasterized based files (i.e. with .tiff or .jpeg extension) require a resolution of at least 300 dpi (dots per inch). Line art should be supplied with a minimum resolution of 800 dpi.

Colour: Please note that images supplied in colour will be published in colour online and black and white in print (unless otherwise arranged). Therefore, it is important that you supply images that are comprehensible in black and white as well (i.e. by using colour with a distinctive pattern or dotted lines). The captions should reflect this by not using words indicating colour.

Dimension: Check that the artworks supplied match or exceed the dimensions of the journal. Images cannot be scaled up after origination

Fonts: The lettering used in the artwork should not vary too much in size and type (usually sans serif font as a default).

Authors services:

For reformatting your manuscript to fit the requirement of the Journal of Civil Engineering Researchers and/or English language editing please send an email to the following address:

researchers.services@gmail.com

Noted: There is a fixed charge for these mentioned services that is a function of the manuscript length. The amount of this charge will be notified through a reply email.

FAQ AND TROUBLESHOOTING FOR AUTHORS

I cannot log in to the system. How do I acquire a new user name and password?

If you cannot remember your username, please write an email to (journals.researchers@gmail.com), who will locate your username and notify you. If you know your username, but cannot remember your password, please click the "Login" link on the left-hand menu at homepage. Below the fields for entering your username and password, you will notice a link that asks "Forgot your password?"; click that link and then enter your email adddress to reset your password. You will be sent an automated message with a temporary password and instructions for how to create a new password. TIP: If you do not receive the automated email in your inbox, please check your SPAM or Junk Mail folder. For any other issues, please contact our Managing Editor,Kamyar Bagherinejad (admin@journals-researchers.com).

How do I locate the online submission form and fill it out?

First you need to register or login (see above). Once you are logged in, make sure the "roles" section of your profile has "Author" selected. Once you assign yourself the role of "Author," save your profile and then click the "New Submission" link on your user home page.

Once you arrive at the submission form page, please read the instructions carefully filling out all necessary information. Unless specified otherwise by the editors, the journal section to be selected for your submission should be "Artlcles." Proceed to the remaining sections, checking all boxes of the submission preparation checklist, and checking the box in the copyright notice section (thus agreeing to journals-researchers's copyright terms). Once the first page is completed, click "Save and Continue." The next page allows you to upload your submission. Use the form to choose your file from your computer. Make sure you click "Upload." The page will refresh and you may then click "Save and Continue." You will then proceed to a page for entering the metadata for your article. Please fill out all required fields and any further information you can provide. Click "Save and Continue." The next page allows you to upload supplementary files (images, audiovisual materials, etc.). These are not required, but if you wish to provide supplementary materials, please upload them here (do no forget to click "Upload." Then click "Save and Continue." This brings you to the final page of the submission form. Please click "Finish Submission" in order to close the

submission process. You wil then be notified by email that your article has been successfully submitted. TIP: If you do not receive the automated email in your inbox, please check your SPAM or Junk Mail folder. For any other issues, please contact our Managing Editor, Kamyar Bagherinejad (admin@journals-researchers.com).

Why am I not receiving any email notifications from HAU?

Unfortunately, some automated messages from Open Journal Systems arrive in users' Spam (or Junk Mail) folders. First, check those folders to see if the message was filtered into there. You may also change the settings of your email by editing your preferences to accept all mail from [jcer] and related journals-researchers.com email accounts.

I am trying to upload a revised article following an initial round of peer-review, but I cannot locate where to upload the article. Where do I submit a revised article?

Follow the login process outlined above and when you successfully login you will see on your user home page a link next to "Author" for "active" articles in our system (usually it is only one article, but if you have mulitple submissions currently in our system, the number could be higher. Click the "Active" link and you will be led to a page that lists your authored articles currently in our system. Click the link under the column labeled "Status" and this will take you to a page showing the current review status of your article. At the very bottom of the screen, you will see an upload form under the heading "Editor decision." Here you may upload your revised article. An automated email will be sent to the editors and you may also notify them directly via email. You may then logout.

I successfully submitted an article; how long will it take for the editors to respond to me with a decision.

For all articles that are recommended for peer-review, the editors of JCER strive to notify authors of a decision within 4-6 weeks. You may contact JCER's Managing Editor, Kamyar Bagherinejad (admin@journals-researchers.com). if you have any questions relating to the review process and its duration.

For all other inquiries, please contact: Kamyar Bagherinejad (Managing Editor)

Privacy Statement

The names and email addresses entered in this journal site will be used exclusively for the stated purposes of this journal and will not be made available for any other purpose or to any other party.

Articles

Section default policy

Make a new submission to the Articles section.

Copyright Notice EditEdit Copyright Notice

Journal of Civil Engineering Researchers follows the regulations of the International Committee on Publication Ethics (COPE) and the ethical principles of publishing articles in this journal are set based on the rules of this committee, and in case of problems, it will be treated according to these rules.

Privacy Statement EditEdit Privacy Statement

The names and email addresses entered in this journal site will be used exclusively for the stated purposes of this journal and will not be made available for any other purpose or to any other party.

Scholars Pavilion

Scholars Pavilion or **Scholars Chartagi** is a monument donated by the Islamic Republic of Iran to the United Nations Office at Vienna. The monument architecture is claimed by the Islamic Republic News Agency of Iran to be a combination of Islamic and Achaemenid architecture, although the latter clearly predominates in the decorative features, with Persian columns and other features from Persepolis and other remains from the Achaemenid dynasty. The Chahartaq pavilion form runs through the architecture of Persia from pre-Islamic times to the present.

Statues of four famous Persian medieval scholars, Omar Khayyam, Al-Biruni, Muhammad ibn Zakariya al-Razi and Ibn-Sina are inside the pavilion. This monument donated in June 2009 in occasion of Iran's peaceful developments in science.

J-Researchers